Revision 2

Effect of alkalis on the reaction of clinopyroxene with Mg-carbonate at 6 GPa: Implications for partial melting of carbonated lherzolite

Anton Shatskiy[1,2*], Ivan V. Podborodnikov[1,2], Anton V. Arefiev[1,2], Konstantin D. Litasov[1,2], Artem D. Chanyshev[1,2], Igor S. Sharygin[1], Nikolai S. Karmanov[1], Eiji Ohtani[1,3]

[1]V.S. Sobolev Institute of Geology and Mineralogy, Russian Academy of Science, Siberian Branch, Novosibirsk 630090, Russia

[2]Novosibirsk State University, Novosibirsk 630090, Russia

[3]Department of Earth and Planetary Material Science, Tohoku University, Sendai 980-8578, Japan

*telephone/fax: +7 (382)-330-75-01, e-mail: anton.antonshatskiy.shatskiy@gmail.com

Abstract

The reaction between clinopyroxene and Mg-carbonate is supposed to define the solidus of carbonated lherzolite at pressures exceeding 5 GPa. To investigate the effect of alkalis on this reaction, subsolidus and melting phase relations in the following systems have been examined at 6 GPa: $CaMgSi_2O_6$ + $2MgCO_3$ (Di + 2Mgs); $CaMgSi_2O_6$ + $NaAlSi_2O_6$ + $2MgCO_3$ (Di + Jd + 2Mgs); $CaMgSi_2O_6$ + $Na_2Mg(CO_3)_2$ (Di + Na_2Mg); and $CaMgSi_2O_6$ + $K_2Mg(CO_3)_2$ (Di + K_2Mg). The Di + 2Mgs system begins to melt at 1400 °C via the approximate reaction $CaMgSi_2O_6$ (clinopyroxene) + $2MgCO_3$ (magnesite) = $CaMg(CO_3)_2$ (liquid) + $Mg_2Si_2O_6$ (orthopyroxene), which leads to an essentially carbonate liquid (L) with composition $Ca_{0.56}Mg_{0.44}CO_3$ + 3.5 mol% SiO_2. The initial melting of the Di + Jd + 2Mgs system occurs at 1350 °C via the reaction $2CaMgSi_2O_6$ (clinopyroxene) + $2NaAlSi_2O_6$ (clinopyroxene) + $8MgCO_3$ (magnesite) = $Mg_3Al_2Si_3O_{12}$ (garnet) + $5MgSiO_3$ (clinopyroxene) + $2CaMg(CO_3)_2$ (liquid) + Na_2CO_3 (liquid) + $3CO_2$ (liquid and/or fluid), which yields the carbonate liquid with approximate composition of $10Na_2CO_3 \cdot 90Ca_{0.5}Mg_{0.5}CO_3$ + 2 mol% SiO_2. The systems Di + Na_2Mg and Di + K_2Mg start to melt at 1100 and 1050 °C, respectively, via the reaction $CaMgSi_2O_6$ (clinopyroxene) + $2(Na \text{ or } K)_2Mg(CO_3)_2$ (solid) = $Mg_2Si_2O_6$ (orthopyroxene) + $(Na \text{ or } K)_4CaMg(CO_3)_4$ (liquid). The resulting melts have the alkali-rich carbonate compositions $Na_2Ca_{0.4}Mg_{0.6}(CO_3)_2$ + 0.4 mol% SiO_2 and $43K_2CO_3 \cdot 57Ca_{0.4}Mg_{0.6}CO_3$ + 0.6 mol% SiO_2. These melts do not undergo significant changes as temperature rises to 1400 °C,

retaining their calcium number and a high Na_2O, K_2O and low SiO_2. We suggest that the clinopyroxene–Mg-carbonate reaction controlling the solidus of carbonated lherzolite is very sensitive to the carbonate composition and shifts from 1400 °C to 1050 °C at 6 GPa, which yields K-rich carbonate melt if the subsolidus assemblage contains the $K_2Mg(CO_3)_2$ compound. Such a decrease in solidus temperature has been previously observed in the K-rich carbonated lherzolite system. Although a presence of eitelite, $Na_2Mg(CO_3)_2$, has a similar effect, this mineral cannot be considered as a potential host of Na in carbonated lherzolite, because the whole Na added into the system dissolves as jadeite component in clinopyroxene if bulk Al/Na ≥ 1. The presence of jadeite component in clinopyroxene has little impact on the temperature of the solidus reaction decreasing it to 1350 °C at 6 GPa.

Keywords: carbonatite, eitelite, $K_2Mg(CO_3)_2$, partial melting, carbonated peridotite, Earth's mantle, high-pressure experiment.

Introduction

High-pressure experimental studies (Dalton and Presnall, 1998a; Dasgupta and Hirschmann, 2007) reveal that dominant melting reaction across the solidus of magnesite-bearing lherzolite is:

$$CaMgSi_2O_6\ (Cpx) + 2MgCO_3\ (Mgs) = CaMg(CO_3)_2\ (L) + Mg_2Si_2O_6\ (Opx). \quad (1)$$

Dalton and Presnall (1998b) experimentally determined the phase relationships in the CaO–MgO–Al_2O_3–SiO_2–CO_2 system (CMAS-CO_2) at 6 GPa. They found the solidus of magnesite-bearing lherzolite at 1380 °C. Further studies in more complex systems revealed that alkalis may decrease the solidus temperature of carbonated peridotite, down to 1190-1220 °C, in the presence of Na_2O (Dasgupta and Hirschmann, 2007) and to 1100 °C in presence of K_2O (Brey et al., 2011). The solidus temperature of anhydrous carbonated mantle rocks, and their resulting near-solidus melt composition, are largely determined by the composition of carbonate component. Therefore, the effect of alkalis on melting of carbonated peridotite depends on the host phase, which may be clinopyroxene or carbonate.

Clinopyroxenes in the garnet lherzolites contain 0.6 to 2.6 mol% Na_2O (corresponding to a 5-20 mol% jadeite component) (Moore and Lock, 2001; Agashev et al., 2013; Kolesnichenko et al., 2017). In a series of high-pressure experiments (6.6 GPa), Dasgupta and Hirschmann (2007) observed a distinct drop in the Na_2O concentrations of Cpx as temperature was increased across the solidus of magnesite-bearing lherzolite. The solidi detected in their study are 200-220 °C cooler than

those found from alkali-free analogue (CMAS-CO_2) compositions. This difference could reflect the influence of additional jadeite component on reaction (1).

On the other hand, Na can be hosted by eitelite, $Na_2Mg(CO_3)_2$. Eitelite remains stable at pressures to at least 6.6 GPa and can coexist with Mgs, in temperatures up to 1200 °C and pressures up to 6 GPa (Shatskiy et al., 2013a; Shatskiy et al., 2016b). Eitelite has been reported as the daughter phase in melt inclusions entrapped in diamond, olivine, Cr-spinel and ilmenite from kimberlites in Siberia, Canada, South Africa and Greenland (Kamenetsky et al., 2013; Kamenetsky et al., 2014; Kaminsky et al., 2016) and in olivine from the deepest known mantle rocks sampled by kimberlite magma – sheared lherzolite xenoliths (190-230 km) from Udachnaya-East kimberlite pipe (Sharygin et al., 2013; Sharygin et al., 2015).

According to experimental results (Brey et al., 2011; Litasov et al., 2013; Shatskiy et al., 2013b; Shatskiy et al., 2016a), $K_2Mg(CO_3)_2$ could be the potential host phase of K in oxidized domains of the upper mantle under anhydrous conditions. The formation of this carbonate, just above the solidus of magnesite-bearing lherzolite, was confirmed in experiments at 8 GPa and 1200 ^{o}C (Brey et al., 2011). Recently, the $K_2Mg(CO_3)_2$ compound was found in microinclusions trapped in peridotitic diamonds together with inclusions of orthopyroxene and carbonate-bearing high-density fluid (Jablon and Navon, 2016).

In addition to the work by (Kushiro et al., 1975; Brey et al., 1983), a dearth of studies on the clinopyroxene-magnesite reaction have been made; yet, the direct impact of alkalis on this reaction has not yet been studied, although indirect data from complex systems exist (Dasgupta and Hirschmann, 2007; Brey et al., 2011). Furthermore, there are very few data that indicate how carbonate melt compositions change as temperature increases above the carbonated lherzolite solidus at pressures of at least 6 GPa (Dalton and Presnall, 1998b; Brey et al., 2011). To ameliorate this situation, and disclose the role of alkali elements on phase relations in carbonate-silicate systems, we have conducted experiments on phase relations in $CaMgSi_2O_6$–$MgCO_3$, $CaMgSi_2O_6$–$NaAlSi_2O_6$–$2MgCO_3$, $CaMgSi_2O_6$–$Na_2Mg(CO_3)_2$ and $CaMgSi_2O_6$–$K_2Mg(CO_3)_2$ systems at a pressure of 6 GPa and over a range of temperatures from 900 to 1800 °C.

Experimental procedures

High-pressure experiments have been conducted using a uniaxial 1500-ton press, 'Discoverer', equipped with DIA-type guide bock (Osugi et al., 1964) installed at the V.S. Sobolev Institute of Geology and Mineralogy SB RAS in Novosibirsk, Russia. "Fujilloy TN-05" 26-mm tungsten

carbide dices with truncation edge length of 12 mm were employed as Kawai-cell anvils. We used ZrO_2 semi-sintered ceramics (OZ-8C, MinoYogyo Co., Ltd) as a pressure medium shaped as a 20.5 mm octahedron with ground edges and corners. Unfired pyrophyllite gaskets, 4.0 mm in both width and thickness were used to seal the compressed volume and support the anvil flanks.

The design of the cell assembly is shown in Shatskiy et al. 2013b (their Fig. 1a). The cell contains several samples, 1 mm in diameter and length, loaded into graphite holders (cassettes) with a 3.5 mm outer diameter, surrounded by an electrically insulating sleeves made of talk dehydrated at 1000 °C for 1 h and ZrO_2 plugs inserted at both heater ends. The high temperature was generated using a graphite heater, 4.5/4.0 mm in outer/inner diameter and 11 mm in length. The sample temperature was monitored via a W-$Re_{3\%/25\%}$ thermocouple, 0.1 mm in diameter, inserted through the heater walls and electrically insulated by Al_2O_3 tubes. Thicker (0.3 mm) thermocouple extensions were inserted from the exterior, through gasket holes, into the pressure medium to the point where the Al_2O_3 tubes begin. No correction for the effect of pressure on the thermocouple electromotive force was applied. The temperature gradient across the sample charges was examined, using thermal modeling software (Hernlund et al., 2006), and was found to be about 5 and 7 °C/mm at 1000 and 1800 °C, respectively.

Room-temperature pressure calibration was performed by monitoring the resistance changes in Bi at 2.5 and 7.7 GPa (Decker et al., 1972) using the four-wire method (Shatskiy et al., 2011). Pressure calibration at high temperature (1100 °C) was carried out using known phase transitions in SiO_2 (quartz-coesite) (Bohlen and Boettcher, 1982) and $CaGeO_3$ (Ono et al., 2011). The pressure deviation from desirable values, during heating to 900–1900 °C, in the cell and press load did not exceed ±0.5 GPa. This was confirmed by in situ X-ray diffraction experiments at the BL04B1 beamline of the SPring-8 synchrotron radiation facility.

In the experiments D010-D019, the silicate component was input as analytical grade oxides (SiO_2, Al_2O_3, MgO), while in runs D025-D073 it was introduced as diopside and jadeite glasses. The glasses were prepared using analytical grade oxides (SiO_2, Al_2O_3, and MgO) and carbonates (Na_2CO_3 and $CaCO_3$). Before weighing, the oxides were dried at 1000 °C and the carbonates at 500 °C. Jadeite and diopside glasses were synthesized in Pt crucibles by heating powders to 1300 and 1500 °C, respectively, followed by rapid quenching in water. The carbonate component was introduced as synthetic Na_2CO_3, K_2CO_3, and natural $Mg_{0.975}Fe_{0.015}Mn_{0.006}Ca_{0.004}CO_3$ magnesite from Brumado (Bahia, Brazil). Starting materials were prepared by blending powders in an agate mortar under acetone and loaded as a powder into graphite cassettes. The bulk compositions of the starting

materials were verified using the EDS spectra, which were collected by rastering an electron beam over a surface area of post-experimental samples with homogeneous textures obtained below the solidus (Tables 1-4). The loaded cassettes were dried at 300 °C for 1–5 h. Prepared assemblies were stored at 200 °C in a vacuum for ≥12 h prior to experiment.

All experiments were performed by compression to a load of 6.5 MN (corresponding to a pressure of 6 GPa) and then heating to a target temperature at a rate of 50-100 °C/min. The temperature was maintained within 2.0 °C of the desired value, using a temperature control mode at a constant press load. The experiments were terminated by turning off the power, resulting in a temperature drop to <100 °C in 10-20 s, followed by slow decompression.

After the experiments were completed, the recovered graphite cassettes were cut using a low-speed diamond saw to get vertical cross-sections of samples. The obtained specimens were mounted into epoxy and polished in low-viscosity oil using 400-, 1000-, and 1500-mesh sandpaper. The sample surface was cleaned using an oil spray between each step of polishing. The final polishing was done on a satin cloth with 3 μm diamond paste. We used petroleum benzene to remove the oil after polishing. The clean samples were stored in petroleum benzene, prior to carbon coating and loading into a scanning electron microscope.

Samples were studied using a MIRA 3 LMU scanning electron microscope (Tescan Orsay Holding) coupled with an INCA energy-dispersive X-ray microanalysis system 450 equipped with the liquid nitrogen-free Large area EDS X-Max-80 Silicon Drift Detector (Oxford Instruments Nanoanalysis Ltd) at V.S. Sobolev IGM SB RAS (Novosibirsk, Russia). The energy-dispersive X-ray spectra (EDS) were collected by using an electron beam-rastering method, in which the stage is stationary while the electron beam moves over the surface area, with dimensions 5-10 μm (for mineral phases) and 50-500 μm (for a quenched melt) at 20 kV accelerating voltage and 1.5 nA beam current. Live counting time for X-ray spectra was 30 s. The EDS spectra were optimized for the quantification using the standard XPP procedure (Pouchou, 1993), which is included in the INCA Energy 450 software. The major element compositions of mineral phases were also analyzed in wavelength dispersive (WDS) mode with a JEOL JXA-8100 microprobe. The accelerating voltage and beam current were 20 kV and 40 nA, respectively. 10-second counting times were used for both peaks and backgrounds. The variation coefficients that characterize the repeatability of a single determination are found to be ~0.5% for WDS and ~0.9% for EDS, which are in the compositional range of the main components (C > 10%). For minor components (1% < C < 10%), the variation coefficients are 1.4% and 3.0%, respectively. For impurities (0.3% < C < 1%), the

coefficients are 2.7% and 13%, respectively (Lavrent'ev et al., 2015). Assuming all CO_2 in the liquid is stored as carbonate ion, the CO_2 content in the liquid was calculated as $CO_2 = MgO + CaO + Na_2O + K_2O - SiO_2 - Al_2O_3$. The validity of this assumption has been verified by mass balance calculations.

Experimental results

The results of the experiments are summarized in Tables 1-4, and illustrated in Fig. 1.

The system $CaMgSi_2O_6$+2$MgCO_3$

At 1350 °C, the sample is represented by a homogeneous aggregate of Cpx, with composition close to $Di_{80}En_{20}$ (mol%) and magnesite, Ca# = 10 (Fig. 1a, 2a,b, 3a,b). The first melt appears at 1400 °C as a layer segregated at the high-temperature side of the capsule (Fig. 2c,d). The melt appears to be in the direct contact with the orthopyroxene Di_7En_{93} layer (Fig. 2d). The lower temperature sample side consists of clinopyroxene $Di_{77}En_{23}$ and magnesite (Ca# = 16) (Fig. 2c,d, Table 1). The melt has an essentially carbonate composition with Ca# = 56 and contains a 3.5 mol% SiO_2 and 46.5 mol% CO_2 (Fig. 4a,b, Table 1). At 1500 °C, Cpx and Mgs completely disappear to form orthopyroxene Di_4En_{96} and a liquid containing 4.8 mol% SiO_2 and 45.2 mol% CO_2 with Ca# = 44 (Fig. 1a, 2c. 4a,b,d, Table 1). Our data are consistent with the subsolidus reaction (1) of the carbonated lherzolite systems (Dalton and Presnall, 1998b; a; Dasgupta and Hirschmann, 2007).

With further increases of temperature, Opx composition remains nearly constant, $Di_{5\text{-}6}En_{95\text{-}94}$, whereas melt becomes more silica-rich and CaO-depleted (Fig. 4a,d, Table 1). The quench products of the melt are represented by dendritic carbonate-silicate aggregate containing quench pyroxenes (q-Px). This q-Px can be distinguished by microprobe analysis. It has compositions falling inside the Opx–Cpx miscibility gap (Gasparik, 2003), varying from $Di_{24}En_{76}$ at 1750 °C to $Di_{18}En_{82}$ at 1800 °C, and suggesting its metastable nature. These crystals display diffusion-limited growth textures (e.g., skeletal and hopper, large interior melt hollows) consistent with large undercooling at rapid quenching (Fig. 2g-i). Furthermore, the distribution of q-Px crystals does not match the temperature field in the sample charge at constant temperature, but reflects a progressive cooling of the sample inward from the periphery during quenching(Fig. 2g-i). It is evident from preferential nucleation of q-Px at the sample corners and their growth toward the center, where the slower temperature drop promotes the crystals to grow to the larger size.

In contrast to the quench pyroxene, the stable orthopyroxene appears as well-shaped euhedral crystals at the lower temperature sample side (Fig. 2e, g) (Fig. 2f, h). Its fraction gradually decreases from 45 to 22 mol%, while temperature increases from 1500 to 1750 °C (Fig. 1a, Table 1). The system achieves complete melting at 1800 °C (Fig 1a, 2i, Table 1). Based on our results (Table 1) and the enstatite melting point (Gasparik, 2003) the temperature dependence of Opx solubility in dolomite melt at 6 GPa can be approximated as follows:

$$C(\mathrm{Opx}) = 430(89) - 0.62(10)\cdot T + 2.26(30)\cdot 10^{-4}\cdot T^{2}, \quad (2)$$

where C(Opx) is orthopyroxene solubility in mol% and T is temperature in °C. The numbers in parentheses are standard deviation (Fig. 5).

The system $CaMgSi_2O_6$–$NaAlSi_2O_6$–$2MgCO_3$

Although components of starting mixture (oxides and carbonates) completely reacted to form a Cpx+Mgs assemblage (Table 2), the samples recovered from the experiments at 900 and 1000 °C show large heterogeneity in the Cpx composition even after sample annealing for 96 h (Fig. 6a, b, Table 2). However, at higher temperatures clinopyroxene forms well-shaped crystals with more uniform composition (Fig. 2c-e, Table 2). Subsolidus assemblage consisting of Cpx and Mgs remains stable up to 1300 °C (Fig. 1b, 2a-e).

At 1350 °C, most of the sample still consists of clinopyroxene-magnesite aggregate (Fig. 6f), while a thin Cpx layer, containing partial melt pockets, appears at the high-temperature sample side (Fig. 6f, g). Note that the incipient melting at this temperature was confirmed in two independent runs using oxide-carbonate and silicate glass-carbonate starting mixtures (Table 2). At 1400 °C, the layer with Cpx and melt expands (Fig. 6d, i). Besides, Grt appears in addition to Cpx and Mgs in the lower-temperature side (Fig. 6h, j). At 1500 °C, Mgs disappears and the sample is represented by the clinopyroxene-garnet aggregate and melt pool segregated at the high-temperature side (Fig. 6k, l). The clinopyroxene-garnet residue remains stable until complete melting of the system, which occurs at 1750 °C (Fig. 1b, Fig. 2k-p).

The melt always quenches to an aggregate of carbonate (Mg-rich dolomite and Ca-bearing Na_2CO_3) and quench-clinopyroxene crystals. As the temperature and silicate solubility in the melt increase, the volume fraction of q-Px crystals increases and their size becomes comparable or even larger than that of the stable Cpx (Fig. 6l, n, p). The morphology of q-Px varies from elongated skeletal hopper crystals with a central void to dendritic ones, which completely differs from well-shaped polyhedral crystals of stable Cpx appearing in the lower temperature zone (Fig. 6 l, n, p).

The largest q-Px dendrites (50-100 μm in diameter) appear in the melt, quenched from 1750 °C, were the system achieved complete melting (Fig. 6r). The composition of q-Px differs from stable Cpx. q-Px has higher Ca# and lower Na_2O content.

Increasing the temperature from 900 to 1300 °C is accompanied by the Ca-Mg exchange between subsolidus phases. This follows from gradual changes in Cpx composition from En_1Di_{99} to $En_{10}Di_{90}$ (Fig. 3b) and a simultaneous increase of Ca# of magnesite from 2 to 6 mol% (Fig. 7, Table 2). At the same time, their modal abundances remain constant (Fig. 1b). Above 1300 °C, the temperature dependence of enstatite solubility in Cpx becomes steeper (Fig. 3b) and Mgs fraction gradually decreases, while its Ca# does not change any more (Fig. 7). The above changes are accompanied by an appearance of a partial melt with Ca# = 47-50 containing 2 mol% SiO_2 and 48 mol% CO_2 (Fig. 4a,b, Table. 2), which is also consistent with reaction (1).

Below solidus, at 900-1300 °C, jadeite content in Cpx ranges between 47 and 53 mol% and does not change systematically. Whereas a further temperature increase is accompanied by a gradual decrease of jadeite concentration of up to 33 mol% at 1500 °C (Fig. 3c, Table 2). At the same time, Na_2O concentration in the melt remains unchanged, 5±1 mol% (Fig. 4c), despite increasing the melt fraction (Fig. 1b). These data, coupled with an appearance of $Prp_{91-94}Grs_{9-6}$ garnet (Fig. 1b, 8), yield the following approximate melting reaction, controlling the solidus of the Di+Jd+2Mgs system at 6 GPa:

$$2CaMgSi_2O_6\ (Cpx) + 2NaAlSi_2O_6\ (Cpx) + 8MgCO_3\ (Mgs) = Mg_3Al_2Si_3O_{12}\ (Grt) + 5MgSiO_3\ (in\ Cpx) + 2CaMg(CO_3)_2\ (L) + Na_2CO_3\ (L) + 3CO_2\ (L\ and/or\ F). \quad (3)$$

Reaction (3) violates the carbonate stoichiometry and requires a liberation of molecular CO_2, which is consistent with appearance of 10-20 μm voids within the melt pool in the experiment at 1700 °C (Fig. 6o, q). Yet, it is not obvious whether molecular CO_2 forms separate fluid phase and/or presents as a solute in the carbonate melt. Note that under high-pressure, carbonate melt can dissolve substantial amounts of molecular CO_2 (12 ± 3 mol% in molten $MgCO_3$ and 23 ± 3 mol% in molten $CaCO_3$ at 2.7 GPa) (Huang and Wyllie, 1976).

The system $CaMgSi_2O_6$+$Na_2Mg(CO_3)_2$

At 900-1050 °C, experimental samples are represented by homogeneous aggregate of clinopyroxene, $Di_{95-98}En_{2-5}$, and eitelite, $Na_2Ca_{0.05}Mg_{0.95}(CO_3)_2$ (Fig. 1c, 9a-c, Table 3). At 1100 °C, eitelite disappears and Cpx fraction decreases from 50 to 30 mol% (Fig. 1c). At this temperature, the sample consists of clinopyroxene, $Di_{90}En_{10}$, orthopyroxene, Di_8En_{92}, and a partial melt with

252 approximate composition [$Na_2Ca_{0.4}Mg_{0.6}(CO_3)_2$ + 0.4 mol% SiO_2] (Fig. 9e, f). These data yield the
253 following melting reaction:

254 $CaMgSi_2O_6$ (Cpx) + $2Na_2Mg(CO_3)_2$ (Na_2Mg) = $Mg_2Si_2O_6$ (Opx) + $Na_4CaMg(CO_3)_4$ (L). (4)

255 From the beginning of melting at 1100 °C, the melt fraction is high, 50 mol% (Fig. 1c).
256 Despite this, the residue does not recrystallize in the lower-temperature side, and the crystal-free
257 melt pool does not form. Instead, numerous euhedral Cpx and Opx crystals are suspended in the
258 melt (Fig. 9e, f). Cpx occurs as stubby prismatic crystals up to 15 μm in size, whereas Opx forms
259 elongated prismatic crystals up to 100 μm in length (Fig. 9e, f). As temperature increases to 1200
260 °C, the crystal-free melt pool appears at the high-temperature zone, but most of the liquid phase
261 remains within the Cpx-Opx aggregate (Fig. 9g). At 1350 °C, most of melt segregates as a separate
262 pool (Fig. 9i). Thus, the increase in the melt pool size (Fig. 9d, g, i) reflects the degree of melt
263 segregation rather than melt fraction. Indeed, the modal abundance of melt established using mass
264 balance calculations increases by only 5 mol% as temperature increases from 1100 to 1400 °C (Fig.
265 1c).

266 The melt composition does not undergo significant changes as the temperature increases from
267 1100 to 1400 °C, retaining its high Na_2O and Ca# and low SiO_2 (Fig. 4). Even at 1400 °C, the melt
268 composition [$45Na_2CO_3 \cdot 55Ca_{0.34}Mg_{0.66}CO_3$ + 4.3 mol% SiO_2] is still very similar with near solidus
269 melt. Although the Opx composition does not exhibit any systematic changes, and varies within
270 $Di_{10-12}En_{88-90}$ (Table 3), Cpx composition gradually evolves toward $Di_{73}En_{27}$ as temperature
271 increases to 1500 °C (Fig. 3a,b). At this temperature, Opx disappears and modal abundance of melt
272 increases to 73 mol% (Fig. 1c, 9i). At this point, the concentration of SiO_2 in the melt increases to
273 15.5 mol%, whereas Na_2O and Ca# decrease to 17 and 34 mol%, respectively (Fig. 4).

274 Quenched mats of essentially silica-free carbonate melts are composed of quenched
275 carbonates: $Na_2Mg(CO_3)_2$ (q-Na_2Mg), $Na_2Ca(CO_3)_2$ (q-Na_2Ca), $Na_2Ca_2(CO_3)_3$ (q-Na_2Ca_2) and
276 minor q-Px. q-Px appears as elongated skeletal crystals with a central void (Fig. 9k). An abundance
277 and size of q-Px crystals increase markedly, as silica content in the melt increases at 1500 °C (Fig.
278 9l, m).
279
280 ***The system $CaMgSi_2O_6$+$K_2Mg(CO_3)_2$***
281 The results of the experiments are summarized in Table 4. Independent of the starting mixture
282 employed, oxide-carbonate or diopside glass-carbonate, subsolidus assemblage, established at 900
283 and 1000 °C, consists of the K_2Mg double carbonate, $K_2Ca_{0.07-0.10}Mg_{0.90-0.93}(CO_3)_2$, and diopside,

$Di_{95}En_5$ (Fig. 1d, 10a, b). The exception is run D070, where the Ca# of Cpx approaches 50, whereas the Ca# of K_2Mg is 3, which can be attributed to the kinetic problem (Table 4). At 1050 °C, the K_2Mg + Cpx aggregate remains in the upper half of the sample, while Cpx and interstitial melt [$43K_2CO_3 \cdot 57Ca_{0.4}Mg_{0.6}CO_3$ + 0.6 mol% SiO_2] coexist in the lower half at the high-temperature side (Fig. 10c, d). Besides, Mgs crystals appear at the interface of the two parts of the sample (Fig. 10c, d). At 1100 °C, the subsolidus assemblage completely disappears and the sample is represented by the Cpx + Opx + L assemblage (Fig. 1d, Fig. 10e). These data suggest the following approximate melting reaction:

$$CaMgSi_2O_6\ (Cpx) + 2K_2Mg(CO_3)_2\ (K_2Mg) = Mg_2Si_2O_6\ (Opx) + K_4CaMg(CO_3)_4\ (L). \quad (5)$$

In the temperature range of 1100-1350 °C, the modal abundance of phases does not change noticeably (Fig. 1d), while the efficiency of melt segregation under the influence of temperature gradient and the size of the melt pools considerably increases with increasing temperature (Fig. 10f, i). As temperature increases from 1050 to 1400 °C, the Ca# and concentration of K_2O in the melt do not change systematically, while the SiO_2 content gradually increases from 0.4-0.6 to 4-5 mol% (Fig. 4). Over this temperature range, the melt composition can be approximated as [42-$45K_2CO_3 \cdot 55$-$58Ca_{0.3-0.4}Mg_{0.6-0.7}CO_3$ + 0.4-4.3 mol% SiO_2]. Clinopyroxene composition gradually evolves from $Di_{95}En_5$ to $Di_{70}En_{30}$ as temperature increases from 900 to 1400 °C. The Opx composition does not exhibit any systematic change and varies within $Di_{4-12}En_{88-96}$ (Table 4). At 1500 °C, the modal abundance of melt increases to 76 mol% (Fig. 1d). At this point, the concentration of SiO_2 in the melt increases to 17 mol%, whereas K_2O decreases to 16 mol% (Fig. 4). This melt quenches to a pyroxene-carbonate aggregate. Quench pyroxenes appear as elongated skeletal crystals with a central void (Fig. 10k-m). Despite their comparable sizes, the morphology of q-Px differs from that of a stable Cpx, which forms well-shaped polyhedral crystals (Fig. 10 l, m).

Discussion

Comparison with carbonate systems

Carbonate would be the dominant melt contributor to the melting reactions in the Cpx + Mg-carbonate systems in our study. Therefore, there is interest to compare these results with those in the silicate-free systems, particularly considering suggestions that the melting relationships in these systems strongly influence the solidus of carbonated lherzolite (Luth, 2006).

The incipient melting in the Di + 2Mgs system would relate to melting phase relations along the $CaCO_3$–$MgCO_3$ join. According to experiments at 6 GPa (Buob et al. (2006), the partial melting

316 at the Mg-side of this system is controlled by peritectic reaction Dol = Mgs + L. However, the
317 composition of peritectic point has distinctly lower Ca# (40) and slightly lower temperature (1350
318 °C) compared with the initial melt (Ca# = 56) established at 1400 °C in the Di + 2Mgs system at 6
319 GPa. Recently we have reexamined phase relations along the $CaCO_3$-$MgCO_3$ join at 6 GPa using the
320 same experimental methodology as in the present study in terms of capsule material, design of high-
321 pressure cell, drying of sample assemblies and chemical analysis of phases. The peritectics was
322 established at Ca# = 58 between 1400 and 1450 °C (our unpublished data), which is consistent with
323 the incipient melting in the Di + 2Mgs system. The composition of the magnesite at the solidus in
324 the present study at 6 GPa has distinctly lower Ca# (9) compared with the magnesite at a peritectic
325 in the silicate-free system (Ca# = 18). Given that the Mg/Ca ratio of magnesite would be controlled
326 by partitioning with Cpx and melt, this difference is not surprising.
327 The incipient melting temperature of the Cpx + Na_2Mg subsolidus assemblage in the Di +
328 Na_2Mg system (1100 °C) is generally consistent with minimum melting temperature of the
329 $Na_2Ca_3(CO_3)_4$ + $Na_4Ca(CO_3)_3$ + $Na_2Mg(CO_3)_2$ assemblage in the Na_2CO_3-$CaCO_3$-$MgCO_3$ system at
330 6 GPa (Shatskiy et al., 2016b). However, the partial melt has slightly lower Ca# (40) than that in the
331 carbonate endmember system. In contrast to the Al-free composition, initial melting of the Cpx +
332 Mgs subsolidus assemblage in the Di + Jd + 2Mgs system occurs at higher temperature (1350 °C),
333 which is very close to the solidus of the alkali-free system, Di + 2Mgs. These results suggest that in
334 the presence of Al, when Al/Na ≥ 1, Na is hosted by Cpx as Jd component, rather than eitelite,
335 $Na_2Mg(CO_3)_2$. As a result, the solidus temperature and incipient melt composition in the Di + Jd +
336 2Mgs system differ from those in the Na-Ca-Mg carbonate system.
337 The initial melting in the Di + K_2Mg system occurs at the same temperature as the minimum
338 melting of the K-Ca-Mg carbonate endmember system. At 1050 °C the initial melt with approximate
339 composition [$43K_2CO_3 \cdot 57Ca_{0.4}Mg_{0.6}CO_3$] coexists with Mgs and K_2Mg, while at 1100 °C solid
340 carbonates are completely consumed and melt composition changes to
341 [$43K_2CO_3 \cdot 57Ca_{0.32}Mg_{0.68}CO_3$] (Fig. 1d, 4). This means that Ca# of a liquid coexisting with Mgs and
342 K_2Mg in the K_2CO_3-$MgCO_3$-$CaCO_3$ system at 1100-1200 °C and 6 GPa should not exceed 30
343 mol%, which is lower than what is expected from the data obtained along the K_2CO_3-$Ca_{0.5}Mg_{0.5}CO_3$
344 join (see Fig. 3c,d in Shatskiy et al., 2016a).
345
346 ***Comparison with lherzolite-CO_2 systems***
347 ***The CMS-CO_2 system***

Canil and Scarfe (1990) experimentally determined the phase relations of synthetic peridotite in the CaO–MgO–SiO_2–CO_2 (CMS-CO_2) system from 4 to 12 GPa. Their starting mixture expressed via mineral fractions (mol%) is 63.6Fo + 21.5Di + 14.9Mgs. Three phases (Ol+CPx+Mgs) were established in the subsolidus conditions at pressure above 5 GPa. According to their results the same assemblage coexists with liquid even 100 °C above the solidus disposed near 1300 °C at 6 GPa. In contrast to their data, our results in the Di+2Mgs system suggests that no melting occurs at 1300 and 1350 °C, whereas at 1400 °C and 6 GPa, Cpx reacts with Mgs to form Opx and silica-poor dolomite melt according to reaction (1) (Fig. 1a).

Although Cpx ($Di_{81-75}En_{19-25}$) and Mgs (Ca# 8-9) compositions established at 1320-1380 °C and 5-7 GPa by Canil and Scarfe (1990) are very similar to that in the Di+2Mgs system (Fig. 3a,b, 7), their partial melt composition (25-39 mol% SiO_2, 0-13 mol% CO_2, Ca# = 10-14) calculated for experiments at 5-7 GPa and 1320-1450 °C using mass balance is completely different from the incipient melt established in the present study at 1400 °C and 6 GPa (Fig. 3a,b). The discrepancy would arise from the mass balance calculations based on the Opx-free supersolidus assemblage. It is possible that Opx was overlooked in their run products, given instrumental restrictions of the ARL SEMQ microprobe used for that study and short run duration (20-150 min). At such short duration, silicate crystals may remain suspended in the liquid (Girnis et al., 2011) and have the size comparable with that of dendritic crystals formed within carbonate-rich melt during quenching.

On the other hand, the temperatures (1200-1355 °C) in Canil and Scarfe (1990) experiments at 6 GPa are lower than that of reaction (1) (1400 °C). Thus, it is not surprising that in all their experiments Opx does not appear and the Cpx- and Mgs-bearing assemblage remains stable. Consequently, an alternative explanation of the lower solidus temperature (1300 °C), essentially silicate composition of quenched melt and identical composition of sub- and supersolidus mineral assemblages (Ol+Cpx+Mgs) established by Canil and Scarfe (1990) is a presence of additional component such as H_2O. However, considering careful drying of loaded sample capsules in their study, this suggestion requires further experimental verification.

The CMAS-CO_2 system

In their manuscript Canil and Scarfe (1990) also reported results on near-solidus phase relations of synthetic lherzolite (CCMAS1) in the CMAS-CO_2 system from 5 to 11 GPa. Their starting mixture expressed via mineral fractions (mol%) is 49.2Fo + 28.1En + 8.8Di + 5.2Grt + 8.8Mgs. They found that lherzolitic assemblage (Ol + Opx + Cpx + Grt) remains stable both above

and below subsolidus established at about 1260 °C at 6 GPa, whereas Mgs is stable in subsolidus runs and disappears across the solidus. The reported solidus temperature is noticeably lower than a position of reaction (1) established in our study (Fig. 1a). Unfortunately, the reason of this discrepancy cannot be clarified because cited manuscript (Canil and Scarfe, 1990) does not contain any details on compositions of phases obtained in the CMAS-CO_2 experiments.

Later, Dalton and Presnall (1998a) continued to study phase relations along the solidus of the CMAS-CO_2 system at pressures ranging from 3 to 7 GPa. Their starting composition can be expressed via mineral fractions (mol%) as 36.7Fo + 31.7En + 8.3Di + 4.9Prp + 18.4Mgs. Six phases (Ol+Opx+CPx+Grt+Mgs+L) were established on the solidus at 1380 °C and 6 GPa (Dalton and Presnall, 1998a). The solidus temperature is consistent with the position of reaction (1) in our study (Fig. 1a). The reported compositions of phases yield following mole fractions below [34.6Ol + 47.4Opx + 4.1Cpx + 3.2Grt +10.8Mgs] and above solidus [35.2Ol + 51.0Opx + 2.8Grt + 6.5Mgs +5.5L]. Note that in the starting composition used by Dalton and Presnall (1998a) as well as in the subsolidus assemblage, the fraction of Mgs more than twice exceeds the Cpx mole fraction. Therefore, in accordance with reaction (1) Cpx must be completely consumed above the solidus in Dalton and Presnall (1998b) experiments. Indeed, to achieve mass balance convergence for their results at 1405-1505 °C, we need to exclude Cpx. After that, the following modal abundances of phases can be obtained: [40.6Ol + 38.9Opx + 6.2Grt + 14.4L] at 1405 °C and [41.7Ol + 31.4Opx + 3.1Grt + 23.6L] at 1505 °C.

Like the present study (Fig. 4), the near-solidus melt at 1380 °C and 6 GPa has essentially dolomitic composition (Ca# = 49 mol%, 4.5 mol% SiO_2, 47.5 mol% CO_2) (Dalton and Presnall, 1998a). However, drastic increase of MgO and SiO_2 in the melt at 1405 °C and 1505 °C (Dalton and Presnall, 1998b) appears to be inconsistent with our results in the Di+2Mgs system (Fig. 4). This discrepancy would be attributed to the differences in the compositions of the Di+2Mgs and CMAS-CO_2 systems. Alternatively, the discrepancy would be caused by applying the wavelength dispersive microprobe technique to determine a bulk composition of polycrystalline quenched products of melt in Dalton and Presnall (1998b) study. The use of stationary electron beam, which diameter is comparable with quenched melt grain size, leads to significant uncertainty of average melt composition (Dalton and Presnall, 1998b). Besides, a stationary electron beam with an acceleration voltage of 15 kV and a current of 10 nA used in their study could result in thermal decomposition of carbonates (Smith, 1986). This, as well as possible presence of small residual silicate crystals within

411 liquid pool in relatively short (6 h) experiments, may cause overestimation of SiO_2 and MgO
412 concentrations in the melt.
413
414 ***The MixKLB-1-CO_2 systems***
415 Dasgupta and Hirschmann (2007) examined near-solidus phase relations in natural peridotite
416 MixKLB-1 with 5.8 mol% CO_2 (PERC2 composition) at 6.6 GPa. The PERC2 composition
417 expressed via mole fraction of minerals is 60.2Ol + 5.9Opx + 10.5Cpx + 4.9Grt + 18.4Mgs, where
418 all minerals have Fe# = 10.3 mol% and Cpx contains 3.6 mol% jadeite. The subsolidus assemblage
419 established at 1250 and 1300 °C includes Ol, Opx, Cpx, Grt, and Mgs. First melt observed at 1330
420 °C. At this temperature, Mgs and Cpx fractions decrease below 1 mol%. Like our study in the
421 Di+Jd+2Mgs system, Dasgupta and Hirschmann (2007) observed distinct change in Cpx
422 composition across the solidus, namely, drop in concentration of jadeite from 2.1 to 1.4 mol% and
423 increase of enstatite concentration from 19 to 28 mol%. These observations as well as an increase in
424 the Grt fraction at 1360 °C are in a good agreement with reaction (3) established in our study.
425 Unlike the Di+Jd+2Mgs system, where $Mg_2Si_2O_6$ liberated above the solidus is completely
426 consumed by the Cpx solid solution, in the PERC2 composition most of $Mg_2Si_2O_6$ forms Opx
427 according to reaction (1). Despite the large difference in jadeite concentration in Cpx and presence
428 of 5.8 mol% FeO, MgO/(MgO+FeO) = 0.9, in the PERC2 composition, the solidus temperatures of
429 these two systems are consistent within experimental uncertainty. Furthermore, the partial melt
430 obtained in the PERC2 system at 1330-1360 °C has essentially carbonate composition (2-3 mol%
431 SiO_2, 45-48 mol% CO_2, 1.2-1.4 mol% Na_2O, Ca# = 40-45) like that established in the Di+Jd+2Mgs
432 system at 1350-1400 °C (Fig. 4). Thus, the presence of Na as jadeite component in Cpx does not
433 affect significantly reaction (1), controlling the solidus of magnesite-bearing lherzolite. Based on
434 our results the maximum temperature decrease in the CaO-MgO-Al_2O_3-SiO_2-Na_2O-CO_2 system with
435 Al/Na ratio ≥ 1 relative to the CMAS-CO_2 system would not exceed 50 °C at 6 GPa. Besides, this
436 comparison also implies that the presence of Fe has no apparent effect on further reduction of the
437 solidus temperature.
438 Brey at al. (2008) also studied the melting phase relations in the system like PERC2
439 (SC1+$MgCO_3$). The SC1+$MgCO_3$ composition expressed via mole fraction of minerals is 54.7Ol +
440 10.7Opx + 10.9Cpx + 5.7Grt + 18.0Mgs, where all minerals have Fe# = 9.2 mol% and Cpx contains
441 4.3 mol% jadeite. They observed partial melting over the entire temperature range beginning from
442 1300 °C at 6 GPa. They succeeded to analyze partial melt quenched at 1350 °C and 6 GPa. The melt

443 has lower Ca# = 34 and surprisingly more silica-rich (9 mol% SiO_2) and sodium-depleted (0.4 mol%
444 Na_2O) composition compared with that in Dasgupta and Hirschmann (2007) study. The mass
445 balance calculations based on Brey et al. (2008) results show that at 1350 °C Cpx and Mgs
446 disappear, whereas fraction of Grt and Opx increases. The calculated mole fractions of phases in
447 their study are [49.5Ol + 11.2Opx + 12.3Cpx + 15.7Grt + 11.0Mgs + (trace)L] at 1300 °C and
448 [47.8Ol + 20.5Opx + 17.7Grt + 13.9L] at 1350 °C. Thus, Brey et al. (2008) results are consistent
449 with our observations and suggest that partial melting of natural carbonated lherzolite at 6 GPa is
450 controlled by combination of reaction (1) and reaction (3) established in our study.
451 Dasgupta and Hirschmann (2007) also examined two compositions with lower bulk CO_2
452 contents, PERC (2.9 mol% CO_2) and PERC3 (1.2 mol% CO_2), keeping proportions of another
453 component identical to the MixKLB-1 peridotite. The principle difference from PERC2 is the lower
454 Mgs mole fraction in subsolidus runs as follows from mass balance calculations: PERC2 [57.4Ol +
455 6.7Opx + 13.2Cpx + 11.1Grt + 11.6Mgs], PERC [62.8Ol + 7.2Opx + 13.0Cpx + 11.1Grt + 5.9Mgs],
456 and PERC3 [64.3Ol + 7.8Opx + 14.4Cpx + 11.1Grt + 2.4Mgs]. Despite of almost the same
457 compositions of subsolidus minerals, the apparent solidus temperatures decreases with decreasing
458 bulk CO_2: 1315±15 °C/5.8 mol% CO_2, 1262±13 °C/2.9 mol% CO_2, 1205±15 °C/1.2 mol% CO_2. The
459 authors attributed these observations to increasing bulk Na_2O/CO_2 mole ratio from 0.04 to 0.21 and
460 connected the decrease in solidus temperature with increasing "availability" of Na_2O in the bulk
461 rock. Our results appear to be inconsistent with the above hypothesis, because bulk Na_2O/CO_2 ratio
462 of the Di + Jd + 2Mgs system is 0.21, while its solidus temperature matches that of PERC2 with
463 Na_2O/CO_2 = 0.04. We suggest that a simple change of the reagent ratio (Cpx/Mgs) would not affect
464 the temperature of reaction (3) and, therefore, cannot increase the "availability" of Na_2O, i.e.
465 redistribution of Na_2O from Cpx (chief reservoir of Na_2O) to carbonate. There should be another
466 reason, which, however, remains unclear owing lack of information on partial melt compositions
467 obtained in the PERC and PERC3 systems.
468
469 ***K-rich carbonated lherzolite***
470 Brey et al. (2011) reported experimental results on melting phase relations in K-rich
471 carbonated lherzolite (LC) at 6-10 GPa. The LC composition expressed via mole fraction of
472 minerals is 54.4Ol + 6.2Opx + 12.9Cpx + 5.3Grt + 8.2Mgs + 13.0K_2Mg, where all minerals have
473 Fe# = 9.0 mol% and Cpx contains 3.4 mol% jadeite. They observed partial melt coexisting with Ol,
474 Opx, and Grt over the entire temperature range of 1200-1600 °C at 6 GPa. Considering the Cpx :

Mgs : K_2Mg proportions in the starting mixture, the established supersolidus assemblage can be explained by a simultaneous operation of reactions (3) and (5). Our results in the Di + K_2Mg system at 6 GPa suggest that $K_2Mg(CO_3)_2$ is a main host of K below the LC solidus, whereas reaction (5) is a dominant solidus reaction, yielding K-rich carbonate melt at 1050 °C. Like the Di + K_2Mg system (Fig. 4), the initial melt in the LC system has K-rich carbonate composition, which does not change significantly with temperature increase from 1200 to 1400 °C (0.5-2.5 SiO_2, 19-21 MgO, 3-5 FeO, 2-4 CaO, 0.3-0.5 Na_2O, 13-17 K_2O, in mol%). Interestingly, the melts from the LC and Di+K_2Mg systems at 6 GPa differ only in Ca# (11-18 and 30-40, respectively); both containing low SiO_2, even though the higher temperature (1400 °C) experiments are 300-350 °C above the solidus. Over a similar temperature range (1400-1600 °C), the liquid compositions at 6 GPa changed more dramatically, especially with respect to the silica concentrations (29 mol% SiO_2 at 1600 °C in LC and 17 mol% SiO_2 at 1500 °C in Di+K_2Mg) (Fig. 4a).

Implications

We suggest that the clinopyroxene–Mg-carbonate reaction controlling the solidus of carbonated lherzolite is very sensitive to the carbonate composition and shifts from 1400 °C to 1050 °C at 6 GPa yielding K-rich carbonate melt [$43K_2CO_3 \cdot 57Ca_{0.4}Mg_{0.6}CO_3$ + 0.6 mol% SiO_2] if subsolidus assemblage contains $K_2Mg(CO_3)_2$ compound. A decrease in solidus temperature at least to 1200 °C has been observed previously in the K-rich carbonated lherzolite system at 6 GPa (Brey et al., 2011). We also found that the partial melt does not undergo significant changes as temperature increases to 1400 °C retaining its Ca#, high K_2O and low SiO_2. These observations suggest that ultrapotassic Mg-rich carbonatite melts from microinclusions in fibrous (Zedgenizov et al., 2007; Klein-BenDavid et al., 2009) and single crystal diamonds (Jablon and Navon, 2016) worldwide could be derived by low degree partial melting of $K_2Mg(CO_3)_2$-bearing lherzolite at temperature of ≥ 1050 °C and pressures near 6 GPa, i.e. at the *P-T* conditions of diamond formation in the lithospheric mantle (Boyd et al., 1985). This idea is consistent with recent finding of the $K_2(Mg,Ca)(CO_3)_2$ compound as microinclusions in peridotitic diamonds along with inclusions of orthopyroxene and ultrapotassic carbonate-bearing high-density fluid (Jablon and Navon, 2016).

We also suggest that eitelite, $Na_2Mg(CO_3)_2$, cannot be considered as a potential host of Na in carbonated lherzolite as far as all Na added into the system is partitioned to clinopyroxene as jadeite component if bulk Al/Na ≥ 1, even if Na is added to the starting mixture as Na_2CO_3. We found that Cpx (diopside-jadeite solid solution) + Mgs assemblage remains stable up to 1350-1400 °C (Fig.

1b), whereas the initial Na-bearing dolomite melt appears at 1350 °C. These results are consistent within experimental uncertainty with the solidus temperature and partial melt composition of natural carbonated lherzolite PERC2 (Dasgupta and Hirschmann, 2007). Thus, the maximum decrease in carbonated lherzolite solidus due to presence of jadeite-bearing Cpx would not exceed 50 °C at 6 GPa.

Nomenclature

Ca# = $100 \cdot Ca/(Ca+Fe+Mg)_{molar}$, Cpx – clinopyroxene, Di – diopside, En – enstatite, Fe# = $100 \cdot Fe/(Fe+Mg)_{molar}$, Fo – forsterite, Grs – grossular, Grt – garnet, Jd – jadeite, K_2Mg – $K_2Mg(CO_3)_2$, L – liquid, F – fluid, Mgs – magnesite, Na_2Mg – eitelite, $Na_2Mg(CO_3)_2$. Ol – olivine, Opx – orthopyroxene, Prp – pyrope.

Acknowledgements

We are very grateful to Robert W Luth for a constructive review, Roland Stalder and Keith Putirka for editorial handling. This work is financially supported by Russian Science Foundation (project No 14-17-00609) and performed under the program of Ministry of education and science of Russian Federation (project No 14.B25.31.0032).

References

Agashev, A.M., Ionov, D.A., Pokhilenko, N.P., Golovin, A.V., Cherepanova, Y., and Sharygin, I.S. (2013) Metasomatism in lithospheric mantle roots: constraints from whole-rock and mineral chemical composition of deformed peridotite xenoliths from kimberlite pipe Udachnaya. Lithos, 160-161, 201-215.

Bohlen, S.R., and Boettcher, A. (1982) The quartz⇆ coesite transformation: a precise determination and the effects of other components. Journal of Geophysical Research: Solid Earth, 87, 7073-7078.

Boyd, F., Gurney, J., and Richardson, S. (1985) Evidence for a 150–200-km thick Archaean lithosphere from diamond inclusion thermobarometry. Nature, 315, 387-389.

Brey, G., Brice, W.R., Ellis, D.J., Green, D.H., Harris, K.L., and Ryabchikov, I.D. (1983) Pyroxene-carbonate reactions in the upper mantle. Earth and Planetary Science Letters, 62, 63-74.

Brey, G.P., Bulatov, V.K., Girnis, A.V., and Lahaye, Y. (2008) Experimental melting of carbonated peridotite at 6-10 GPa. Journal of Petrology, 49, 797-821.

Brey, G.P., Bulatov, V.K., and Girnis, A.V. (2011) Melting of K-rich carbonated peridotite at 6-10 GPa and the stability of K-phases in the upper mantle. Chemical Geology, 281, 333-342.

Buob, A., Luth, R.W., Schmidt, M.W., and Ulmer, P. (2006) Experiments on $CaCO_3$-$MgCO_3$ solid solutions at high pressure and temperature. American Mineralogist, 91, 435-440.

Canil, D., and Scarfe, C.M. (1990) Phase relations in peridotite+CO_2 systems to 12 GPa: implications for the origin of kimberlite and carbonate stability in the Earth's upper mantle. Journal of Geophysical Research: Solid Earth, 95, 15805-15816.

Dalton, J.A., and Presnall, D.C. (1998a) Carbonatitic melts along the solidus of model lherzolite in the system CaO-MgO-Al_2O_3-SiO_2-CO_2 from 3 to 7 GPa. Contributions to Mineralogy and Petrology, 131, 123-135.

-. (1998b) The continuum of primary carbonatitic-kimberlitic melt compositions in equilibrium with lherzolite: Data from the system CaO-MgO-Al_2O_3-SiO_2-CO_2 at 6 GPa. Journal of Petrology, 39, 1953-1964.

Dasgupta, R., and Hirschmann, M.M. (2007) Effect of variable carbonate concentration on the solidus of mantle peridotite. American Mineralogist, 92, 370-379.

Decker, D.L., Bassett, W.A., Merrill, L., Hall, H.T., and Barnett, J.D. (1972) High-pressure calibration a critical review. J. Phys. Chem. Ref. Data., 1, 1-79.

Gasparik, T. (2003) Phase diagrams for geoscientists. An Atlas of the Earth's Interior, Springer Ed.

Girnis, A.V., Bulatov, V.K., and Brey, G.P. (2011) Formation of primary kimberlite melts - Constraints from experiments at 6-12 GPa and variable CO_2/H_2O. Lithos, 127, 401-413.

Hernlund, J., Leinenweber, K., Locke, D., and Tyburczy, J.A. (2006) A numerical model for steady-state temperature distributions in solid-medium high-pressure cell assemblies. American Mineralogist, 91, 295-305.

Huang, W.L., and Wyllie, P.J. (1976) Melting relationships in the systems CaO-CO_2 and MgO-CO_2 to 33 kilobars. Geochimica Et Cosmochimica Acta, 40, 129-132.

Jablon, B.M., and Navon, O. (2016) Most diamonds were created equal. Earth and Planetary Science Letters, 443, 41-47.

568 Kamenetsky, V.S., Grütter, H., Kamenetsky, M.B., and Gömann, K. (2013) Parental carbonatitic
569 melt of the Koala kimberlite (Canada): Constraints from melt inclusions in olivine and Cr-
570 spinel, and groundmass carbonate. Chemical Geology, 353, 96-111.
571 Kamenetsky, V.S., Golovin, A.V., Maas, R., Giuliani, A., Kamenetsky, M.B., and Weiss, Y. (2014)
572 Towards a new model for kimberlite petrogenesis: Evidence from unaltered kimberlites and
573 mantle minerals. Earth-Science Reviews, 139, 145-167.
574 Kaminsky, F.V., Ryabchikov, I.D., and Wirth, R. (2016) A primary natrocarbonatitic association in
575 the Deep Earth. Mineralogy and Petrology, 110, 387-398.
576 Klein-BenDavid, O., Logvinova, A.M., Schrauder, M., Spetius, Z.V., Weiss, Y., Hauri, E.H.,
577 Kaminsky, F.V., Sobolev, N.V., and Navon, O. (2009) High-Mg carbonatitic
578 microinclusions in some Yakutian diamonds - a new type of diamond-forming fluid. Lithos,
579 112, 648-659.
580 Kolesnichenko, M.V., Zedgenizov, D.A., Litasov, K.D., Safonova, I.Y., and Ragozin, A.L. (2017)
581 Heterogeneous distribution of water in the mantle beneath the central Siberian Craton:
582 Implications from the Udachnaya Kimberlite Pipe. Gondwana Research,
583 http://dx.doi.org/10.1016/j.gr.2016.09.011.
584 Kushiro, I., Satake, H., and Akimoto, S. (1975) Carbonate-silicate reactions at high presures and
585 possible presence of dolomite and magnesite in the upper mantle. Earth and Planetary
586 Science Letters, 28, 116-120.
587 Lavrent'ev, Y.G., Karmanov, N., and Usova, L. (2015) Electron probe microanalysis of minerals:
588 Microanalyzer or scanning electron microscope? Russian Geology and Geophysics, 56,
589 1154-1161.
590 Litasov, K.D., Shatskiy, A., Ohtani, E., and Yaxley, G.M. (2013) The solidus of alkaline carbonatite
591 in the deep mantle. Geology, 41, 79-82.
592 Luth, R.W. (2006) Experimental study of the $CaMgSi_2O_6$-CO_2 system at 3-8 GPa. Contributions to
593 Mineralogy and Petrology, 151, 141-157.
594 Moore, A.E., and Lock, N.P. (2001) The origin of mantle-derived megacrysts and sheared
595 peridotites-evidence from kimberlites in the northern Lesotho Orange Free State (South
596 Africa) and Botswana pipe clusters. South African Journal of Geology, 104, 23-38.
597 Ono, S., Kikegawa, T., and Higo, Y. (2011) In situ observation of a garnet/perovskite transition in
598 $CaGeO_3$. Physics and Chemistry of Minerals, 38, 735-740.

599 Osugi, J., Shimizu, K., Inoue, K., and Yasunami, K. (1964) A compact cubic anvil high pressure
600 apparatus. Review of Physical Chemistry of Japan, 34, 1-6.
601 Pouchou, J.-L. (1993) X-Ray microanalysis of stratified specimens. Analytica chimica acta, 283, 81-
602 97.
603 Sharygin, I., Litasov, K., Shatskiy, A., Golovin, A., Ohtani, E., and Pokhilenko, N. (2015) Melting
604 phase relations of the Udachnaya-East group-I kimberlite at 3.0-6.5 GPa: experimental
605 evidence for alkali-carbonatite composition of primary kimberlite melts and implications for
606 mantle plumes. Gondwana Research, 28, 1391-1414.
607 Sharygin, I.S., Golovin, A.V., Korsakov, A.V., and Pokhilenko, N.P. (2013) Eitelite in sheared
608 peridotite xenoliths from Udachnaya-East kimberlite pipe (Russia) – a new locality and host
609 rock type. European Journal of Mineralogy, 25, 825-834.
610 Shatskiy, A., Katsura, T., Litasov, K.D., Shcherbakova, A.V., Borzdov, Y.M., Yamazaki, D.,
611 Yoneda, A., Ohtani, E., and Ito, E. (2011) High pressure generation using scaled-up Kawai-
612 cell. Physics of the Earth and Planetary Interiors, 189, 92-108.
613 Shatskiy, A., Gavryushkin, P.N., Sharygin, I.S., Litasov, K.D., Kupriyanov, I.N., Higo, Y., Borzdov,
614 Y.M., Funakoshi, K., Palyanov, Y.N., and Ohtani, E. (2013a) Melting and subsolidus phase
615 relations in the system Na_2CO_3-$MgCO_3$+-H_2O at 6 GPa and the stability of $Na_2Mg(CO_3)_2$ in
616 the upper mantle. American Mineralogist, 98, 2172-2182.
617 Shatskiy, A., Sharygin, I.S., Gavryushkin, P.N., Litasov, K.D., Borzdov, Y.M., Shcherbakova, A.V.,
618 Higo, Y., Funakoshi, K., Palyanov, Y.N., and Ohtani, E. (2013b) The system K_2CO_3-$MgCO_3$
619 at 6 GPa and 900-1450 ºC. American Mineralogist, 98, 1593-1603.
620 Shatskiy, A., Litasov, K.D., Palyanov, Y.N., and Ohtani, E. (2016a) Phase relations on the K_2CO_3-
621 $CaCO_3$-$MgCO_3$ join at 6 GPa and 900-1400 °C: implication for incipient melting in
622 carbonated mantle domains. American Mineralogist, 101, 437-447.
623 Shatskiy, A., Litasov, K.D., Sharygin, I.S., Egonin, I.A., Mironov, A.M., Palyanov, Y.N., and
624 Ohtani, E. (2016b) The system Na_2CO_3–$CaCO_3$–$MgCO_3$ at 6 GPa and 900-1250 °C and its
625 relation to the partial melting of carbonated mantle. High Pressure Research, 36, 23-41.
626 Smith, M.P. (1986) Silver coating inhibits electron microprobe beam damage of carbonates:
627 Research method paper. Journal of Sedimentary Research, 56, 560-561.
628 Zedgenizov, D.A., Rege, S., Griffin, W.L., Kagi, H., and Shatsky, V.S. (2007) Composition of
629 trapped fluids in cuboid fibrous diamonds from the Udachnaya kimberlite: LAM-ICPMS
630 analysis. Chemical Geology, 240, 151-162.

631

632 **Figure captions**

633

634 Fig. 1. Modal abundances of phases present as a function of temperature in the systems
635 $CaMgSi_2O_6 + 2MgCO_3$ (a), $CaMgSi_2O_6 + NaAlSi_2O_6 + 2MgCO_3$ (b), $CaMgSi_2O_6 + Na_2Mg(CO_3)_2$
636 (c), and $CaMgSi_2O_6 + K_2Mg(CO_3)_2$ (d) at 6.0 GPa. Modes are in mol% were determined from the
637 bulk compositions of starting mixtures and compositions of phases measured by electron
638 microprobe.

639

640 Fig. 2. Representative BSE micrographs of sample cross-sections from experiments in the
641 $CaMgSi_2O_6 + 2MgCO_3$ system at 6.0 GPa. The lower side of images a-f, i and the upper side of
642 images g, h correspond to the high-temperature edge of the capsule. q-Px – quench pyroxenes. HT –
643 high-temperature side. LT – low-temperature side. Gravity vector is directed downwards.

644

645 Fig. 3. Variations of diopside (a), enstatite (b), jadeite (c), and tschermakite $MgAlSiAlO_6$ (d)
646 components in clinopyroxene with temperature in the studied systems. Diagrams (a) and (b) also
647 contain the data for the $Mg_2Si_2O_6$-$CaMgSi_2O_6$ system (black solid line Di+En) (Gasparik, 2003).

648

649 Fig. 4. Run temperature plotted against selected oxide concentrations (a-c) and Ca# (d) in
650 liquid phase obtained in the systems $CaMgSi_2O_6 + 2MgCO_3$ (Di + 2Mgs), $CaMgSi_2O_6 + NaAlSi_2O_6$
651 $+ 2MgCO_3$ (Di + Jd + 2Mgs), $CaMgSi_2O_6 + Na_2Mg(CO_3)_2$ (Di + Na_2Mg), and $CaMgSi_2O_6 +$
652 $K_2Mg(CO_3)_2$ (Di + K_2Mg) at pressure of 6.0 GPa. The liquid composition in the Di + Jd + 2Mgs
653 system recalculated assuming that all molecular CO_2 is dissolved in the melt.

654

655 Fig. 5. The temperature dependence of orthopyroxene solubility, *C*(Opx), in dolomite melt at
656 6 GPa. T_m(En) – enstatite melting point (Gasparik, 2003).

657

658 Fig. 6. Representative BSE images of sample cross-sections from experiments in the
659 $CaMgSi_2O_6 + NaAlSi_2O_6 + 2MgCO_3$ system at 6.0 GPa. See Fig. 1 for abbreviations. q-Px – quench
660 pyroxenes. HT – high-temperature side. LT – low-temperature side. Gravity vector is directed
661 downwards.

662

Fig. 7. The temperature dependence of Ca# (mol%) of Mg-carbonates obtained in carbonate-silicate systems (this study) compared with that synthesized in the Ca-Mg, Na-Ca-Mg and K-Ca-Mg carbonate systems at 6 GPa (Buob et al., 2006; Shatskiy et al., 2016a; Shatskiy et al., 2016b).

Fig. 8. The temperature dependence of Ca# (mol%) of garnet from experiments in the $CaMgSi_2O_6 + NaAlSi_2O_6 + 2MgCO_3$ system at 6.0 GPa.

Fig. 9. Representative BSE images of sample cross-sections from experiments in the $CaMgSi_2O_6 + Na_2Mg(CO_3)_2$ system at 6.0 GPa. q-Px – quench pyroxenes, q-Na_2Mg – quench $Na_2Mg(CO_3)_2$, q-Na_2Ca – quench $Na_2Ca(CO_3)_2$, q-Na_2Ca_2 – quench $Na_2Ca_2(CO_3)_3$. HT – high-temperature side. LT – low-temperature side. Gravity vector is directed downwards. Gravity is directed downwards.

Fig. 10. Representative BSE images of sample cross-sections from experiments in the $CaMgSi_2O_6 + K_2Mg(CO_3)_2$ system at 6.0 GPa. q-Px – quench pyroxenes, q-K_2Mg – quench $K_2Mg(CO_3)_2$. HT – high-temperature side. LT – low-temperature side. Gravity vector is directed downwards. Gravity is directed downwards.

Table 1. Summary of run conditions, composition of phases (mol%) and their mole proportions (MFP) in the $CaMgSi_2O_6 + 2MgCO_3$ system at 6.0 GPa

Run#	*T*, °C	*t*, h.	Phase	n	SiO_2	MgO	CaO	CO_2	BD	MFP
System composition					25.0	37.5	12.5	25.0		
D019[1]	1350	16	Bulk	3	25.9(6)	37.1(3)	12.5(0)	–	24.5(4)	
			Cpx	17	50.4(3)	30.2(9)	19.4(9)	–	–	49.8(3)
			Mgs	15	–	44.9(4)	5.1(2)	50	51.0(4)	50.0(3)
D027[2]	1350	24	Bulk	1	25.8	37.8	12.6	–	23.8	
			Cpx	7	50.4(6)	29.6(3)	20.0(3)	–	–	49.8(3)
			Mgs	4	–	45.4(2)	4.6(1)	50	51.0(2)	50.1(3)
D010[1]	1400	24	Bulk	1	25.7	36.7	11.5	–	26.2	
			Cpx	8	49.9(7)	30.8(1.5)	19.3(1.2)	–	–	21.3(0)
			Opx	6	50.1(2)	48.1(8)	1.8(5)	–	–	27.4(0)
			Mgs	4	–	42.1(4)	7.9(1)	50	51.0(5)	32.1(0)
			L	4	3.5(8)	22.1(1.6)	27.9(2.1)	46.5	54.6(4.1)	19.3(0)
D012[1]	1500	16	Opx	11	49.9(4)	49.0(4)	1.1(1)	–	–	44.9(2)
			L	5	4.8(1)	27.9(3)	22.1(1)	45.2	45.9(4)	55.2(3)
D036[2]	1550	8	Opx	6	50.2(1)	48.5(2)	1.3(1)	–	–	44.0(6)
			L	2	5.6(0)	28.2(1)	21.8(1)	44.4	44.4(0)	56.3(7)
D018[1]	1600	2	Opx	20	50.0(9)	48.0(7)	2.0(4)	–	–	39.7(0)
			L	11	8.5(3.6)	30.6(1.9)	19.4(1.5)	41.5	38.4(3.8)	60.3(0)
D025[2]	1700	2	Opx	9	50.1(3)	48.3(3)	1.5(1)	–	–	31.3(1.2)
			L	3	14.0(6)	31.7(5)	18.3(2)	36.0	29.3(1.3)	69.2(1.5)
D029[2]	1750	1	Opx	8	50.3(2)	48.2(4)	1.5(1)	–	–	22.1(2)
			L	4	17.9(2)	34.3(3)	15.7(2)	32.1	35.7(7)	77.9(3)
D039[2]	1800	0.5	L	2	26.0(2)	36.5(1)	13.3(2)	24.2	24.1(0)	100

Notes: "–"– phase absent; *t* – run duration; n – number of EDS analyses averaged. Mole fractions of phases (MFP) were determined from mass balance calculations using microprobe analyses of phases. Values within parentheses are standard deviation in the last decimal place reported. Assuming all CO_2 in the liquids in carbonate ion form, CO_2 contents of the liquids were calculated as $CO_2 = MgO + CaO + Na_2O + K_2O – SiO_2 – Al_2O_3$. BD – CO_2 contents estimated from the difference between 100% and the analysis total. [1] – Starting mixture = $2SiO_2 + 2MgO + CaCO_3 + MgCO_3$; [2] – starting mixture = $CaMgSi_2O_6$(glass) + $2MgCO_3$.

Table 2. Summary of run conditions, composition of phases (mol%) and their mole proportions (MFP) in the $CaMgSi_2O_6 + NaAlSi_2O_6 + 2MgCO_3$ system at 6.0 GPa

Run#	*T*, °C	*t*, h.	Phase	n	SiO_2	Al_2O_3	MgO	CaO	Na_2O	CO_2	BD	MFP
System composition					36.4	4.5	27.3	9.1	4.5	18.2		
D011[1]	900	71	Bulk	4	36.5(1)	4.7(1)	28.0(5)	9.7(4)	4.5(0)	–	16.7(1.1)	
			Cpx	18	58.3(2.7)	7.6(2.9)	13.7(4.4)	12.9(4.0)	7.6(2.9)	–	–	62.8(8)
			Mgs	3	n.d.	n.d.	49.2(1)	0.8(4)	n.d.	50	51.2(2)	37.2(7)
D016[1]	1000	96	Bulk	1	36.6	4.3	28.0	9.1	4.8	–	17.2	
			Cpx	15	56.9(2.0)	6.5(1.8)	15.9(2.8)	13.9(2.3)	6.8(1.9)	–	–	63.9(5)
			Mgs	4	n.d.	n.d.	48.5(4)	1.5(5)	n.d.	50	51.5(4)	35.9(4)
D015[1]	1100	48	Bulk	1	36.9	4.8	27.5	9.1	4.5	–	17.2	
			Cpx	7/5	57.3(5)	7.7(7)	15.4(8)	12.3(1.0)	7.3(6)	–	–	63.7(7)
			Mgs	6	n.d.	n.d.	48.4(3)	1.6(1)	n.d.	50	51.9(3)	36.3(6)
D014[1]	1200	25	Bulk	1	37.2	4.6	27.0	8.8	4.7	–	17.8	
			Cpx	5/3	57.5(9)	7.3(7)	16.2(1.1)	11.7(7)	7.2(7)	–	–	63.6(7)
			Mgs	4/1	n.d.	n.d.	46.2(3)	2.7(2)	n.d.	50	50.4(5)	36.3(6)
D013[1]	1300	49	Cpx	7/5	56.8(1.1)	7.1(8)	17.7(7)	11.8(9)	6.6(5)	–	–	63.9(8)
			Mgs	4	n.d.	n.d.	46.9(3)	3.0(1)	n.d.	50	51.6(4)	35.4(7)
D019[1]	1350	16	Bulk	1	37.0	4.7	27.9	9.0	4.4	–	17.0	
			Cpx	7	56.9(4)	7.5(3)	19.4(4)	9.7(3)	6.5(2)	–	–	63.2(2)
			Mgs	5	n.d.	n.d.	47.4(4)	2.6(2)	n.d.	50	52.5(4)	26.3(3)
			L	8	2.2(1.0)	0.3(1)	23.5(8)	20.6(4)	5.8(7)	47.5	52.2(1.3)	10.6(4)
D027[2]	1350	24	Bulk	1	36.7	4.9	27.8	8.8	4.4	–	17.5	
			Cpx	17	56.7(7)	6.6(6)	19.2(1.2)	11.2(6)	6.3(5)	–	–	63.8(7)
			Mgs	9	n.d.	n.d.	46.7(4)	3.3(1)	n.d.	50	51.6(4)	29.9(1.3)
			L	1	1.7	0.2	22.8	23.0	4.2	48.1	49.6	6.1(1.6)
D017[1]	1400	8	Cpx	22	56.1(9)	6.8(7)	23.2(1.7)	8.0(9)	5.9(5)	–	–	63.4(1.8)
			Grt	15	43.0(7)	13.8(6)	39.3(1.3)	3.7(8)	n.d.	–	–	1.6(2.3)
			Mgs	13	n.d.	n.d.	47.4(5)	2.6(2)	n.d.	50	51.4(5)	15.3(1.5)
			CO_2	–	–	–	–	–	–	100	–	1.6(6)
			L	5	0.7(6)	0.2(1)	25.6(4)	19.2(2)	5.2(5)	49.1	49.6(7)	18.3(1.3)
D012[1]	1500	16	Bulk	1	36.4	4.5	27.3	9.7	4.6	–	17.5	
			Cpx	3/5	54.6(1)	5.5(1)	28.2(4)	7.3(0)	4.4(0)	–	–	55.2(7)
			Grt	5/2	42.8(3)	13.8(1)	40.2(6)	3.2(4)	n.d.	–	–	9.6(8)
			CO_2	–	–	–	–	–	–	100	–	6.0(3)
			L	3	7.4(3)	0.6(0)	26.9(4)	16.6(2)	6.5(2)	42.0	47.0(4)	29.1(6)
			L+CO_2	–	6.1	0.5	22.3	13.8	5.4	51.8	–	35.1(7)
D036[2]	1550	8	Bulk	1	36.3	4.6	27.9	9.2	4.9	–	17.0	
			Cpx	8	55.1(4)	5.9(2)	28.0(3)	6.4(3)	4.7(2)	–	–	58.9(1.0)
			Grt	5	43.6(3)	13.4(2)	40.2(4)	2.8(1)	n.d.	–	–	5.3(1.2)
			CO_2	–	–	–	–	–	–	100	–	4.4(4)
			L	4	5.3(1.7)	0.5(1)	28.0(4)	16.1(2)	5.9(4)	44.2	36.4(6)	31.3(8)
			L+CO_2	–	4.7	0.5	24.6	14.1	5.2	51.0	–	35.7(9)
D033[2]	1650	3	Bulk	1	36.4	4.5	27.3	9.7	4.6	–	17.5	
			Cpx	14	55.3(4)	6.2(1)	27.5(4)	6.3(2)	4.7(1)	–	–	51.2(2)
			Grt	5	43.7(5)	13.4(1)	40.1(1)	2.6(1)	n.d.	–	–	5.8(2)
			CO_2	–	–	–	–	–	–	100	–	5.7(1)
			L	7	14.9(4)	1.5(1)	29.2(7)	15.4(3)	5.4(2)	33.7	37.0(1.2)	37.2(2)
			L+CO_2	–	12.9	1.3	25.3	13.4	4.7	42.4	–	42.9(2)
D025[2]	1700	2	Bulk	1	36.2	4.7	27.2	9.4	4.7	–	17.7	
			Cpx	12	55.6(2)	6.6(1)	27.1(2)	5.7(1)	5.0(1)	–	–	14.5(1.0)
			Grt	11	43.6(4)	13.5(6)	40.2(6)	2.5(2)	n.d.	–	–	6.8(1.0)
			CO_2	–	–	–	–	–	–	100	–	13.7(2)
			L	7	38.9(6)	4.3(1)	31.6(3)	12.5(2)	6.0(1)	6.9	23.1(7)	65.2(1.4)

			$L+CO_2$	–	32.1	3.6	26.1	10.3	4.9	23.0	–	78.9(1.7)
D029[2]	1750	1	$L+CO_2$	2	36.4(1)	4.5(1)	28.3(2)	9.3(2)	4.4(2)	17.1	17.7(6)	100

Notes: * – free fluid phase and/or molecular CO_2 dissolved in the liquid. n – number of EDS or EDS/WDS analyses averaged. $L+CO_2$ – the liquid composition assuming that all molecular CO_2 dissolved in the melt; n.d. – not determined; [1] – starting mixture = $4SiO_2 + 0.5Al_2O_3 + 2.5MgO + CaCO_3 + 0.5MgCO_3 + 0.5Na_2CO_3$; [2] – starting mixture = $CaMgSi_2O_6$(glass) + $NaAlSi_2O_6$(glass) + $2MgCO_3$. See Table 1 notes for other abbreviations.

Table 3. Summary of run conditions, composition of phases (mol%) and their mole proportions (MFP) in the $CaMgSi_2O_6 + Na_2Mg(CO_3)_2$ system at 6.0 GPa

Run#	*T*, °C	*t*, h.	Phase	n	SiO_2	MgO	CaO	Na_2O	CO_2	BD	MFP
System composition					25.0	25.0	12.5	12.5	25.0		
D011[1]	900	71	Cpx	7/3	50.6(4)	25.5(3)	23.4(1)	0.5(1)	–	–	49.8(4)
			Na_2Mg	9	n.d.	24.4(1)	1.1(6)	24.5(7)	50	51.0(9)	50.1(4)
D070[2]	900	96	Bulk	1	25.1	24.4	12.0	12.9	–	25.6	
			Cpx	11	50.8(6)	24.8(3)	23.7(5)	0.7(2)	–	–	49.3(6)
			Na_2Mg	8	n.d.	25.8(2)	1.1(3)	23.2(2)	50	52.6(4)	50.3(6)
D016[1]	1000	96	Bulk	1	25.0	25.6	12.6	12.6	–	24.3	
			Cpx	13	50.6(5)	25.8(2)	23.1(3)	0.5(0)	–	–	49.9(5)
			Na_2Mg	9	n.d.	24.2(3)	1.1(1)	24.8(2)	50	50.7(1)	50.0(5)
D073[2]	1000	96	Bulk	1	26.3	24.5	11.9	12.9	–	24.4	
			Cpx	9	50.1(5)	25.4(7)	24.0(6)	0.4(3)	–	–	49.8(2)
			Na_2Mg	11	n.d.	24.693)	1.3(1)	24.1(6)	50	54.5(7)	50.2(2)
D026[2]	1050	96	Cpx	13	50.4(7)	25.6(3)	23.4(5)	0.6(2)	–	–	49.9(4)
			Na_2Mg	9	n.d.	23.9(3)	1.5(0)	24.7(4)	50	50.0(6)	50.1(4)
D015[1]	1100	48	Cpx	5	50.5(4)	27.1(7)	22.2(2)	0.2(0)	–	–	31.4(3)
			Opx	6	49.8(5)	48.1(7)	2.1(5)	n.d.	–	–	18.0(3)
			L	2	0.4(0)	15.3(1)	10.1(4)	24.6(3)	49.6	49.4(0)	50.5(2)
D014[1]	1200	25	Cpx	6	50.4(2)	28.1(9)	21.4(1.0)	0.1(1)	–	–	30.8(5)
			Opx	9	50.0(5)	47.1(8)	2.8(6)	–	–	–	18.6(4)
			L	2	0.5(1)	14.8(0)	10.5(3)	24.7(0)	49.5	50.1(4)	50.6(2)
D038[2]	1250	25	Cpx	37	50.6(9)	30.2(9)	19.0(5)	0.3(3)	–	–	34.9(1.5)
			Opx	10	50.2(1.0)	47.0(6)	2.9(4)	n.d.	–	–	14.4(1.3)
			L	3	0.7(1)	14.9(3)	10.4(2)	24.2(2)	49.8	51.4(5)	50.6(5)
D013[1]	1300	49	Cpx	6/4	50.4(3)	30.2(9)	19.2(1.1)	0.2(0)	–	–	34.8(3)
			Opx	10/3	50.0(5)	47.4(6)	2.6(2)	n.d.	–	–	13.1(3)
			L	5	1.8(1)	15.8(1)	10.4(1)	23.9(5)	48.0	48.2(7)	52.1(1)
D027[2]	1350	24	Cpx	7	50.6(2)	30.8(5)	18.3(4)	0.3(1)	–	–	37.3(1.4)
			Opx	6	50.2(1.0)	47.5(7)	2.3(3)	n.d.	–	–	10.3(1.3)
			L	4	2.2(1)	16.1(3)	10.0(1)	24.0(4)	47.8	48.7(7)	52.4(5)
D017[1]	1400	8	Cpx	14	50.3(3)	31.3(2.0)	18.2(2.0)	0.2(1)	–	–	34.3(3)
			Opx	15	49.9(9)	47.2(1.4)	2.9(5)	n.d.	–	–	10.8(3)
			L	7	4.3(4)	16.7(4)	10.8(4)	22.5(4)	45.7	47.6(5)	54.8(1)
D012[1]	1500	16	Cpx	3/5	50.4(8)	33.4(8)	16.1(7)	0.2(0)	–	–	27.0(2)
			L	2	15.5(1)	22.1(1)	11.2(1)	17.0(1)	34.2	34.2(1)	73.0(2)

Notes: [1] – Starting mixture = $2SiO_2 + 2MgO + CaCO_3 + Na_2CO_3$; [2] – starting mixture = $CaMgSi_2O_6$(glass) + $MgCO_3$ + Na_2CO_3. See notes of Tables 1 and 2 for abbreviations.

Table 4. Summary of run conditions, composition of phases (mol%) and their mole proportions (MFP) in the $CaMgSi_2O_6 + K_2Mg(CO_3)_2$ system at 6.0 GPa

Run#	*T*, °C	*t*, h.	Phase	n	SiO_2	MgO	CaO	K_2O	CO_2	BD	MFP
System composition					25.0	25.0	12.5	12.5	25.0	–	–
D011[1]	900	71	Cpx	9	49.6(7)	25.6(3)	23.3(6)	1.5(5)	–	–	50.4(8)
			K_2Mg	7	n.d.	23.2(3)	2.5(1)	24.2(3)	50	49.2(6)	50.0(8)
D070[2]	900	96	Bulk	1	23.5	23.2	11.6	12.2	–	29.6	
			Cpx	13	50.7(4)	24.6(4)	24.3(3)	0.4(2)	–	–	49.5(3)
			K_2Mg	11	n.d.	25.2(6)	0.8(3)	24.0(2)	50	51.1(8)	50.4(3)
D016[1]	1000	96	Cpx	7	49.8(7)	26.3(0)	23.5(0)	0.4(0)	–	–	50.0(2)
			K_2Mg	8	n.d.	23.9(4)	1.7(2)	24.3(2)	50	49.8(8)	50.0(2)
D073[2]	1000	96	Bulk	1	24.0	24.0	11.9	12.4	–	27.6	
			Cpx	5	50.2(9)	25.8(6)	23.2(5)	0.8(6)	–	–	49.9(1)
			K_2Mg	7	n.d.	24.3(7)	1.6(4)	24.1(3)	50	52.3(9)	50.0(1)
D026[2]	1050	96	Bulk	1	23.4	25.3	11.6	12.3	–	27.2	
			Cpx	5	50.2(2)	26.4(1)	23.1(3)	0.3(1)	–	–	49.8(2)
			Mgs	4	n.d.	49.0(4)	1.0(1)	n.d.	50	–	0.3(3)
			K_2Mg	16	n.d.	23.9(3)	1.1(1)	25.0(3)	50	49.6(6)	45.5(9)
			L	1	0.6	17.2	11.2	20.6	49.4	53.0(5)	4.3(8)
D015[1]	1100	48	Cpx	12	49.6(9)	27.7(6)	21.8(7)	0.9(5)	–	–	37.9(4.3)
			Opx	13	50.0(9)	48.4(7)	1.6(3)	n.d.	–	–	10.9(3.7)
			L	7	0.4(1)	19.2(1.0)	9.1(1.2)	21.7(1.1)	49.6	50.6(8)	50.8(1.9)
D031[2]	1150	53	Cpx	10	50.5(3)	27.5(3)	22.0(2)	0.1(0)	–	–	35.4(1.3)
			Opx	13	50.5(3)	48.6(4)	0.9(1)	n.d.	–	–	11.4(1.1)
			L	6	2.5(1)	18.5(5)	8.8(3)	22.7(8)	47.5	54.6(1.1)	53.0(6)
D014[1]	1200	25	Cpx	9/3	50.1(4)	29.1(8)	20.4(7)	0.4(2)	–	–	39.9(2.9)
			Opx	7/3	50.1(7)	47.0(6)	3.0(5)	n.d.	–	–	8.0(2.6)
			L	25	1.4(1.4)	19.1(9)	8.5(1.1)	22.3(1.0)	48.6	49.9(1.7)	51.9(1.2)
D038[2]	1250	25	Cpx	5	50.5(4)	28.5(6)	20.8(4)	0.1(0)	–	–	37.3(7)
			Opx	4	50.3(5)	48.6(2)	1.1(2)	n.d.	–	–	7.2(6)
			L	5	4.8(2)	19.3(2)	8.1(3)	22.5(3)	45.2	53.4(5)	55.4(3)
D013[1]	1300	49	Cpx	3/5	50.0(1)	29.7(6)	20.3(5)	0.1(0)	–	–	37.2(6)
			Opx	4/2	49.9(5)	47.8(7)	2.2(3)	n.d.	–	–	7.7(6)
			L	5	4.5(3)	18.7(3)	8.9(1)	22.3(3)	45.5	47.3(7)	55.0(3)
D027[2]	1350	24	Cpx	13	50.5(4)	30.4(4)	19.1(4)	n.d.	–	–	36.9(3.1)
			Opx	8	50.2(1)	48.6(2)	1.3(2)	n.d.	–	–	7.5(2.8)
			L	6	4.3(3)	18.8(2)	10.2(3)	21.0(2)	45.7	42.5(7)	55.3(1.3)
D017[1]	1400	8	Cpx	21	50.0(4)	32.4(6)	17.5(6)	0.1(1)	–	–	45.6(9)
			L	8	3.8(5)	18.4(4)	9.7(4)	21.9(3)	46.2	50.0(1.0)	54.5(1.0)
D028[2]	1500	6	Cpx	9	50.4(4)	30.4(3)	19.1(2)	0.1(0)	–	–	24.3(3)
			L	4	16.8(7)	23.4(4)	10.5(1)	16.1(3)	33.2	34.4(1.0)	75.6(4)

Notes: [1] – starting mixture = $2SiO_2 + 2MgO + CaCO_3 + K_2CO_3$; [2] – starting mixture = $CaMgSi_2O_6$(glass) + $MgCO_3$ + K_2CO_3. See notes of Tables 1 and 2 for abbreviations.

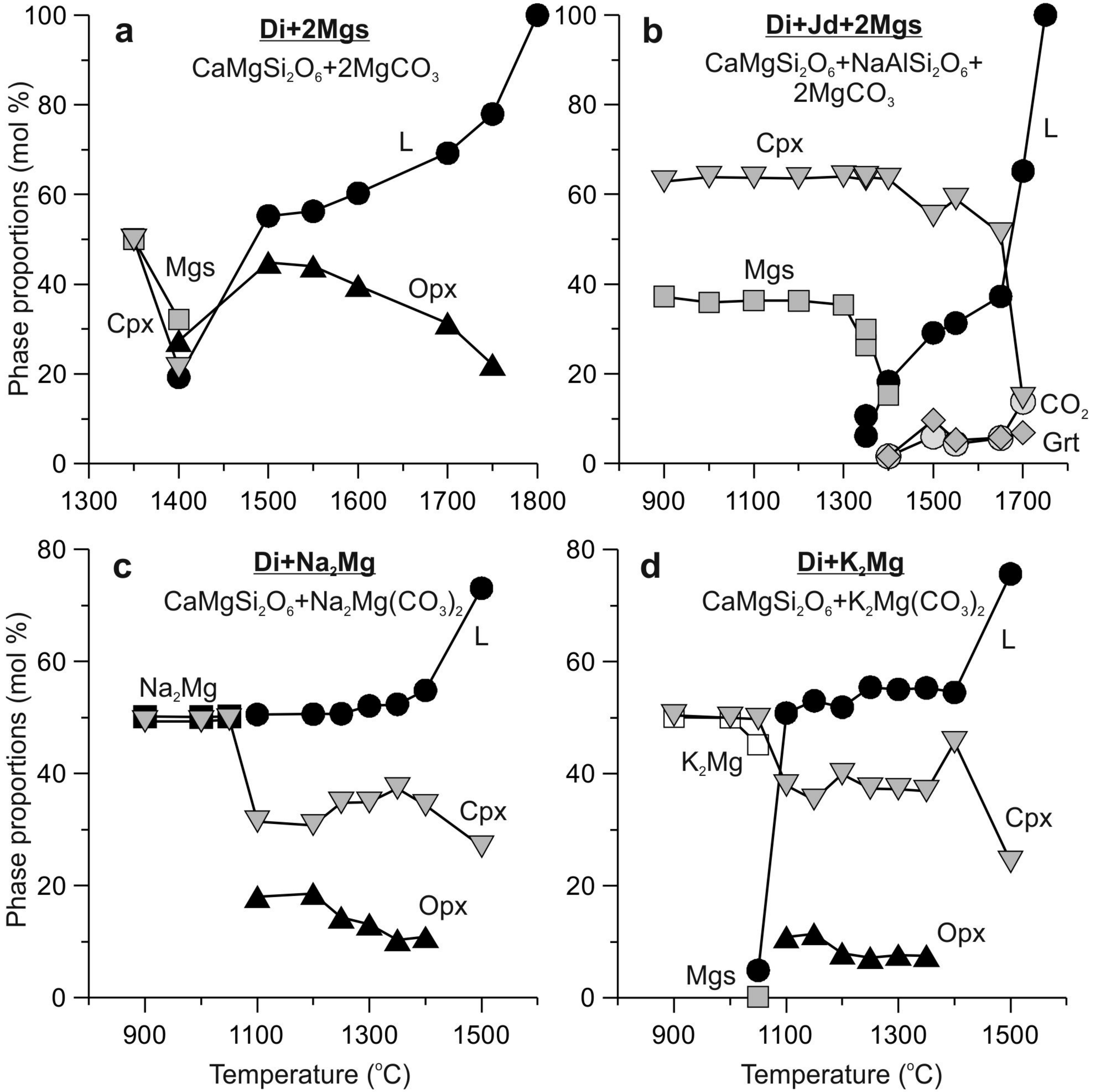
a
Di+2Mgs
CaMgSi2O6+2MgCO3
L
Mgs
Opx
Cpx
Phase proportions (mol %)
100
80
60
40
20
0
1300
1400
1500
1600
1700
1800
b
Di+Jd+2Mgs
CaMgSi2O6+NaAlSi2O6+
2MgCO3
Cpx
L
Mgs
CO2
Grt
900
1100
1300
1500
1700
c
Di+Na2Mg
CaMgSi2O6+Na2Mg(CO3)2
L
Na2Mg
Cpx
Opx
Temperature (°C)
d
Di+K2Mg
CaMgSi2O6+K2Mg(CO3)2
L
K2Mg
Cpx
Opx
Mgs
▲ - Orthopyroxene (Opx), ▽ - Clinopyroxene (Cpx), ◆ - Garnet (Grt),
■ - Na2Mg(CO3)2 (Na2Mg), □ - K2Mg(CO3)2 (K2Mg), ▩ - Magnesite (Mgs), ● - Liquid (L).

a. D027, 1350 °C, 24 h.

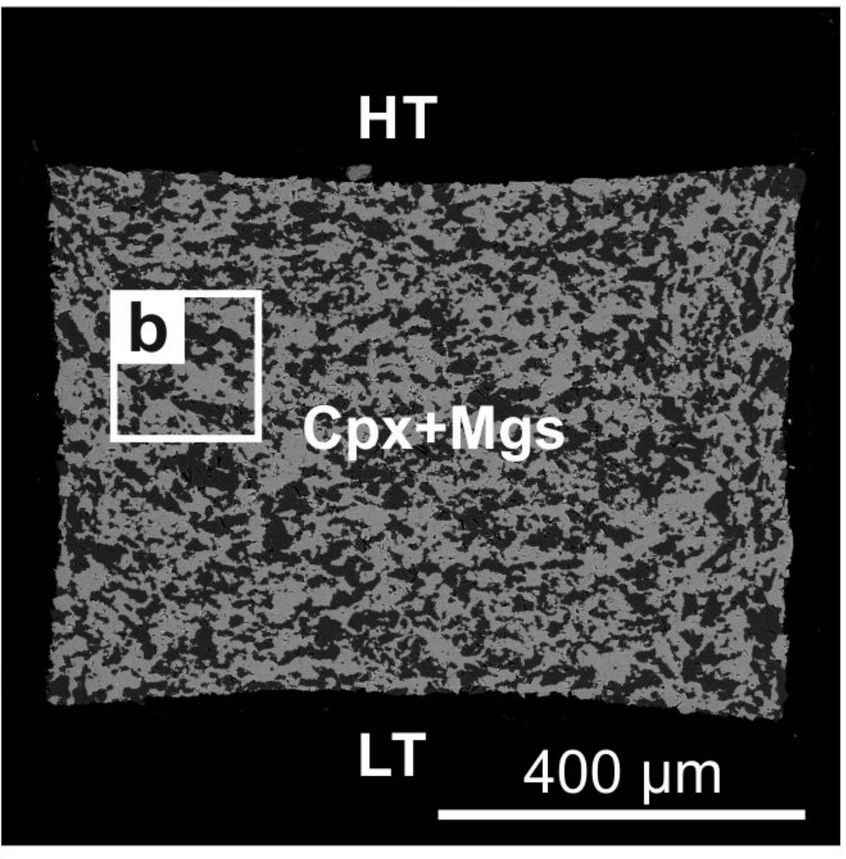

b. D027, 1350 °C, 24 h.

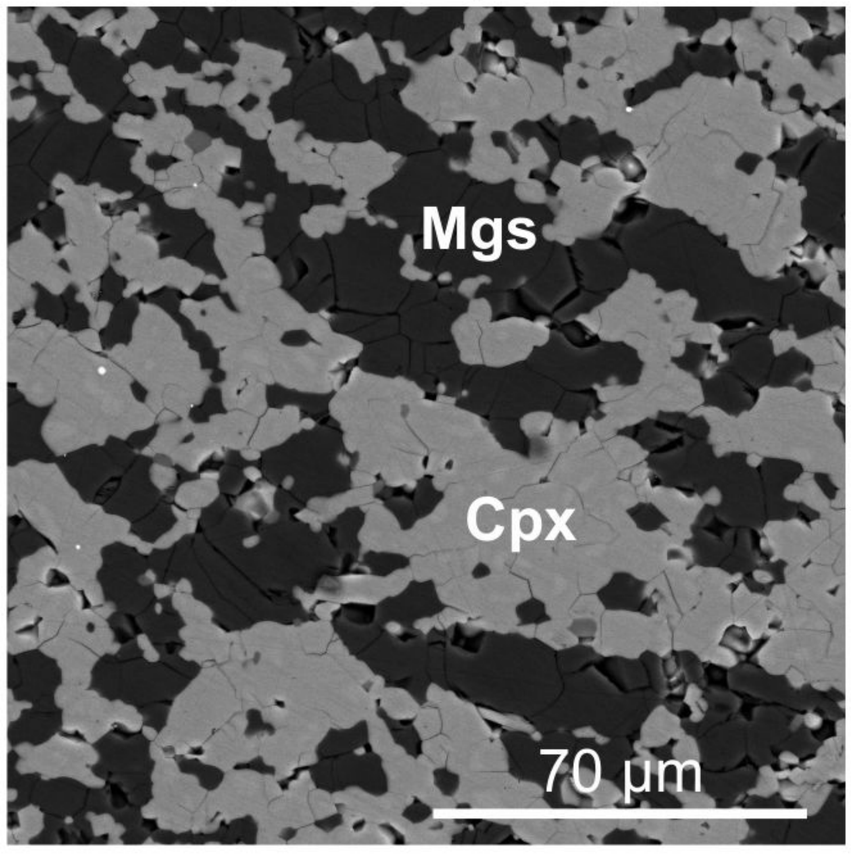

c. D010, 1400 °C, 24 h.

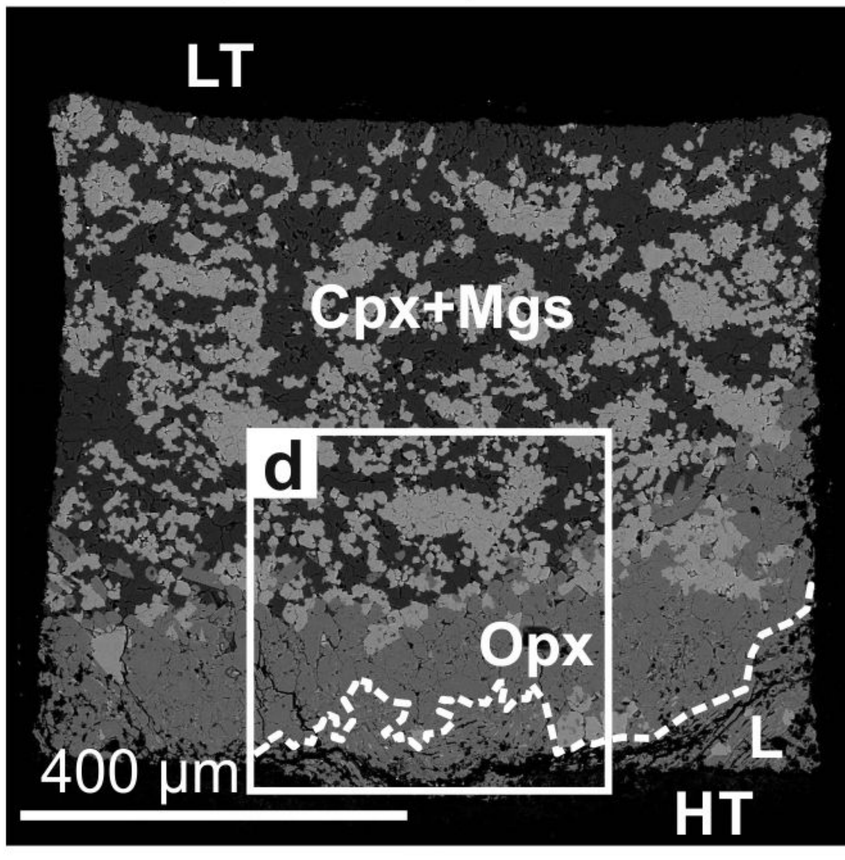

d. D010, 1400 °C, 24 h.

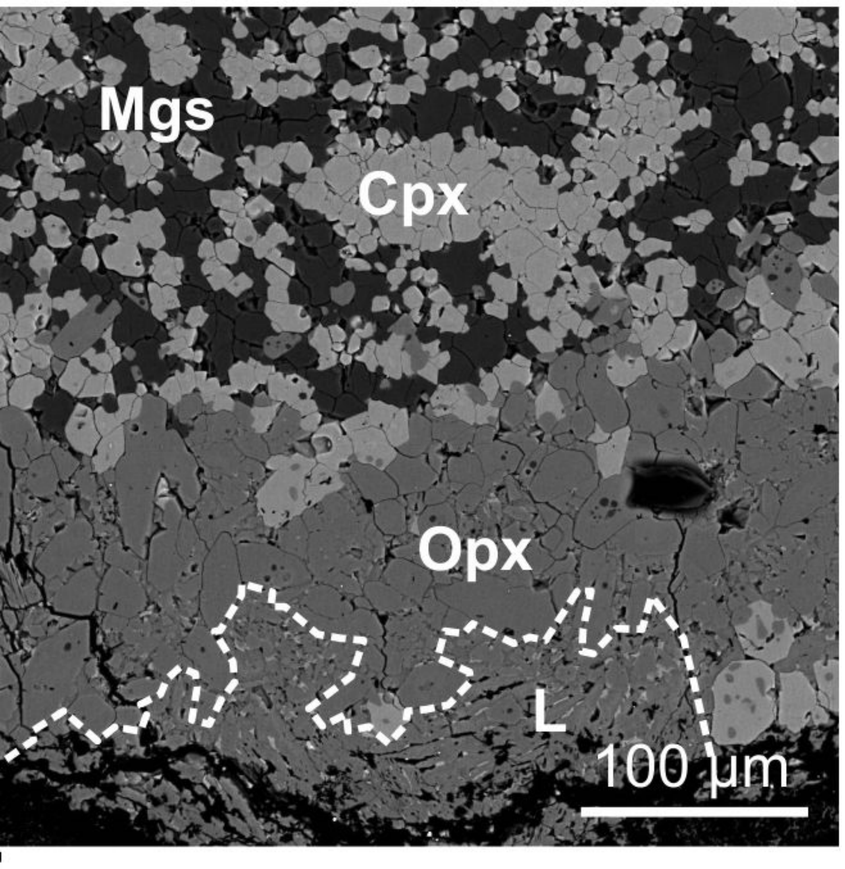

e. D012, 1500 °C, 16 h.

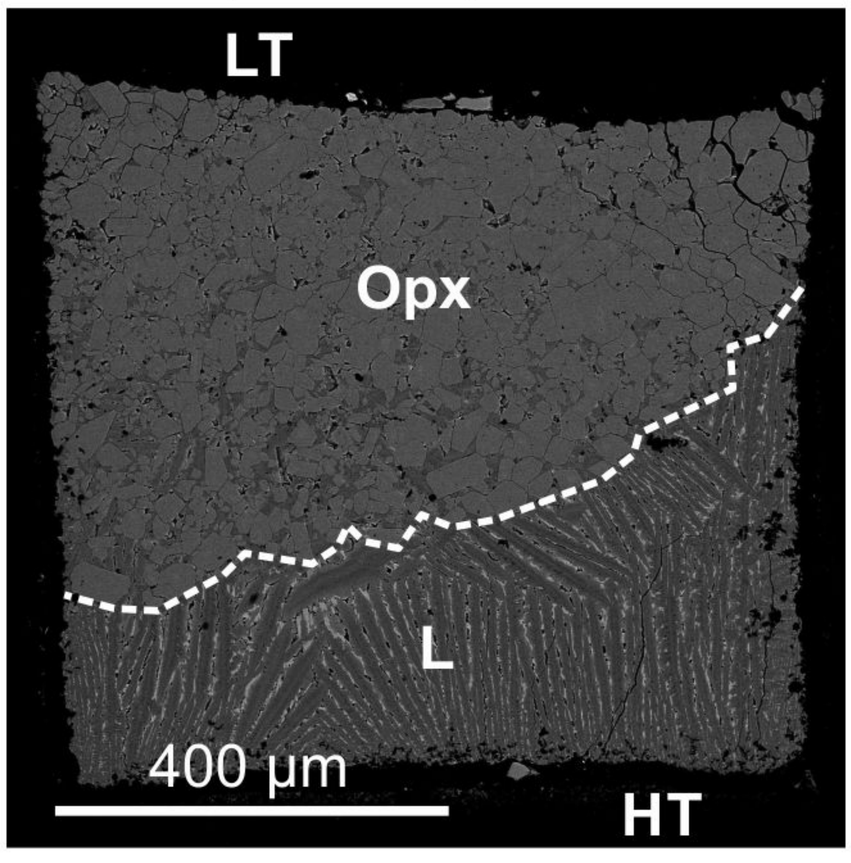

f. D036, 1550 °C, 8 h.

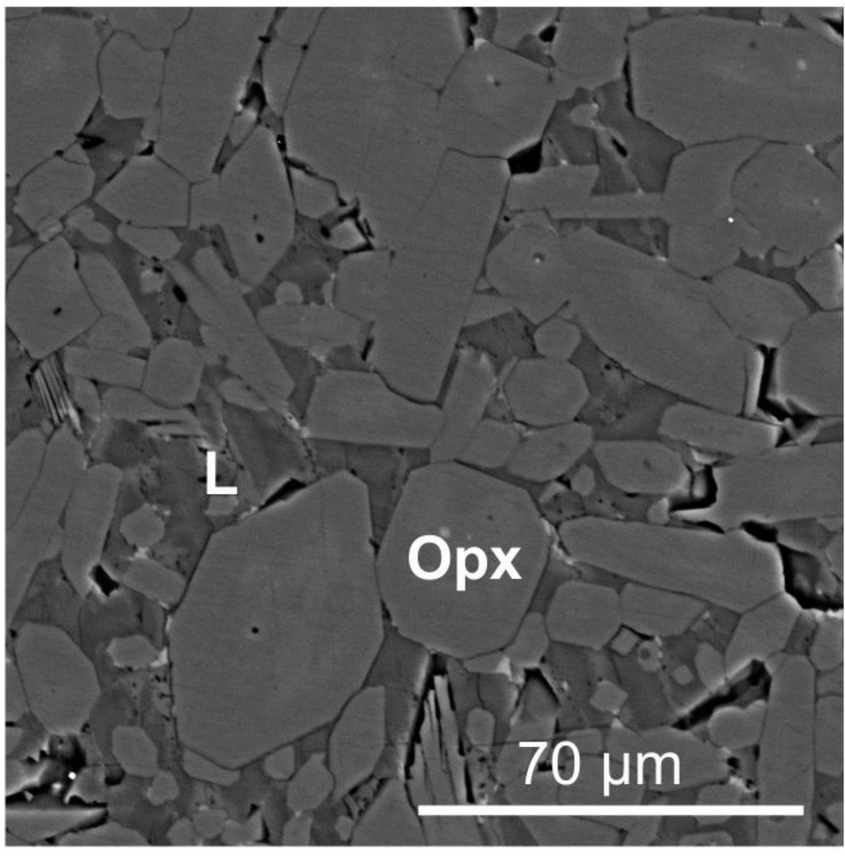

g. D029, 1750 °C, 1 h.

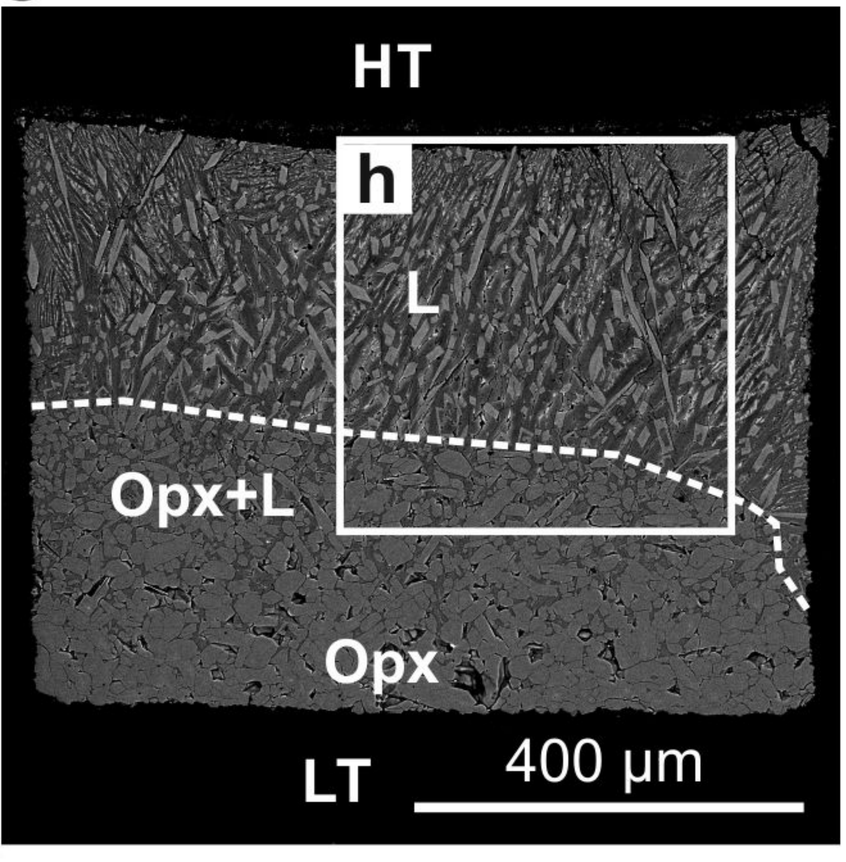

h. D029, 1750 °C, 1 h.

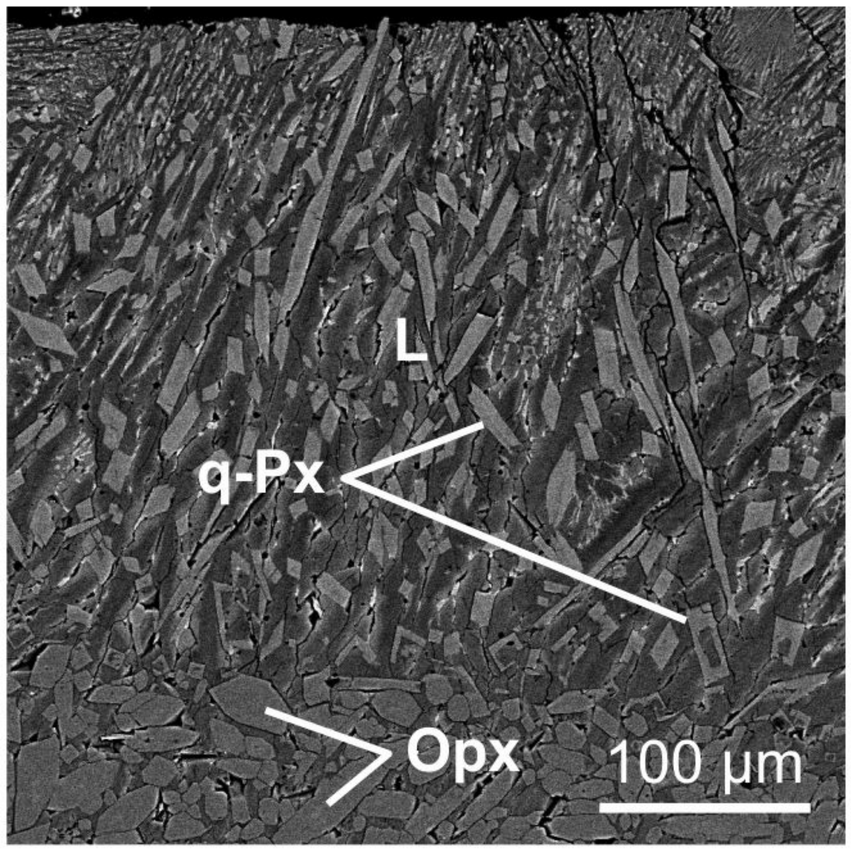

i. D039, 1800 °C, 0.5 h.

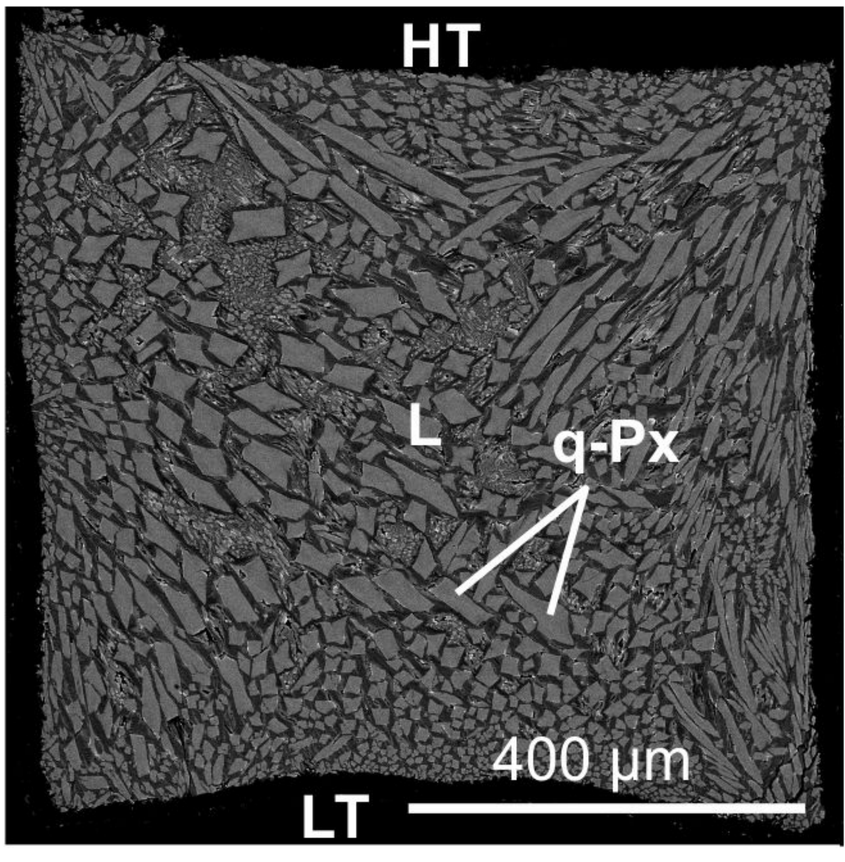

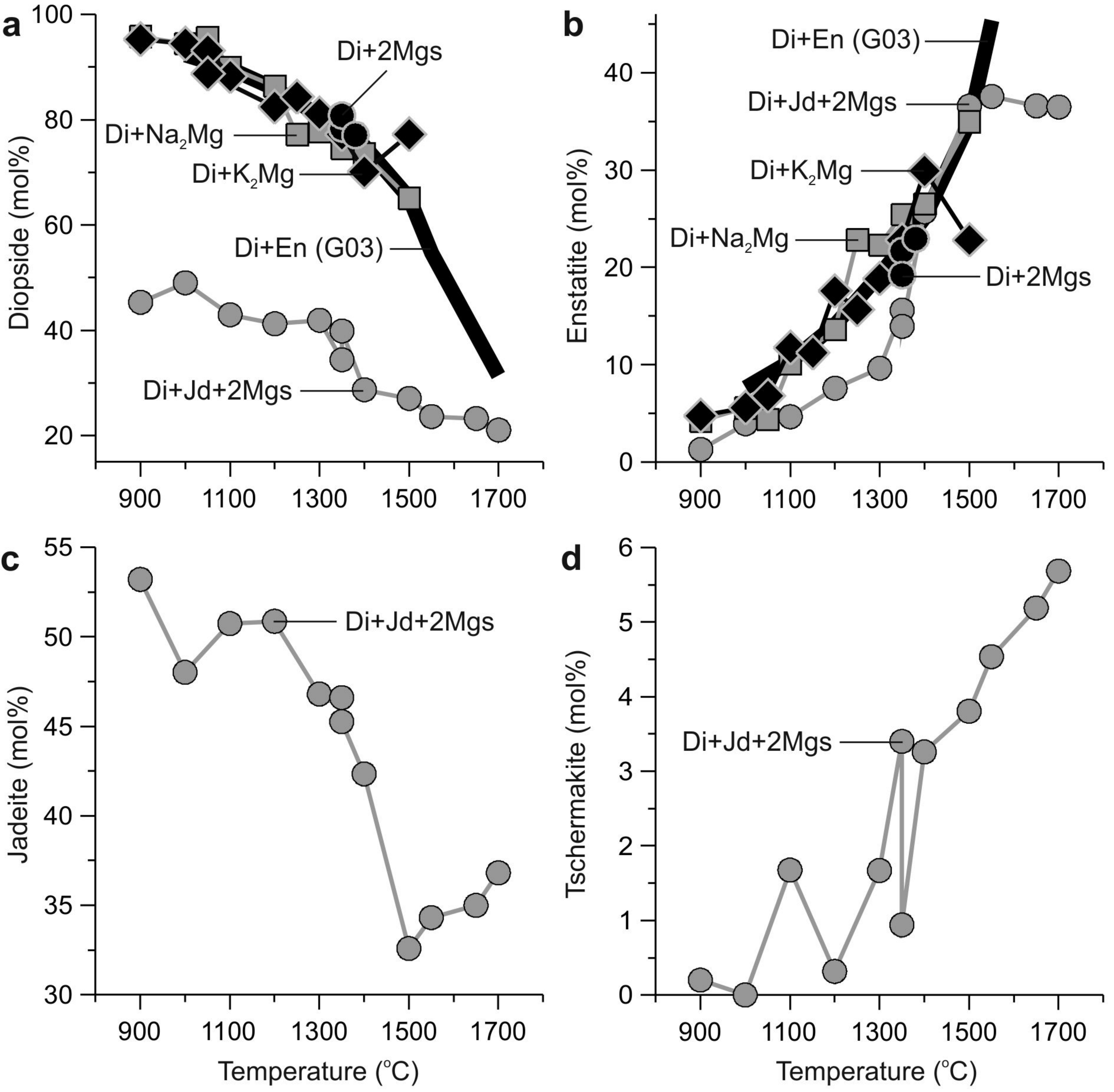
a
Diopside (mol%)
Di+2Mgs
Di+Na2Mg
Di+K2Mg
Di+En (G03)
Di+Jd+2Mgs
b
Enstatite (mol%)
Di+En (G03)
Di+Jd+2Mgs
Di+K2Mg
Di+Na2Mg
Di+2Mgs
c
Jadeite (mol%)
Di+Jd+2Mgs
d
Tschermakite (mol%)
Di+Jd+2Mgs
Temperature (°C)
Temperature (°C)

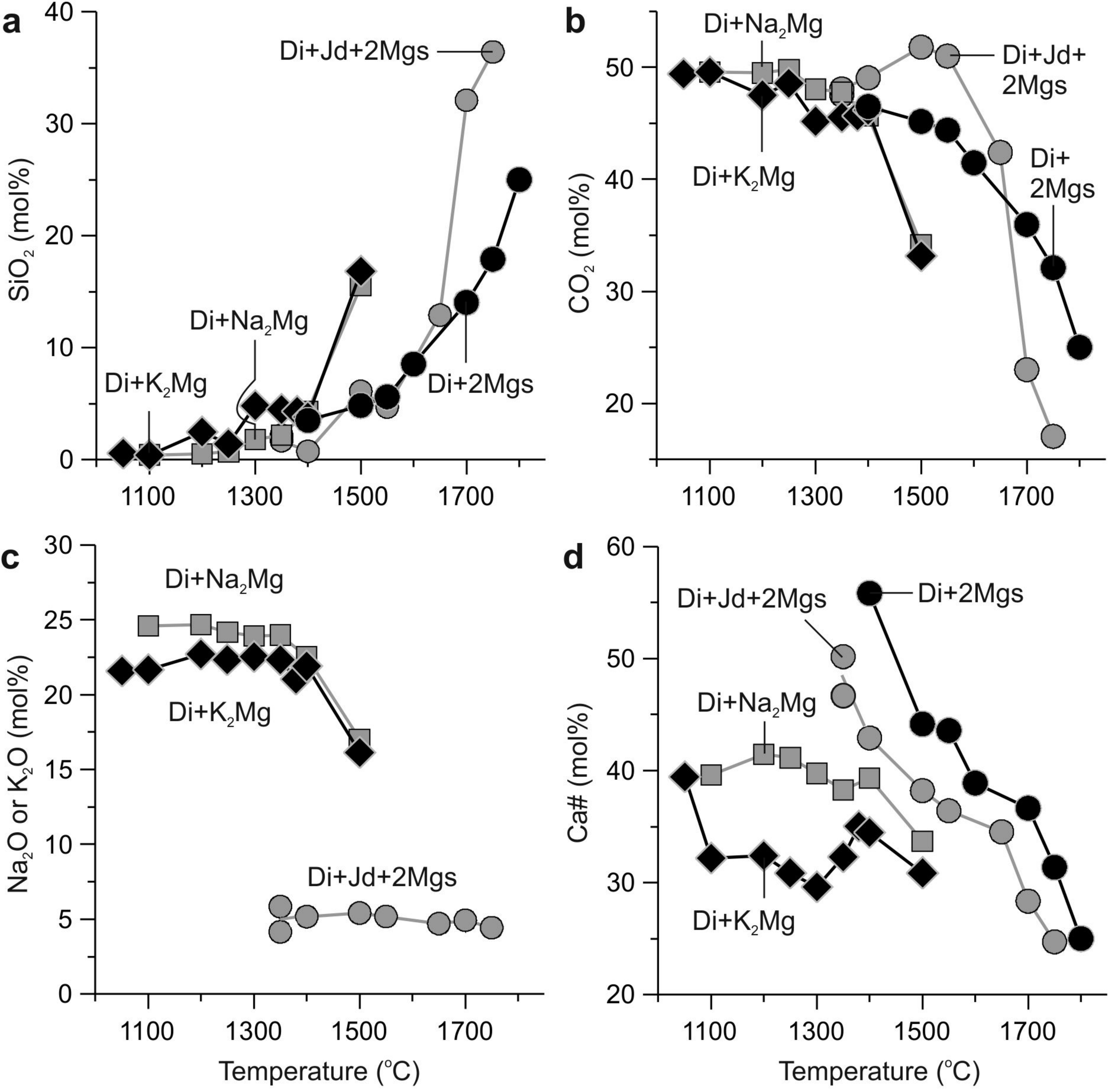
a
b
c
d
SiO2 (mol%)
CO2 (mol%)
Na2O or K2O (mol%)
Ca# (mol%)
Temperature (°C)
Di+Jd+2Mgs
Di+Na2Mg
Di+K2Mg
Di+2Mgs
Di+Jd+
2Mgs
Di+
2Mgs
0
10
20
30
40
50
60
5
15
25
1100
1300
1500
1700

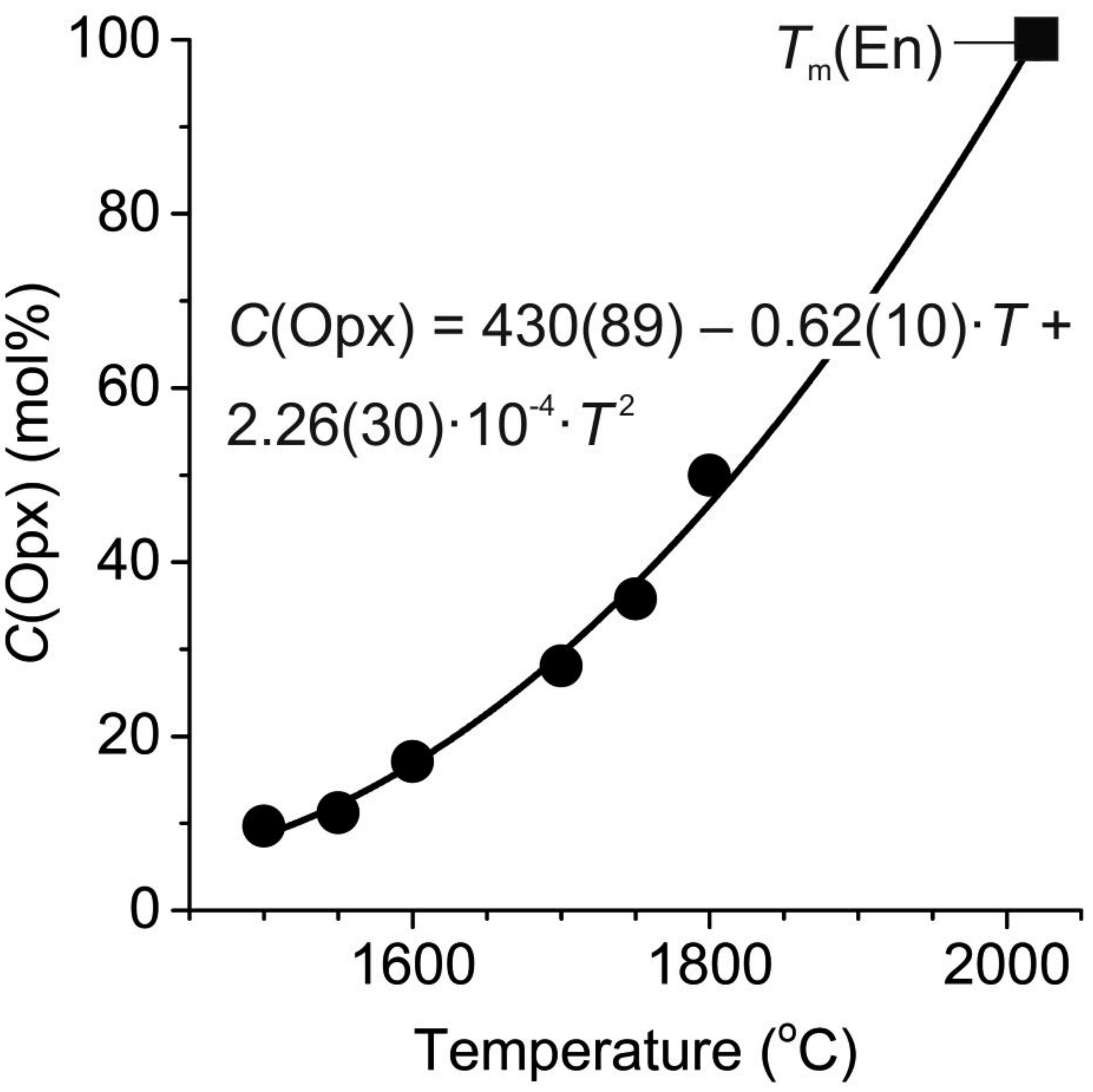
100
80
60
40
20
0
C(Opx) (mol%)
T_m(En)
$C(\mathrm{Opx}) = 430(89) - 0.62(10)\cdot T + 2.26(30)\cdot 10^{-4}\cdot T^2$
1600
1800
2000
Temperature (°C)

a. D011, 900 ℃, 71 h.

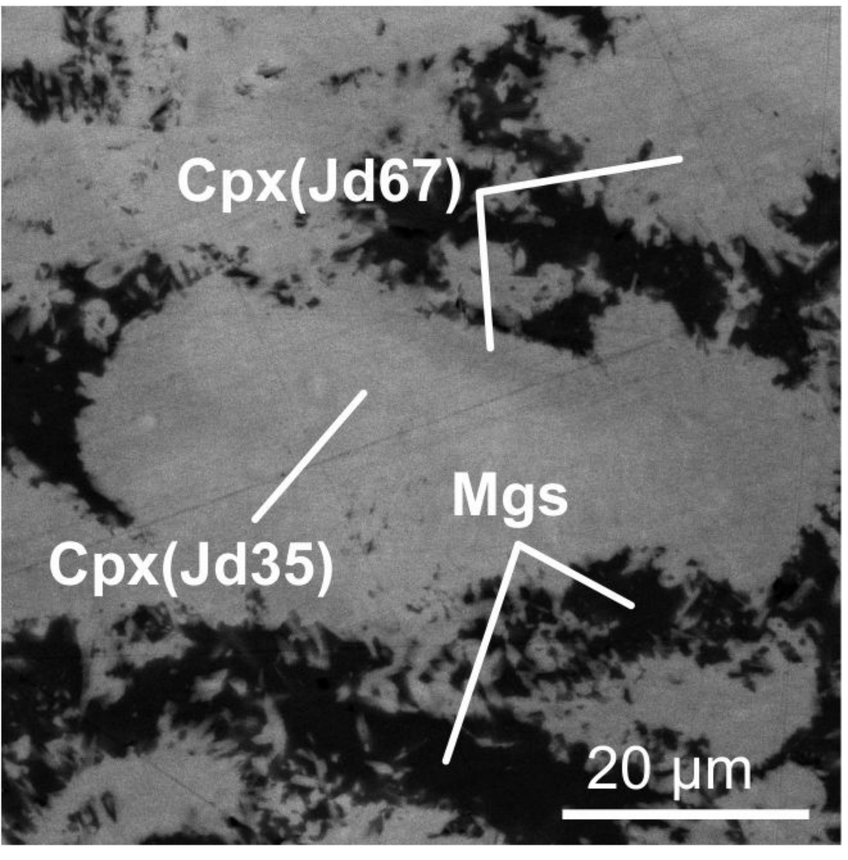

b. D016, 1000 ℃, 96 h.

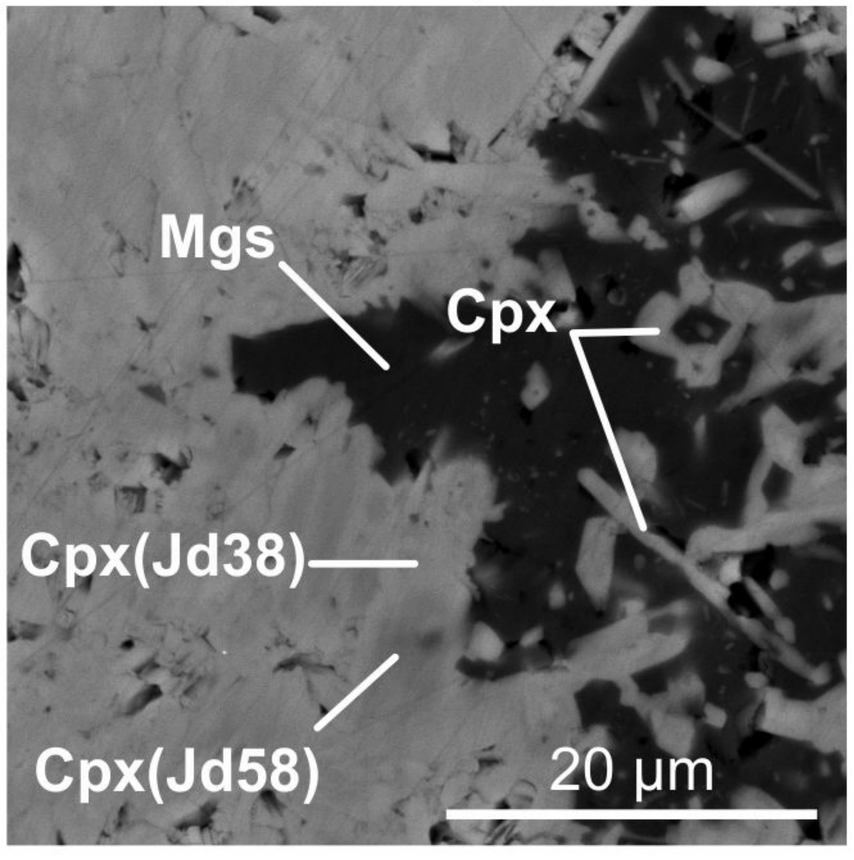

c. D015, 1100 ℃, 48 h.

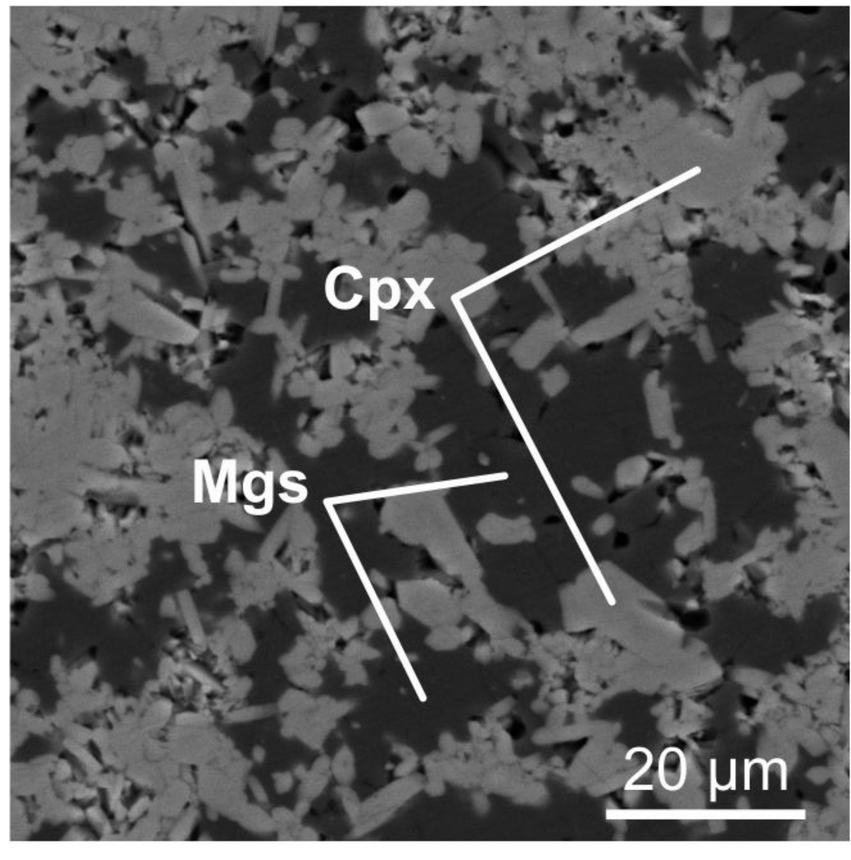

d. D014, 1200 ℃, 25 h.

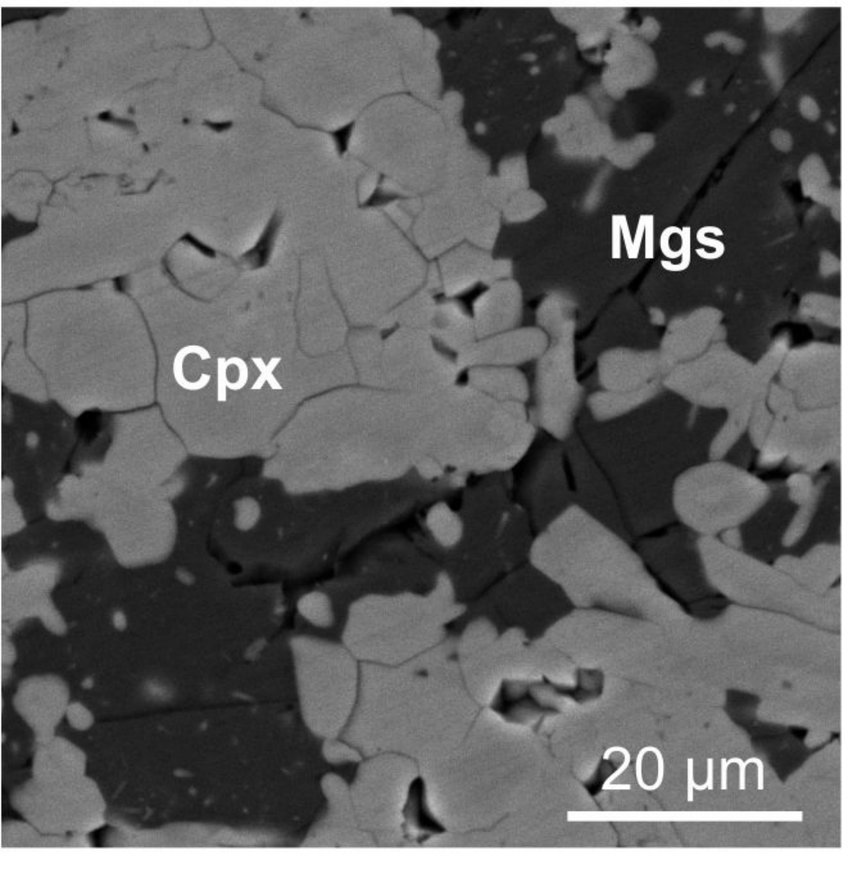

e. D013, 1300 ℃, 49 h.

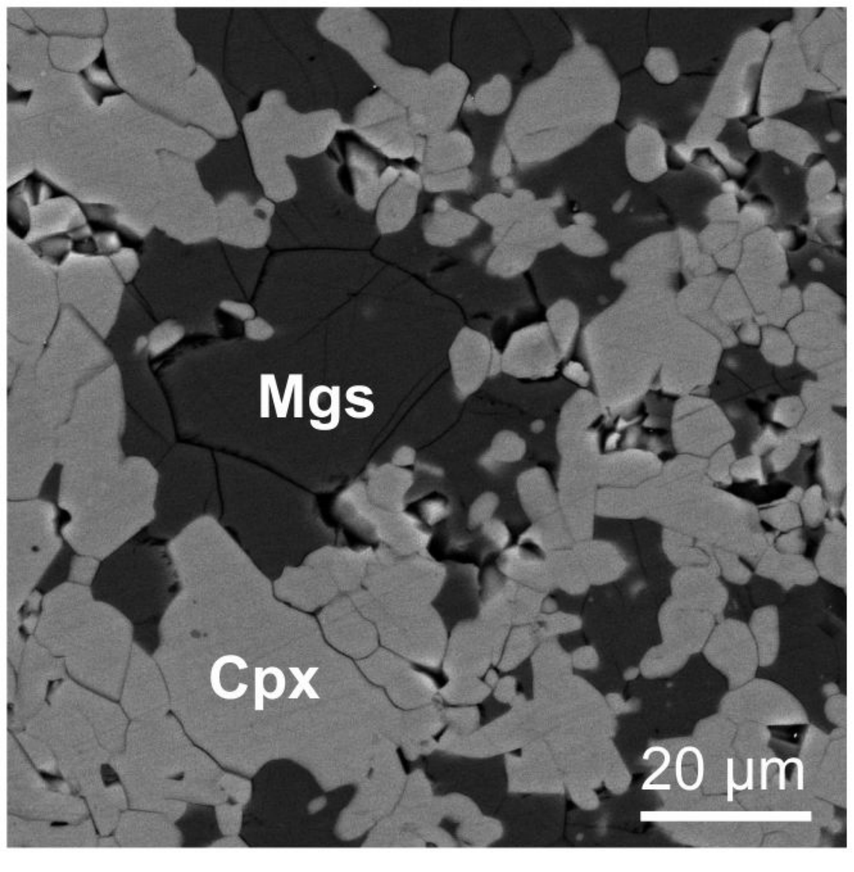

f. D027, 1350 ℃, 24 h.

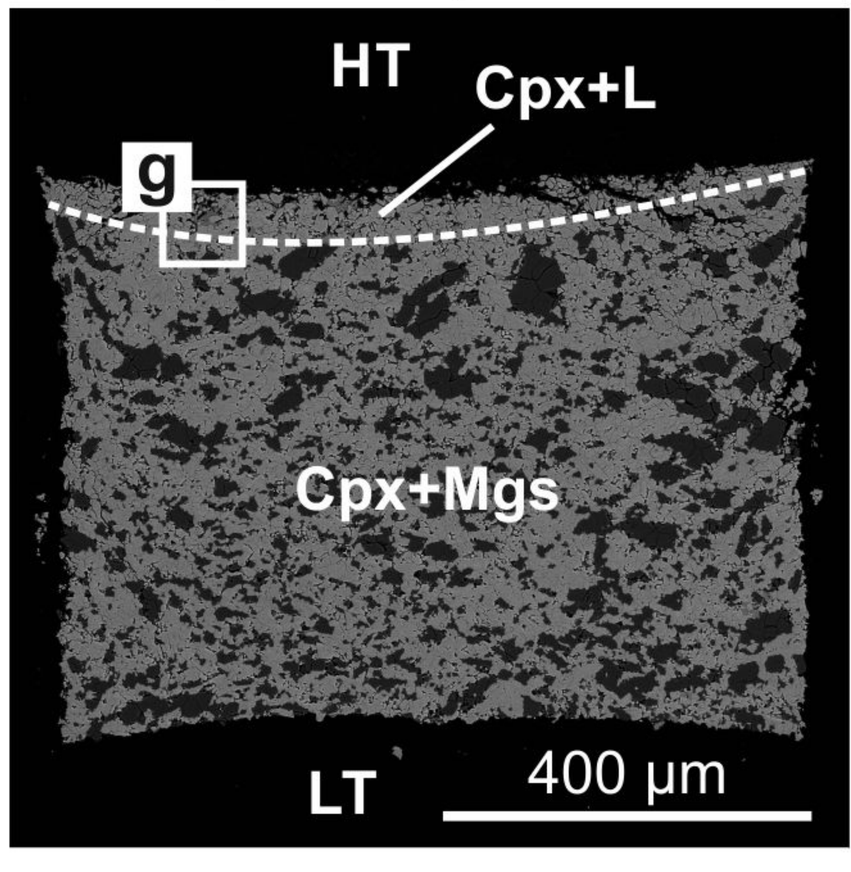

g. D027, 1350 ℃, 24 h.

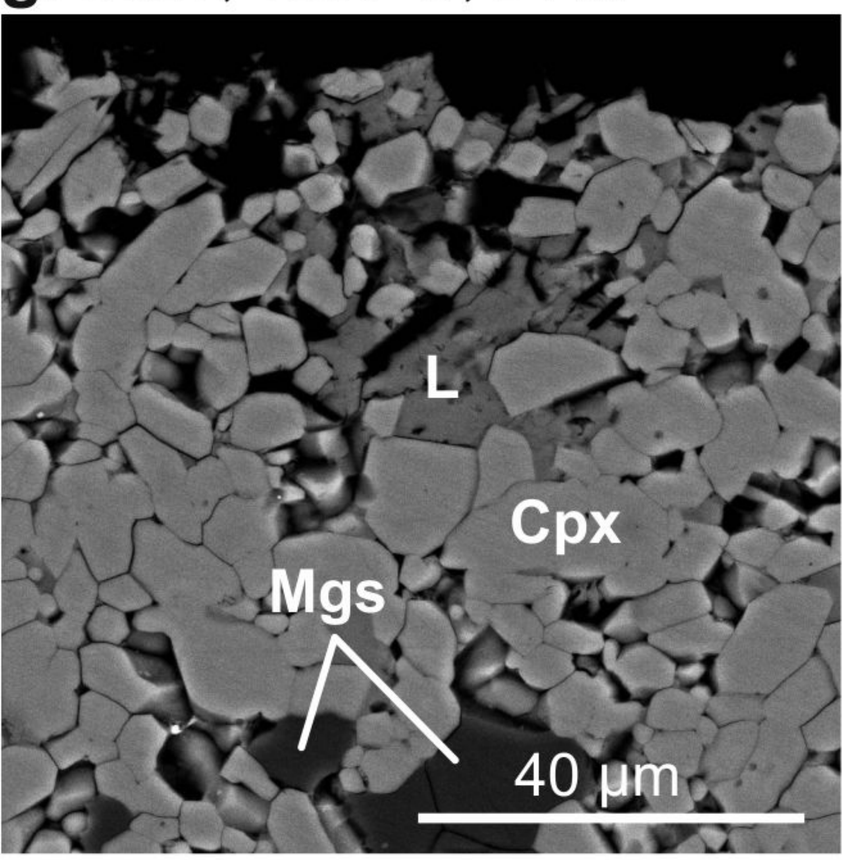

h. D017, 1400 ℃, 8 h.

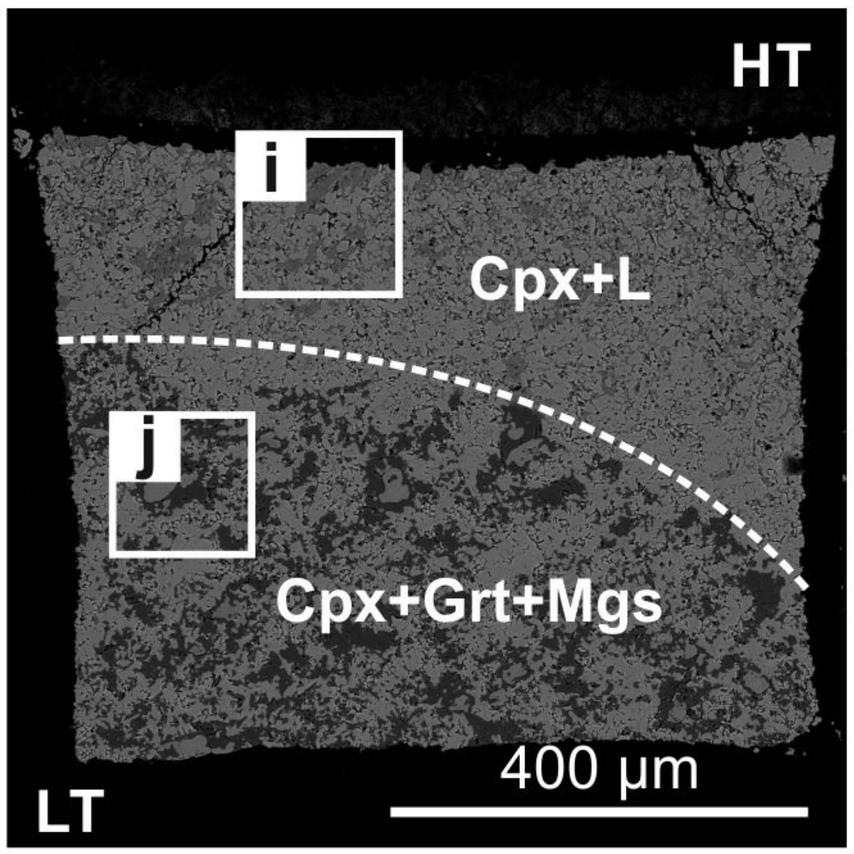

i. D017, 1400 ℃, 8 h.

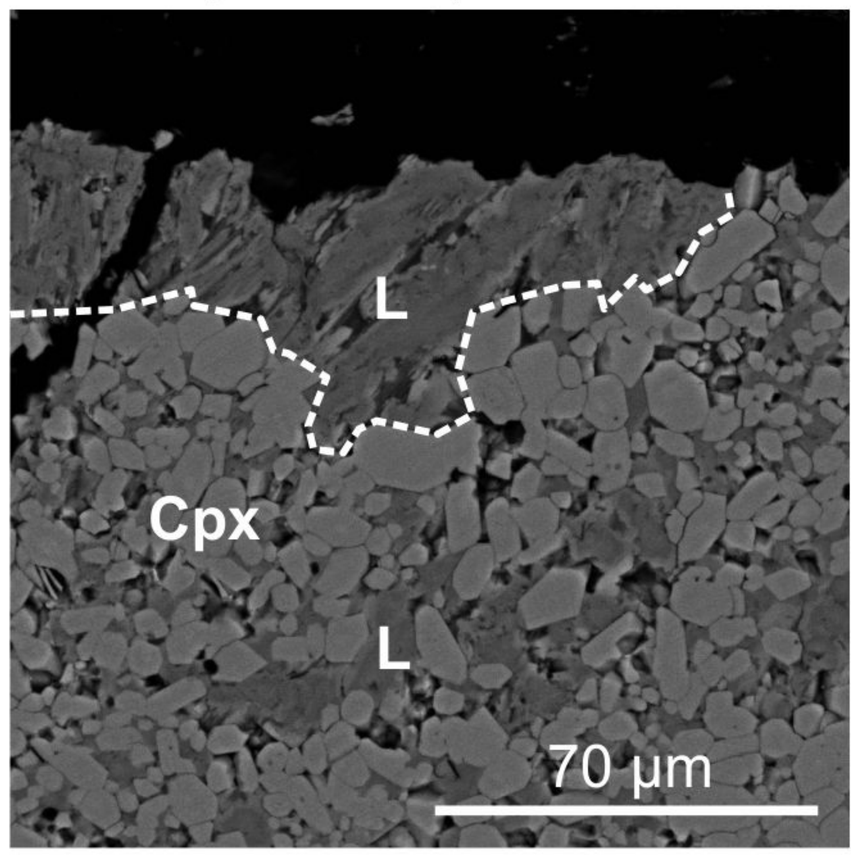

j. D017, 1400 °C, 8 h.

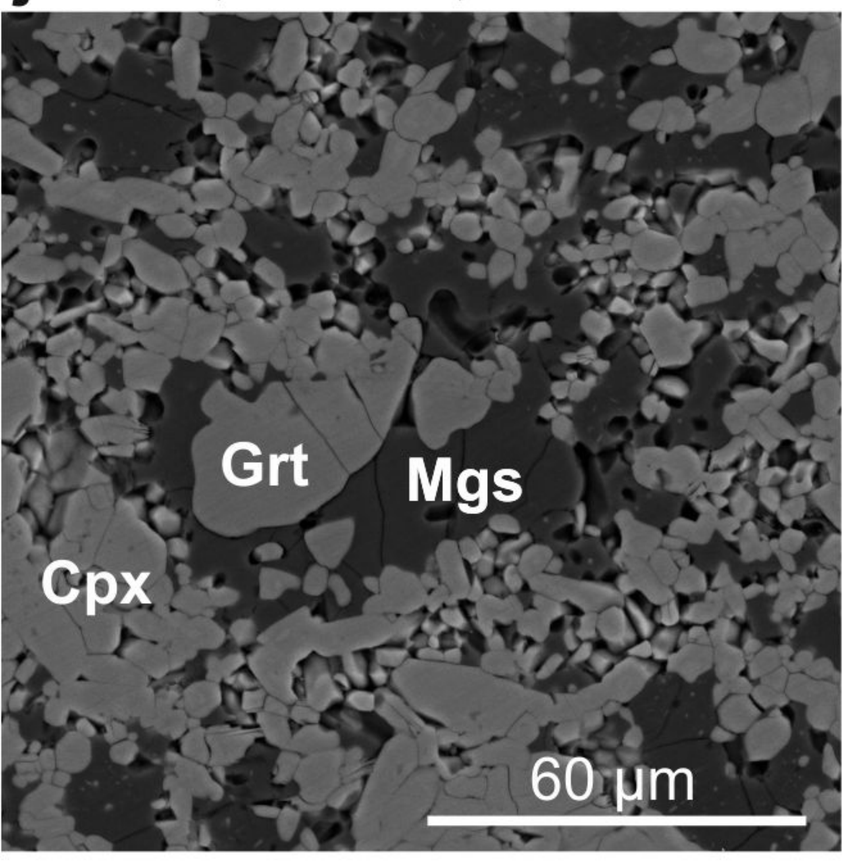

k. D012, 1500 °C, 16 h.

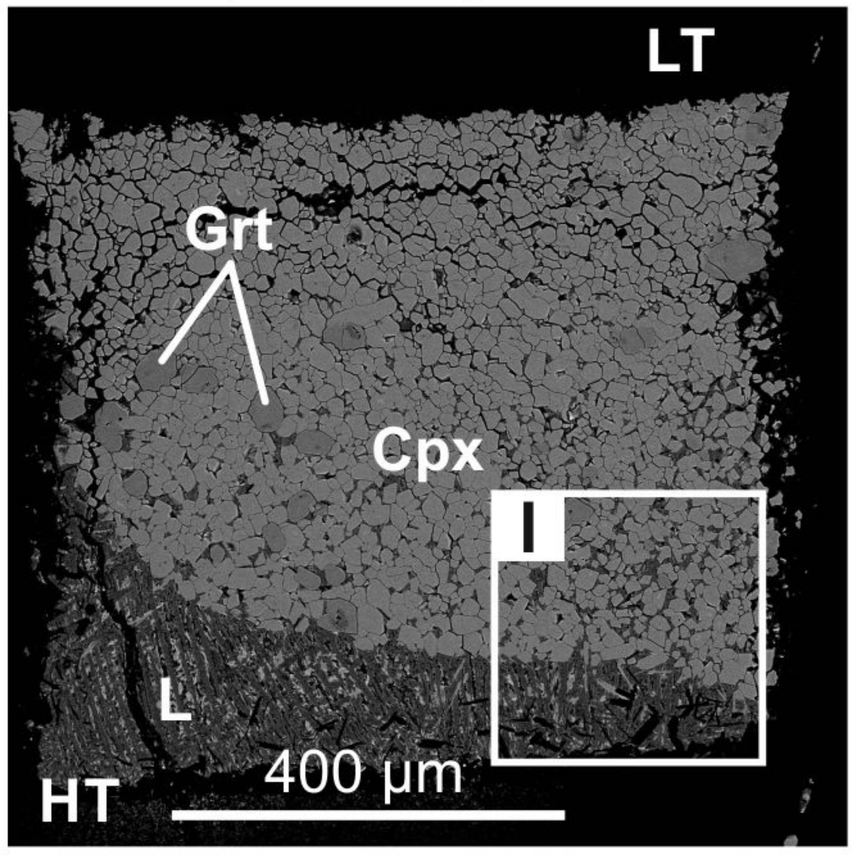

l. D012, 1500 °C, 16 h.

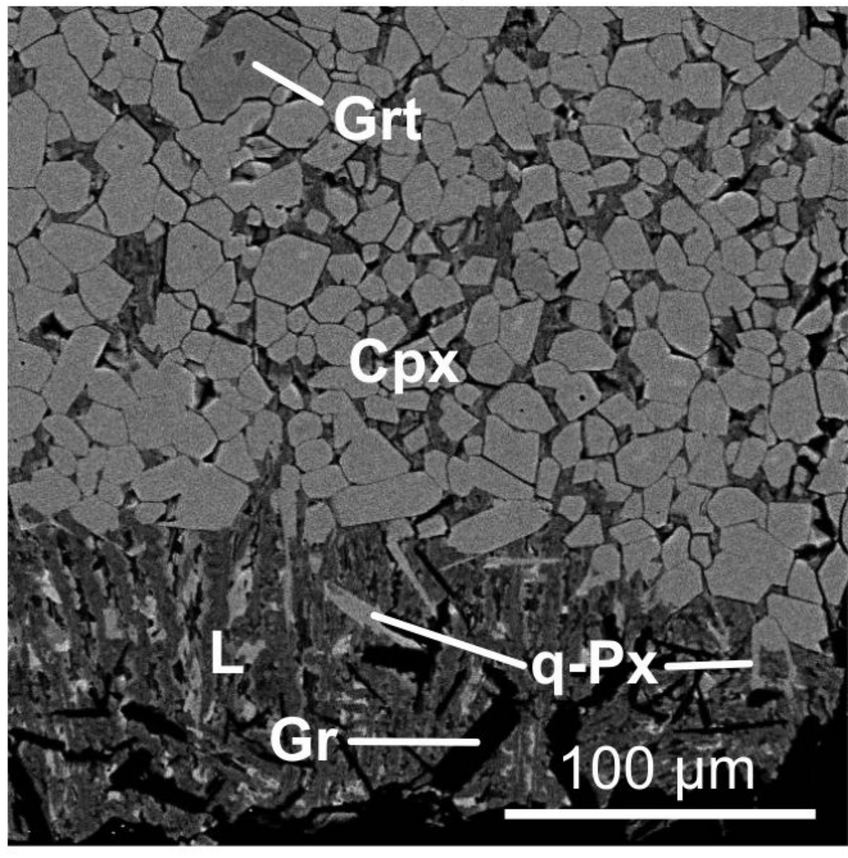

m. D036, 1550 °C, 8 h.

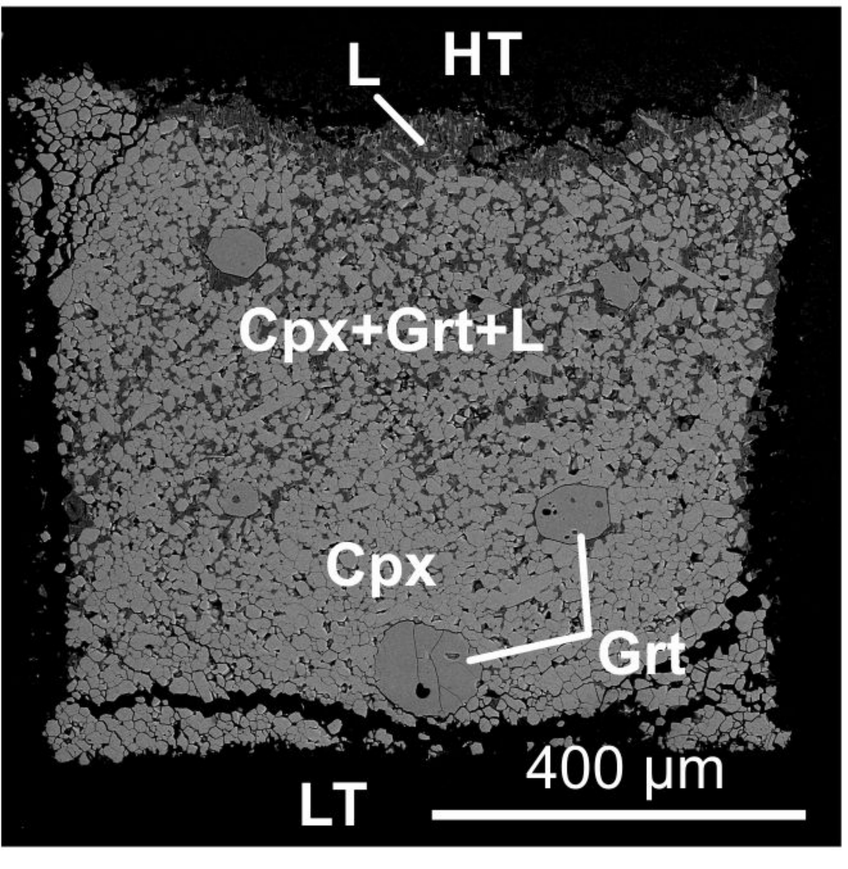

n. D033, 1650 °C, 3 h.

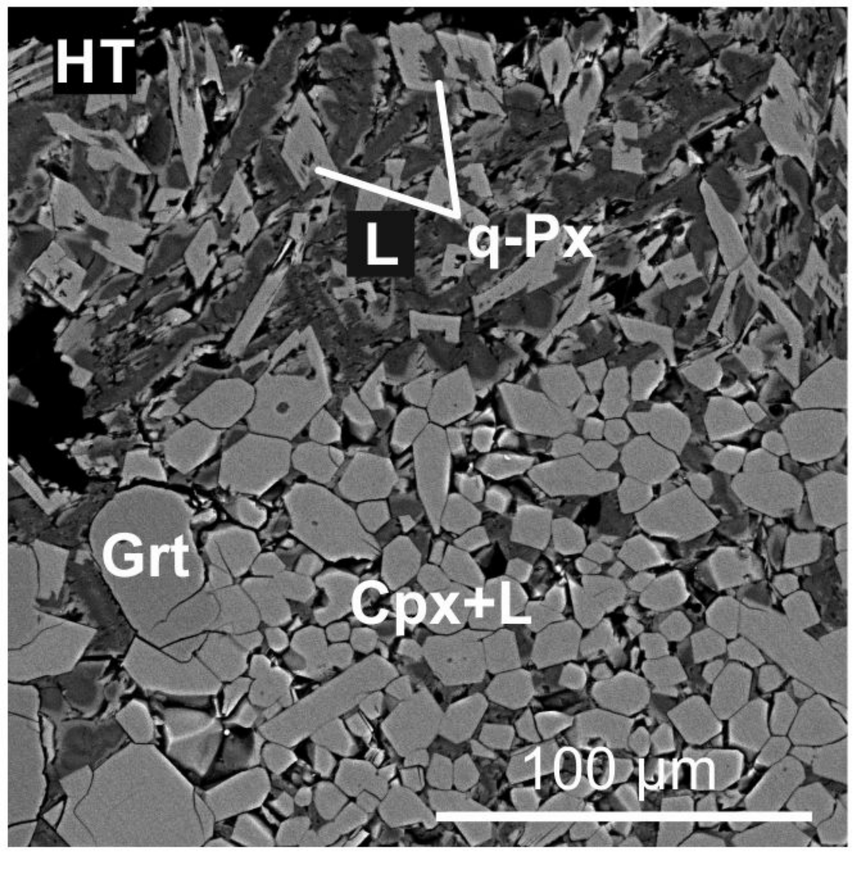

o. D025, 1700 °C, 2 h.

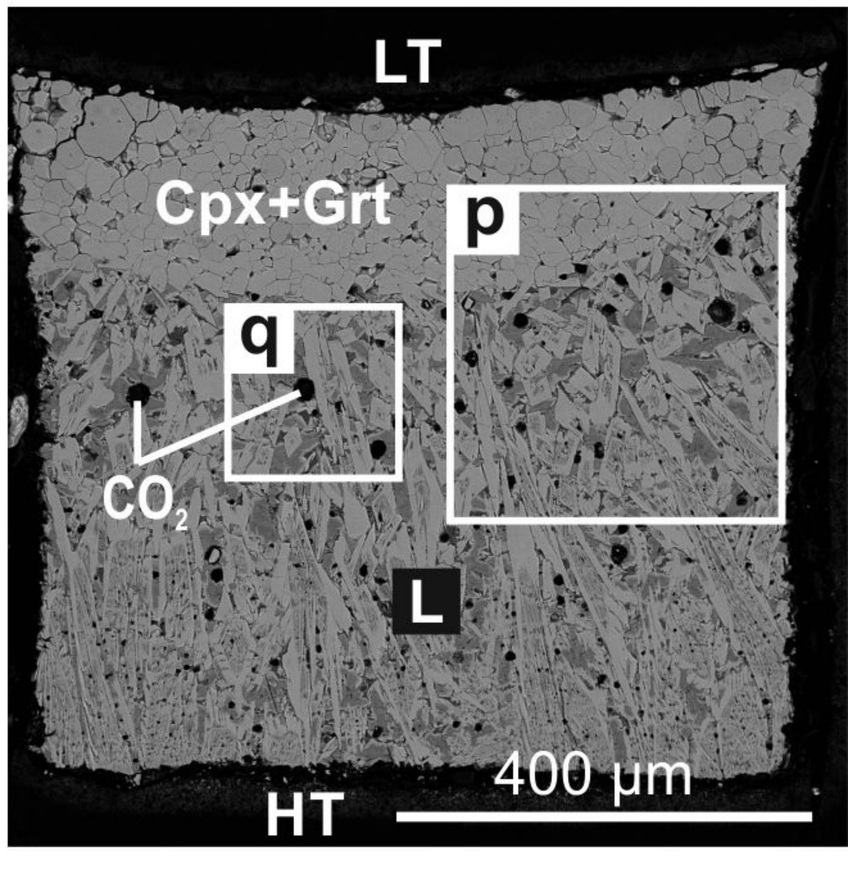

p. D025, 1700 °C, 2 h.

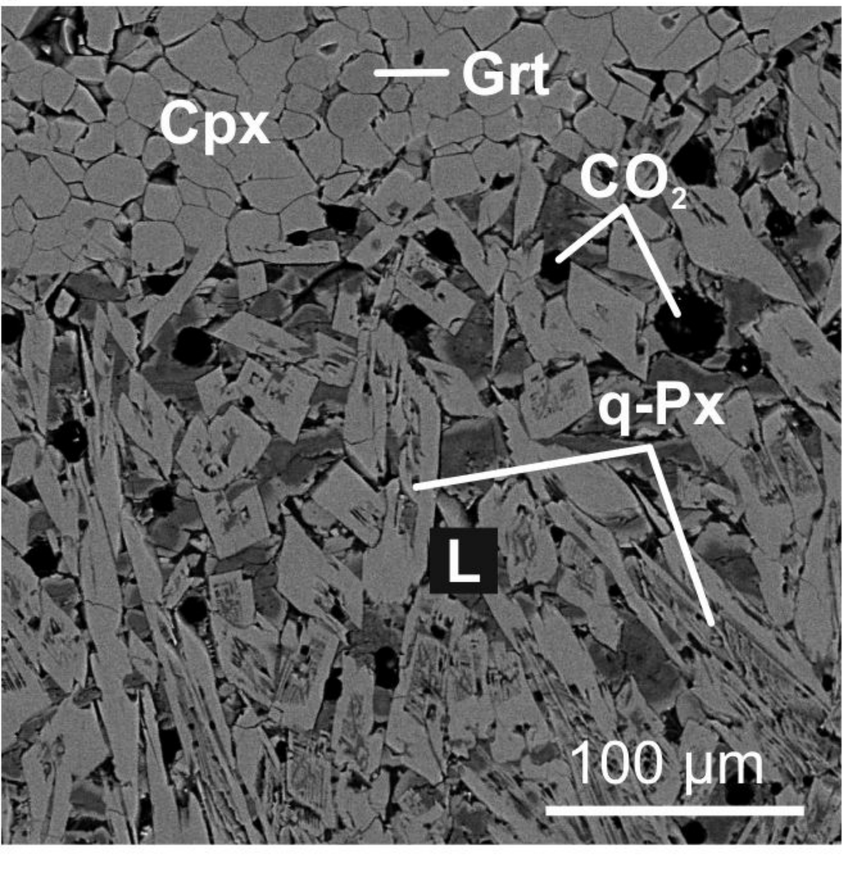

q. D025, 1700 °C, 2 h.

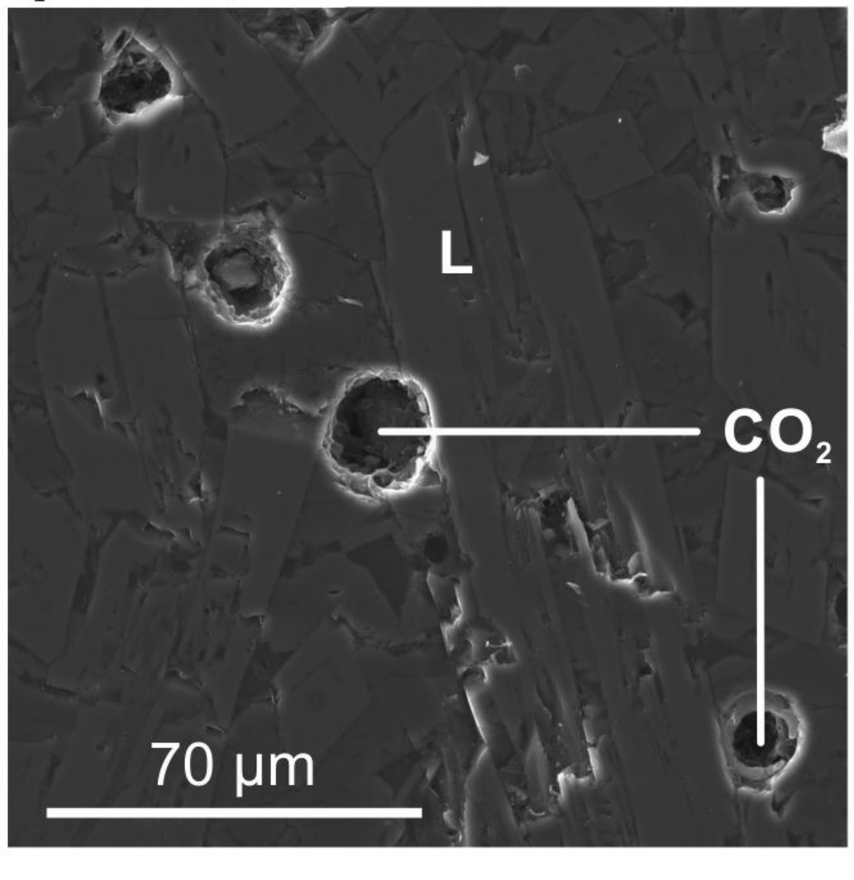

r. D029, 1750 °C, 1 h.

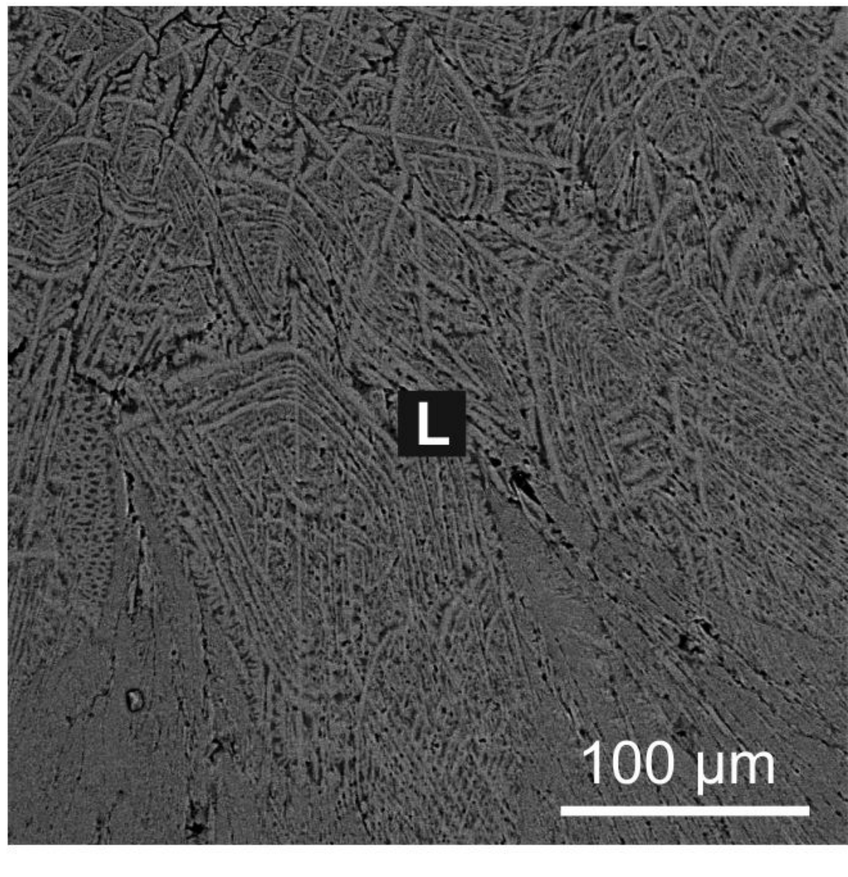

Magnesite:

- Ca-Mg-CO_3;

- Di+2Mgs;

- Di+Jd+2Mgs;

Ca# (mol%)

18
16
14
12
10
8
6
4
2

900 1000 1100 1200 1300 1400

Temperature (°C)

Na_2Mg carbonate:

- Na_2-Ca-Mg-CO_3;

- Di+Na_2Mg;

K_2Mg carbonate:

- K_2-Ca-Mg-CO_3;

- Di+K_2Mg.

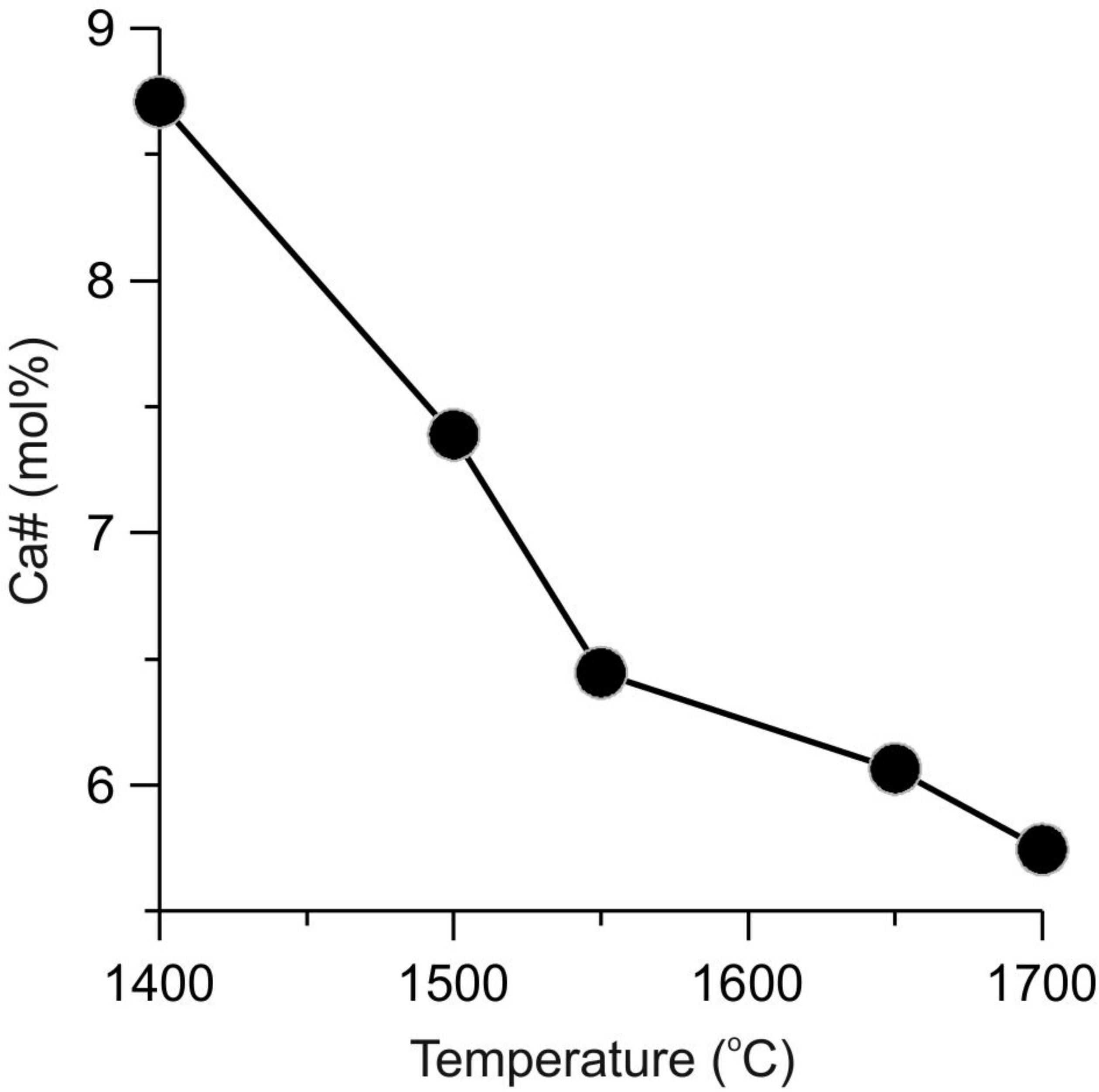
9
8
7
6
Ca# (mol%)
1400
1500
1600
1700
Temperature (°C)

a, b. 900 °C.

a. D011, 71 h.

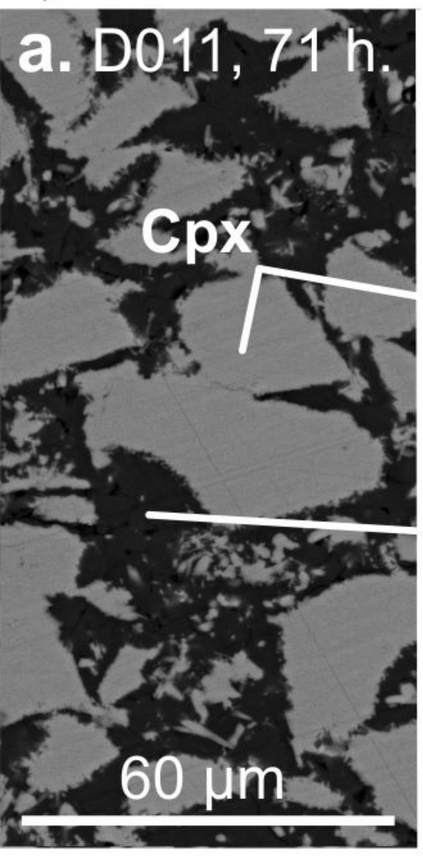

b. D070, 96 h.

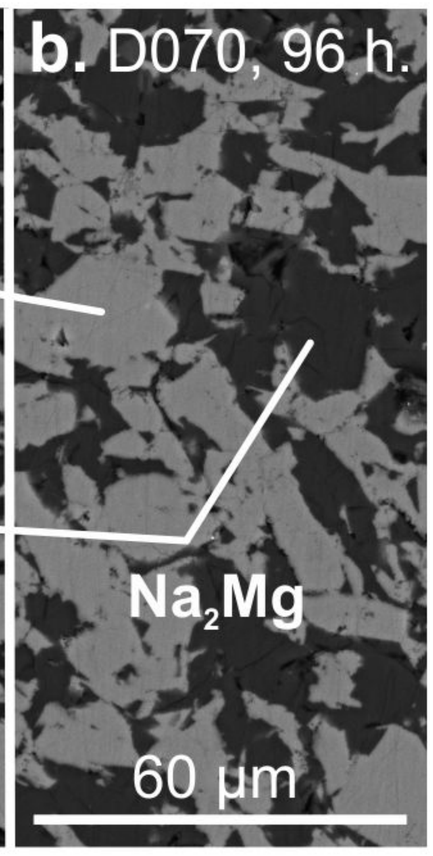

c. D026, 1050 °C, 96 h.

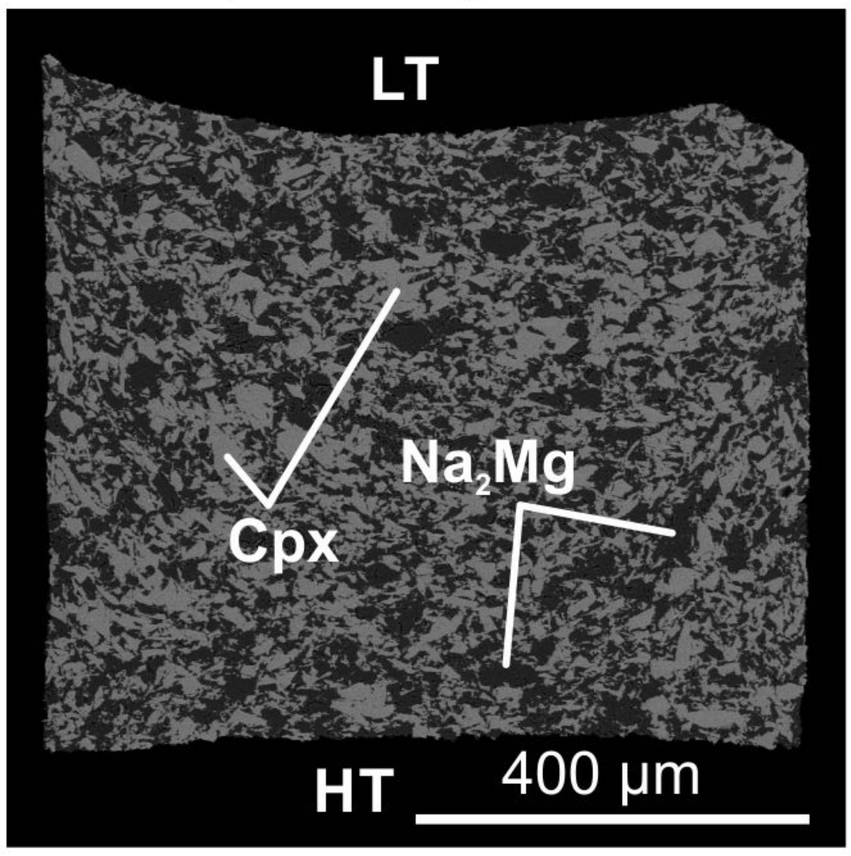

d. D015, 1100 °C, 48 h.

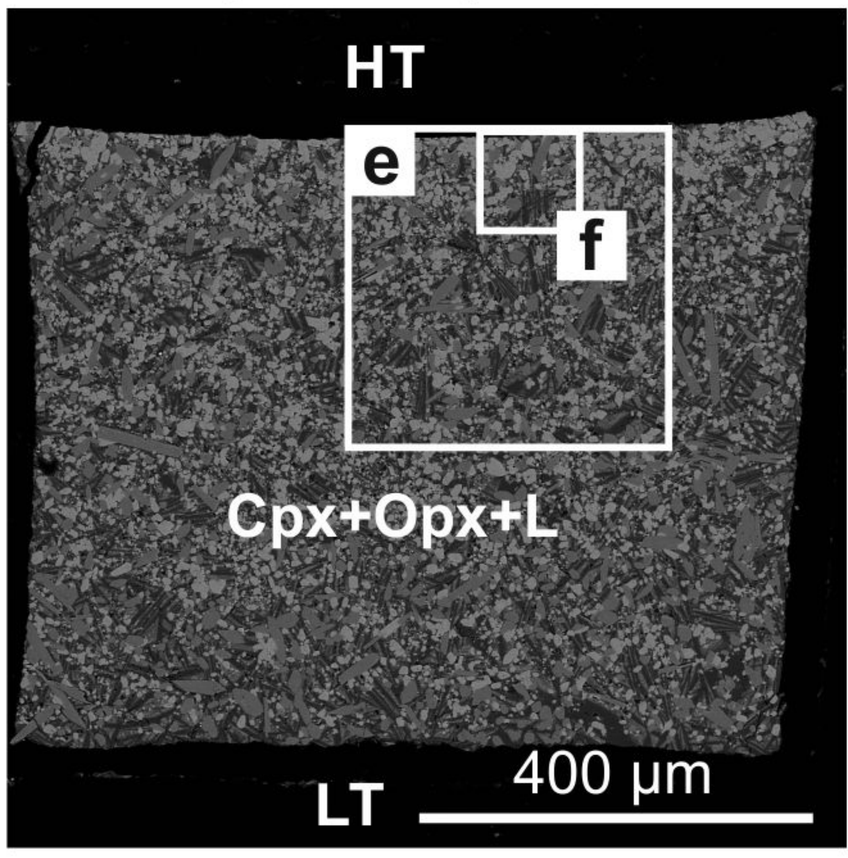

e. D015, 1100 °C, 48 h.

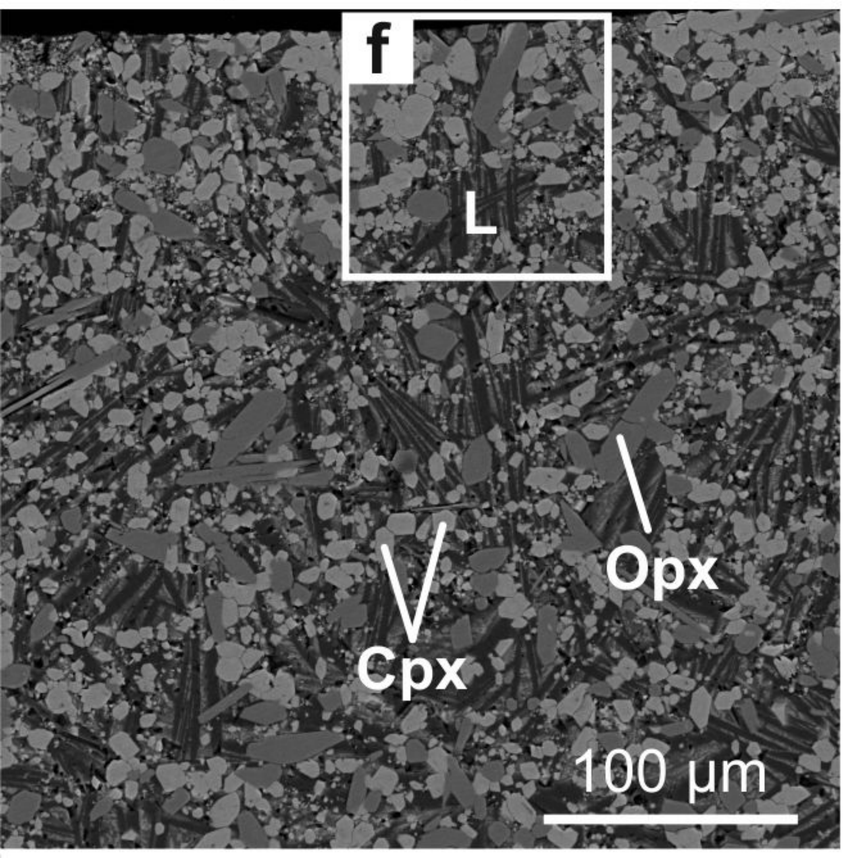

f. D015, 1100 °C, 48 h.

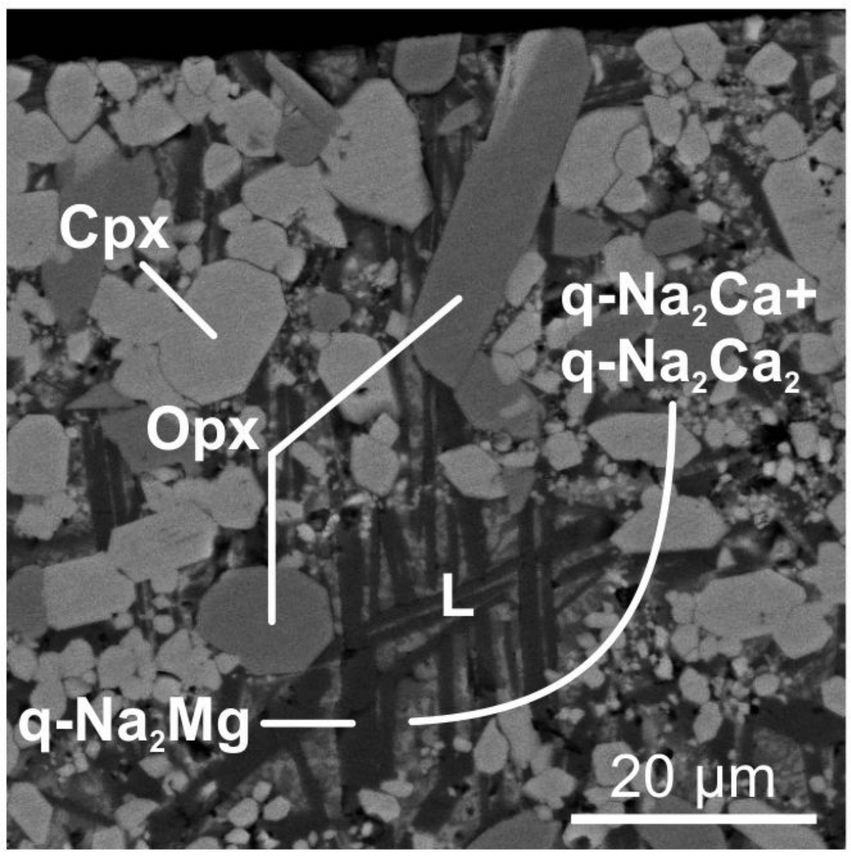

g. D014, 1200 °C, 25 h.

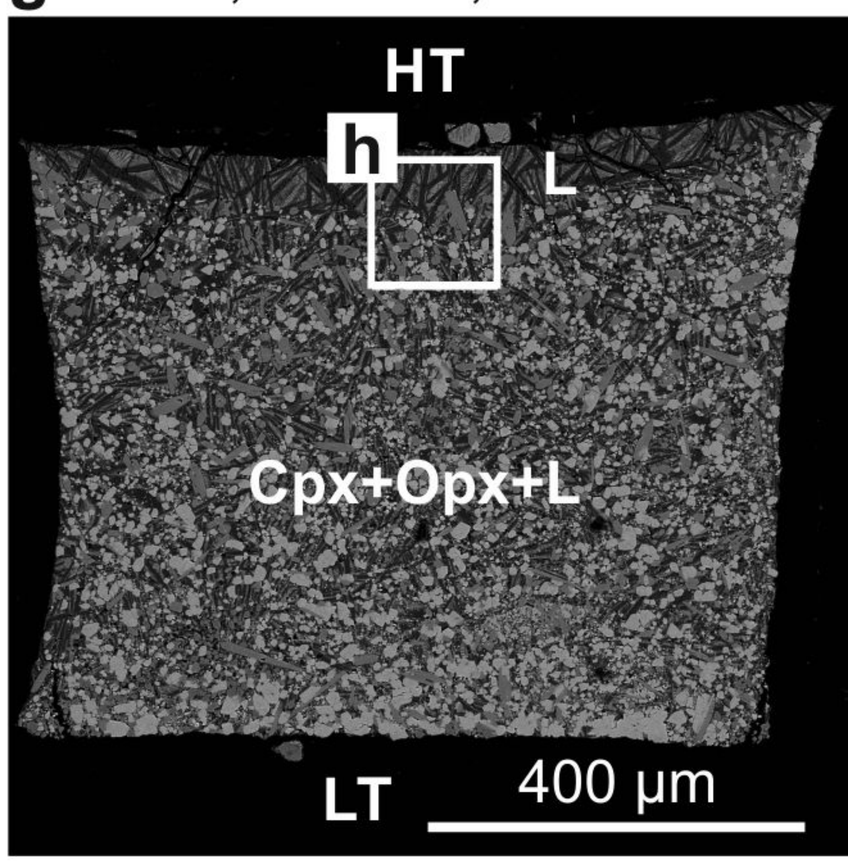

h. D014, 1200 °C, 25 h.

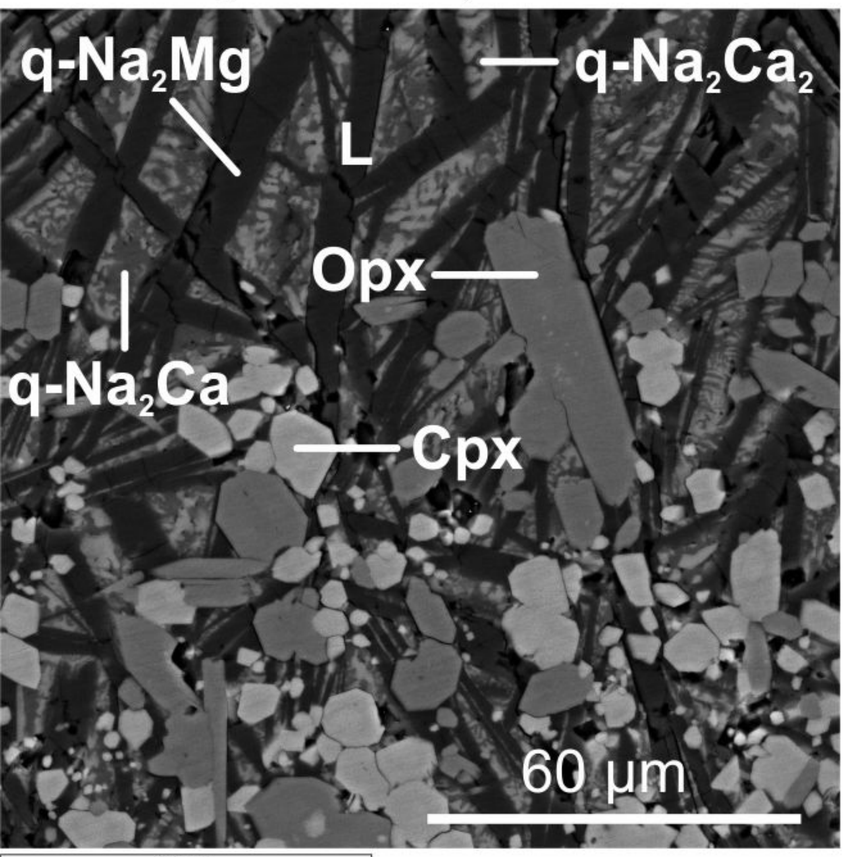

i. D027, 1350 °C, 24 h.

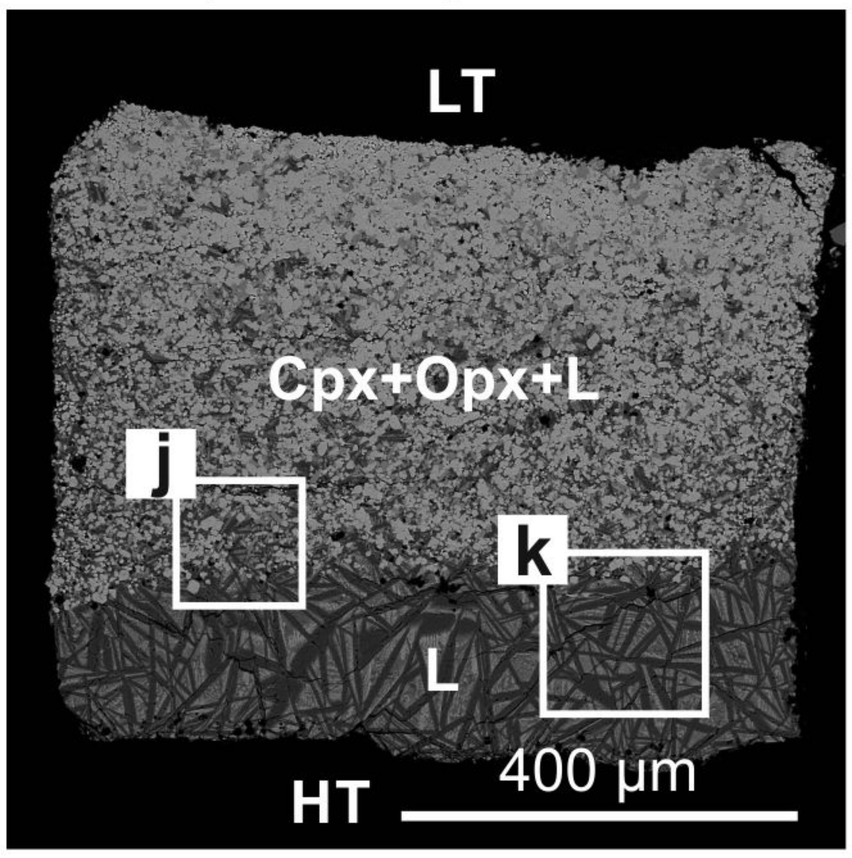

j. D027, 1350 °C, 24 h.

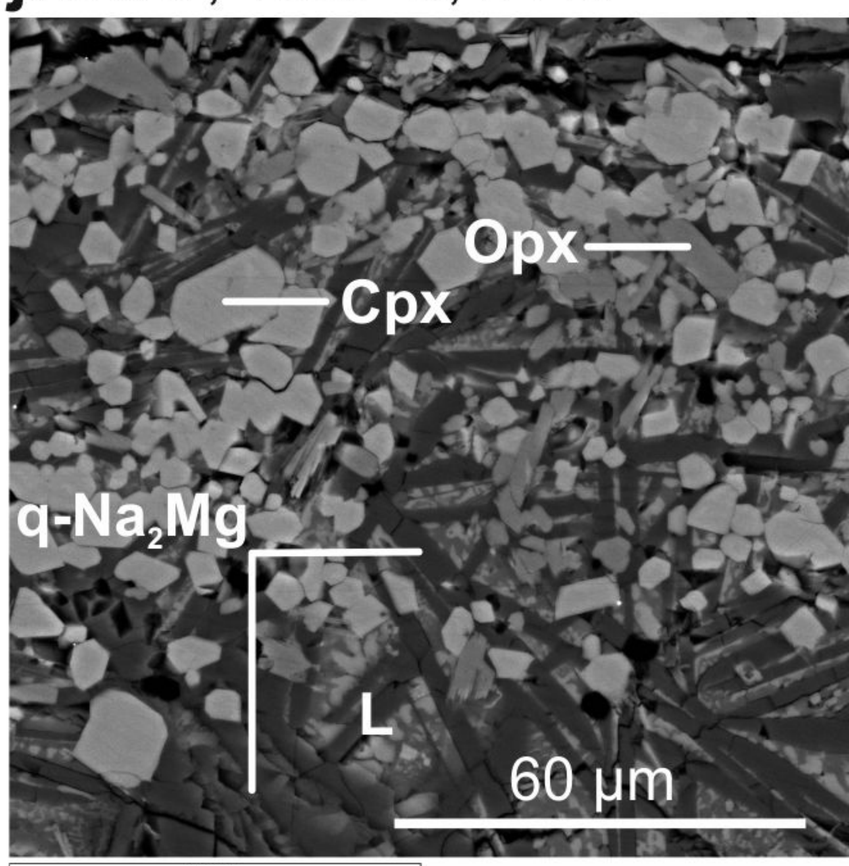

k. D027, 1350 °C, 24 h.

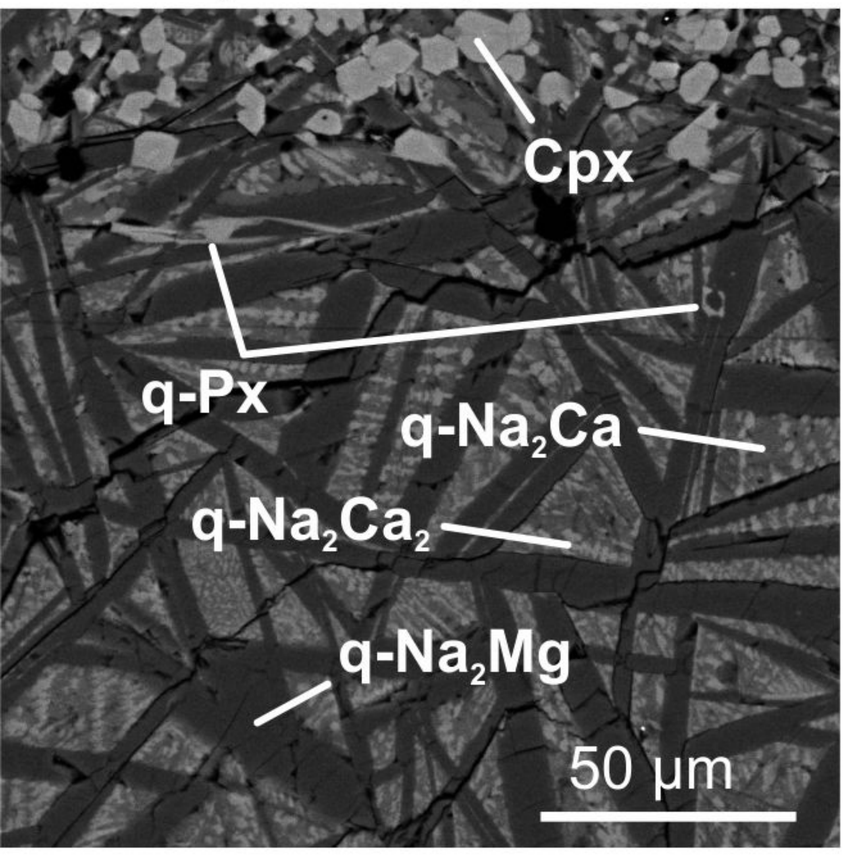

l. D012, 1500 °C, 16 h.

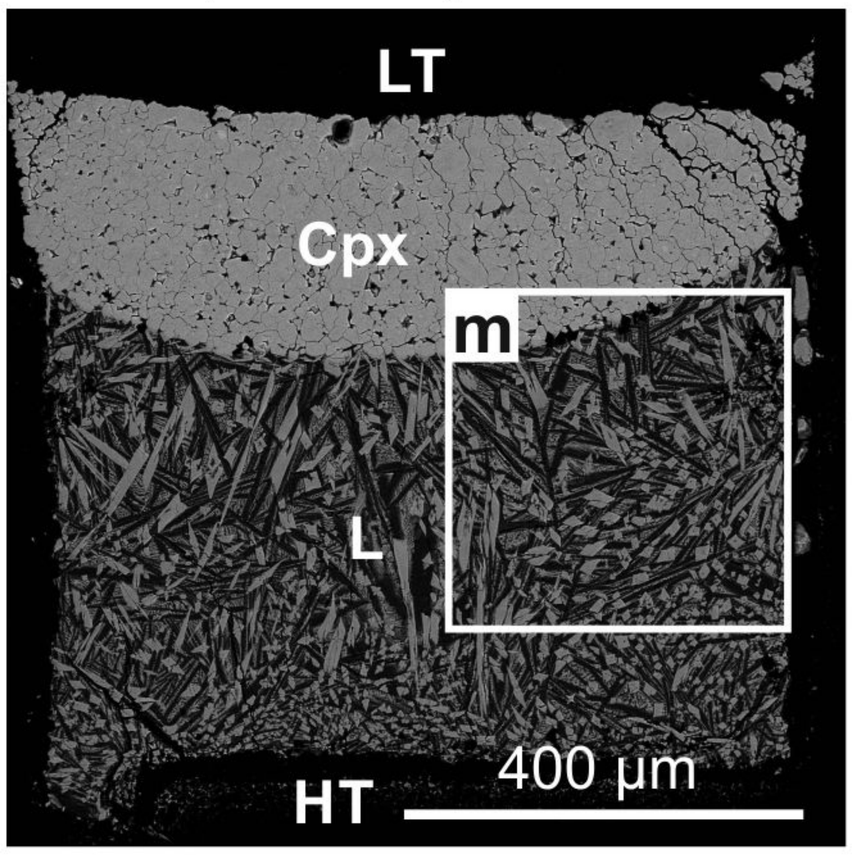

m. D012, 1500 °C, 16 h.

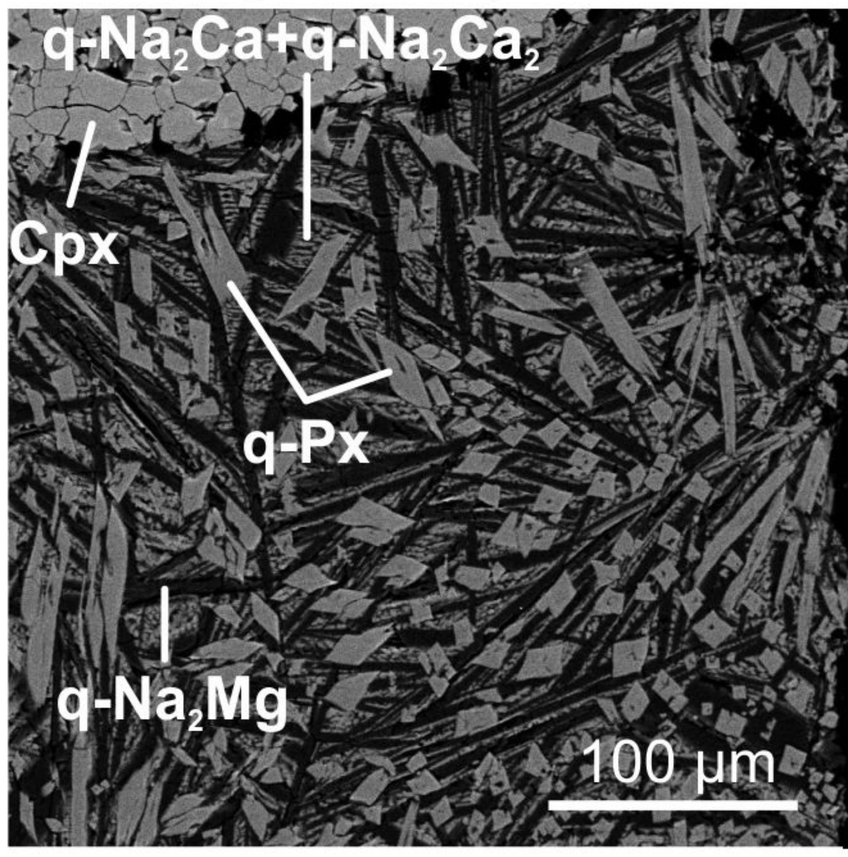

a. D070, 900 °C, 96 h.

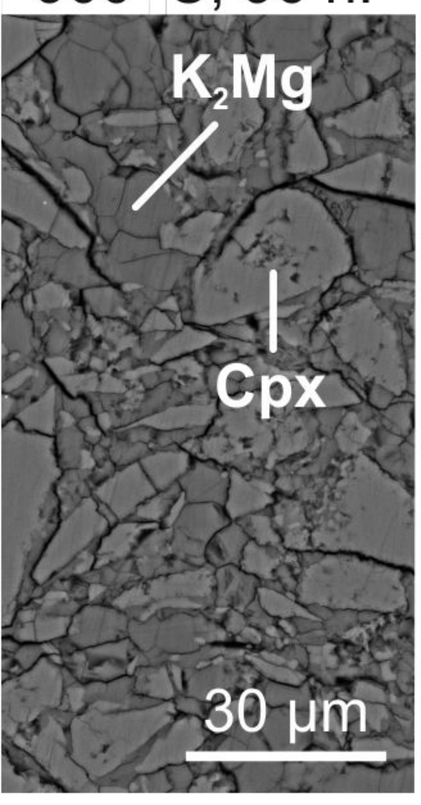

b. D073, 1000 °C, 96 h.

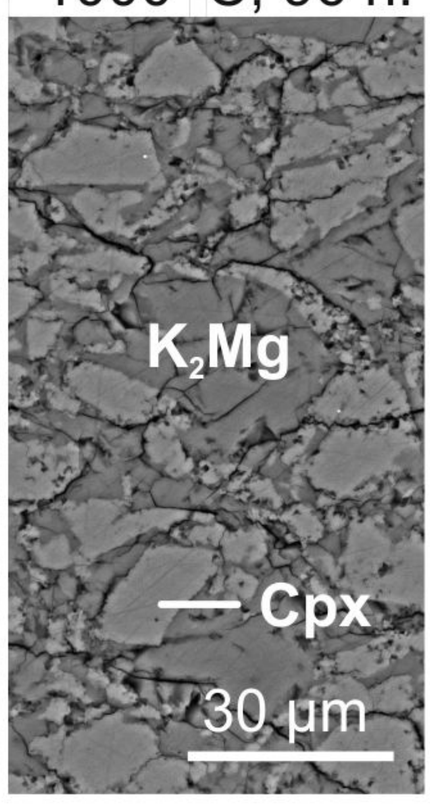

c. D026, 1050 °C, 96 h.

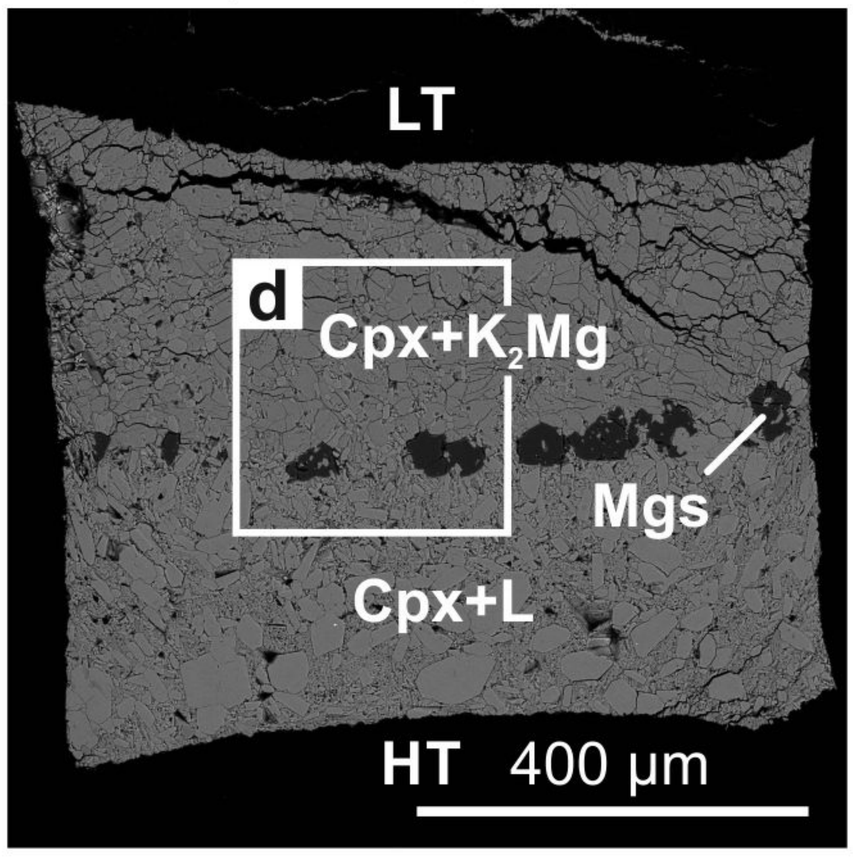

d. D026, 1050 °C, 96 h.

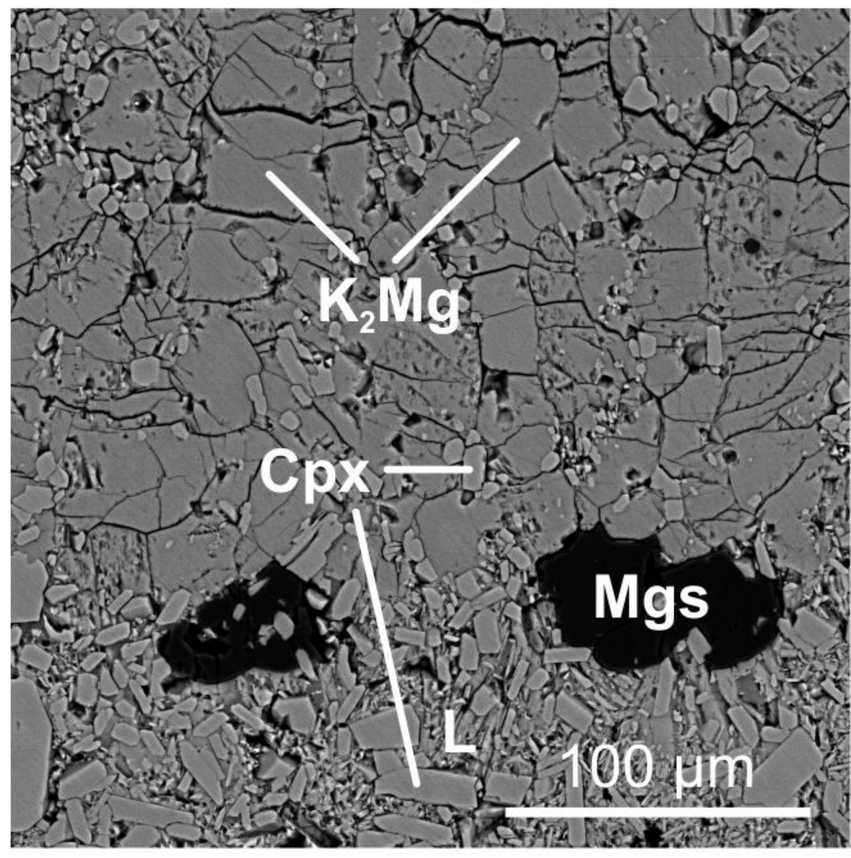

e. D015, 1100 °C, 48 h.

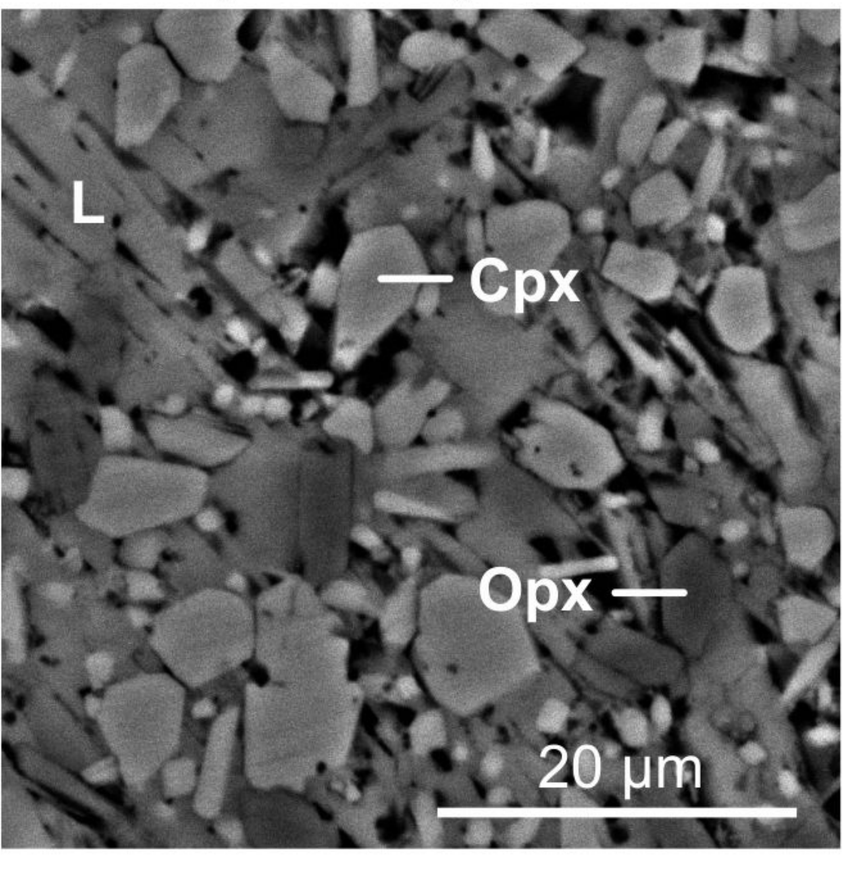

f. D031, 1150 °C, 53 h.

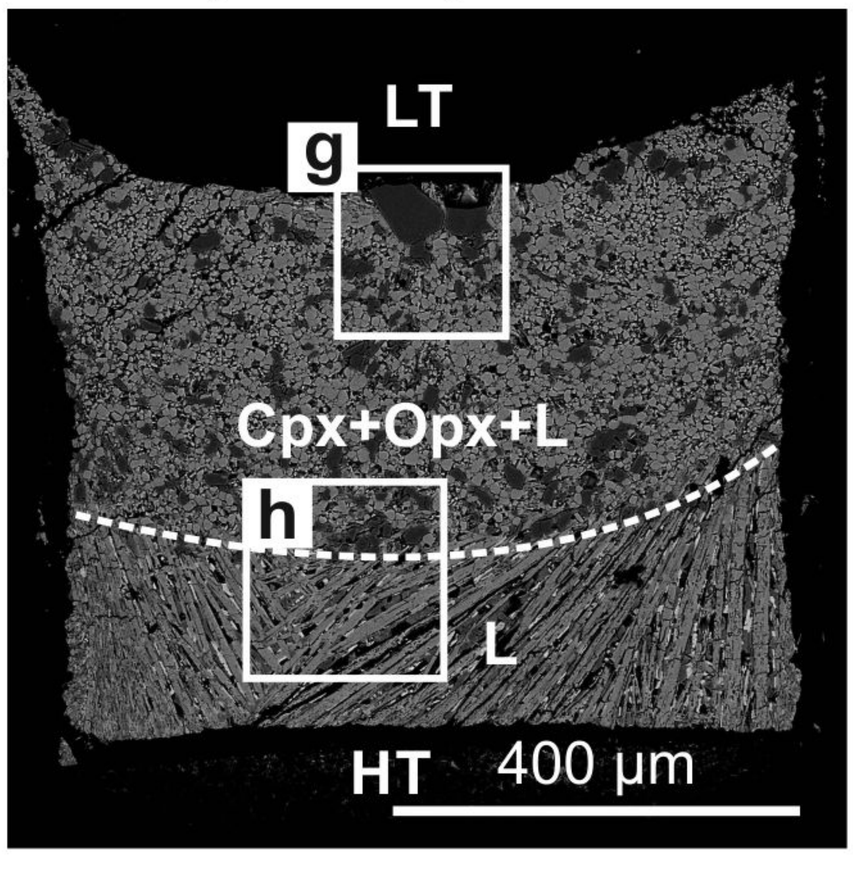

g. D031, 1150 °C, 53 h.

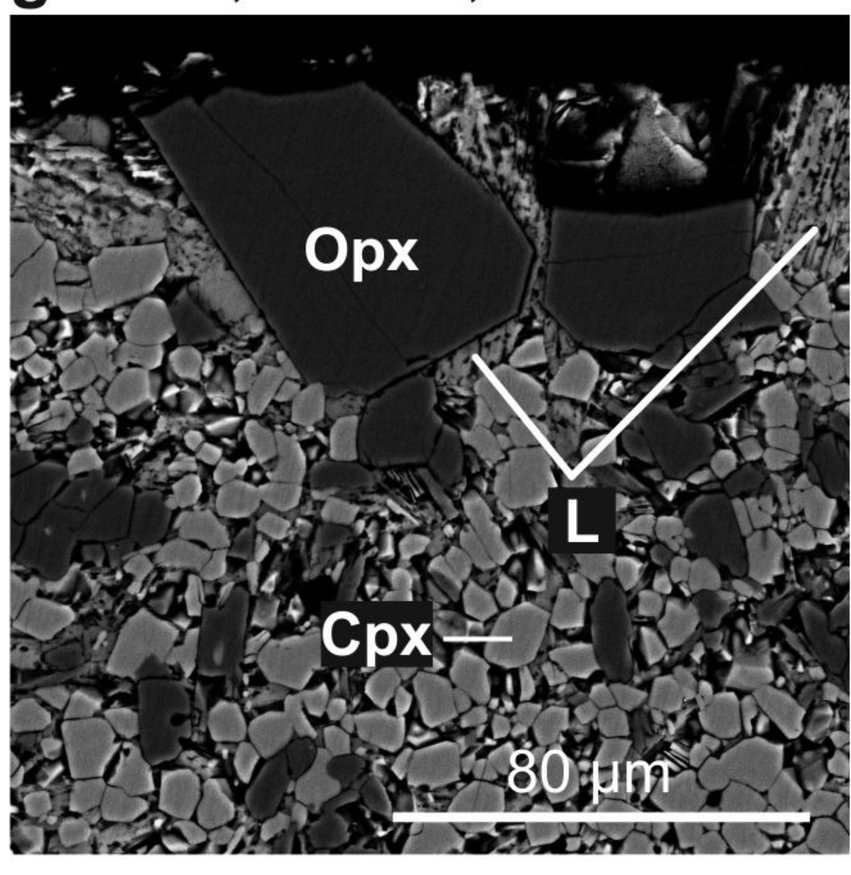

h. D031, 1150 °C, 53 h.

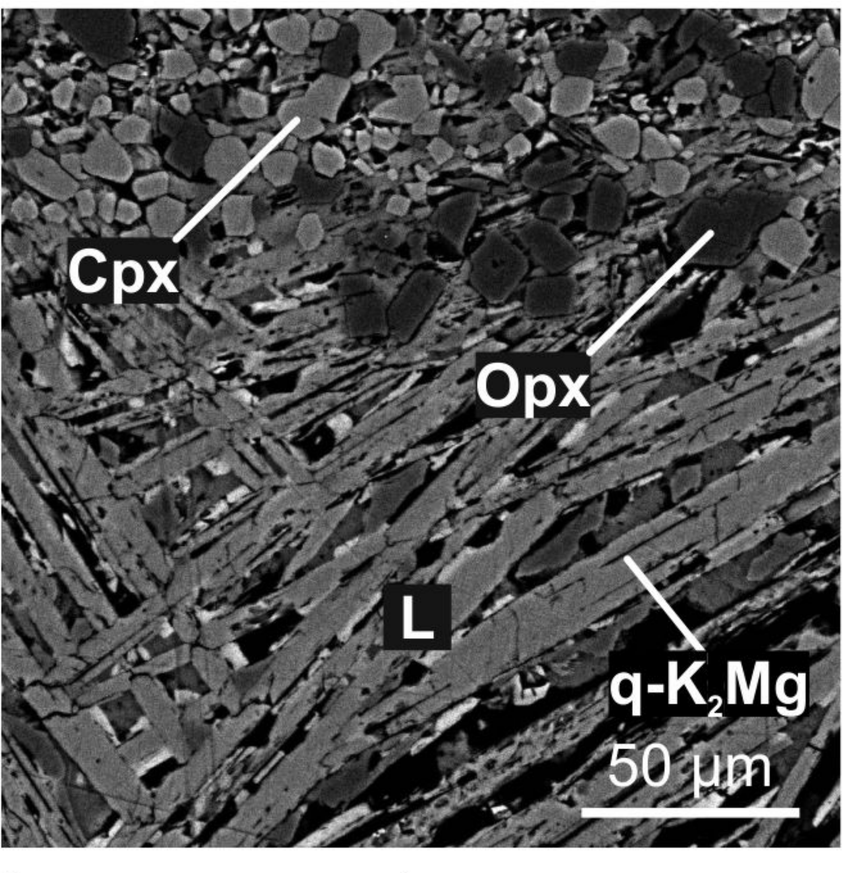

i. D027, 1350 °C, 24 h.

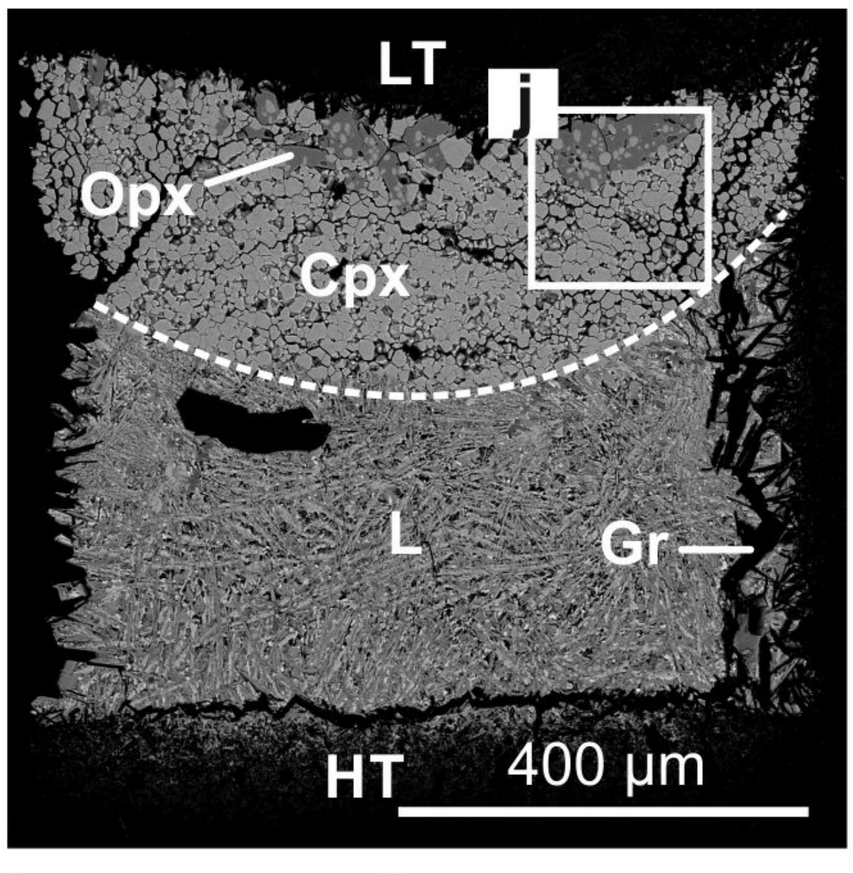

j. D027, 1350 °C, 24 h.

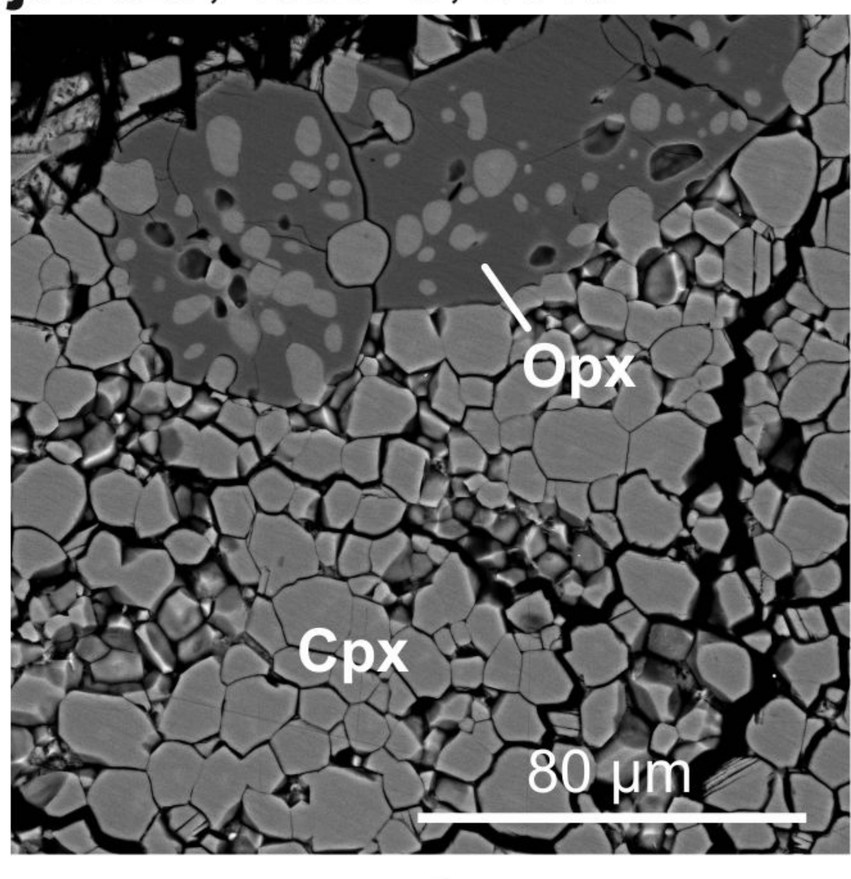

k. D028, 1500 °C, 6 h.

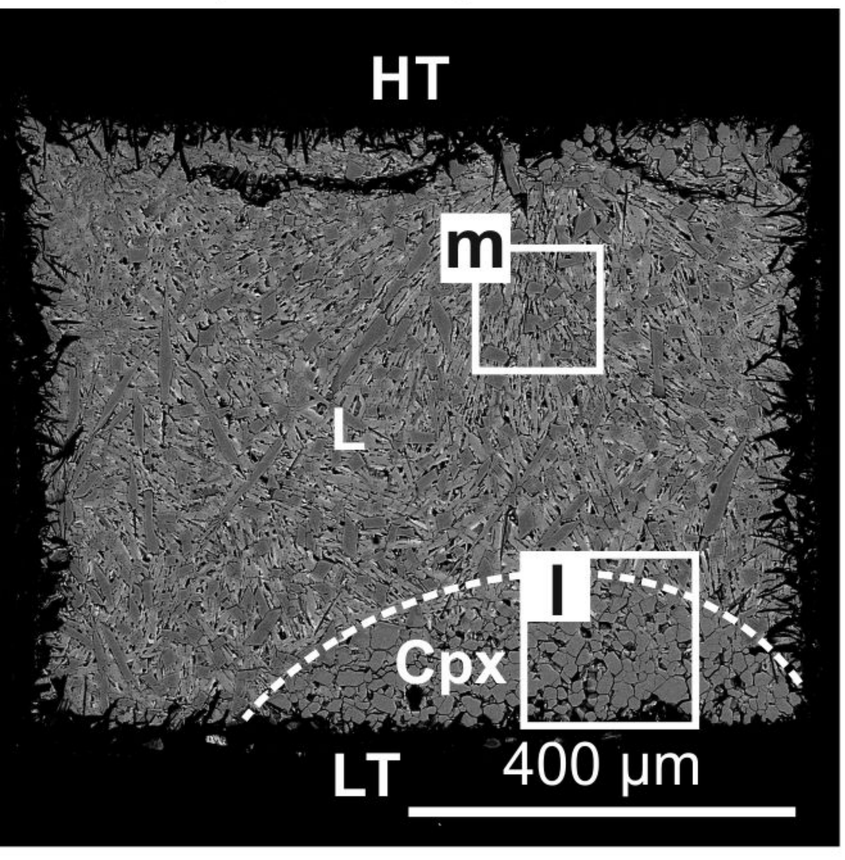

l. D028, 1500 °C, 6 h.

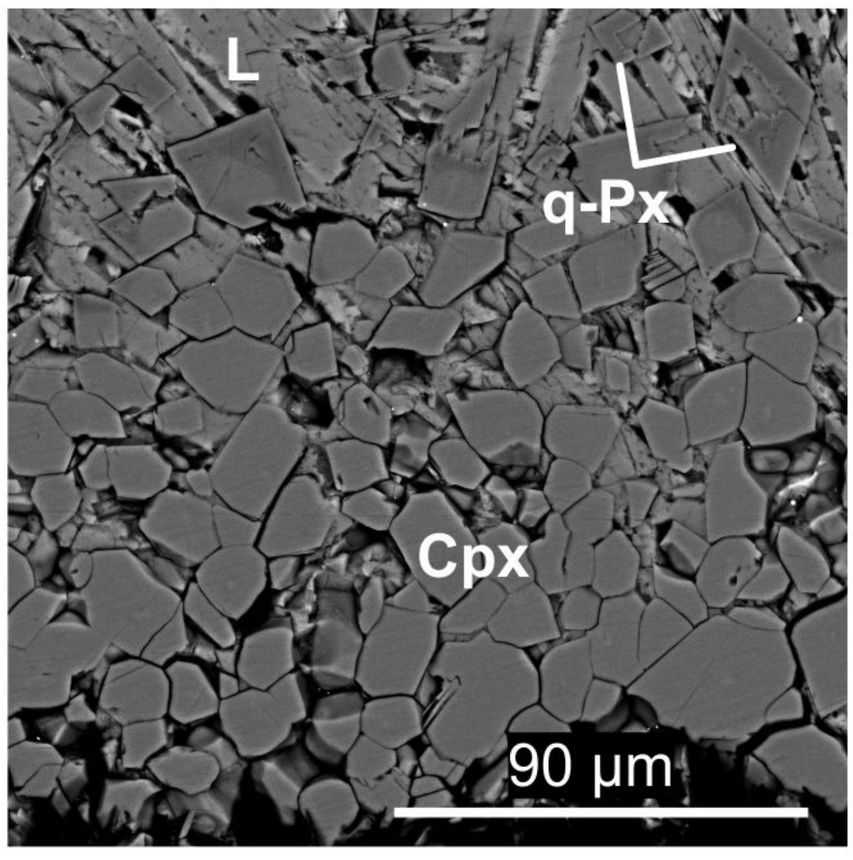

m. D028, 1500 °C, 6 h.